Hydrogen problems related to reactor accidents

Bujor, A.

Publication date:
1993

Document Version
Publisher's PDF, also known as Version of record

RISØ

Risø-R-706(EN)

Hydrogen Problems Related to Reactor Accidents

A. Bujor

Risø National Laboratory, Roskilde, Denmark
September 1993

Hydrogen Problems Related to Reactor Accidents

Risø-R-706(EN)

A. Bujor

Risø National Laboratory, Roskilde, Denmark
September 1993

Abstract At reactor accidents, the combustion of hydrogen causes pressure and temperature transients which pose supplementary loads in containment. In certain conditions, they could be at hazardous levels and impair the integrity of the containment and the operability of the safety systems.

The mechanisms of the chemical reactions specific for the hydrogen-oxygen system are presented ir Chap. 2. The conditions in which a burning can occur and the various combustion modes, including the transition to detonation are also described.

In Chap. 3 the related safety aspects and mitigation methods are discussed. Examples for particular applications and safety approaches for various types of reactors, included those promoted for the advanced reactors are also given.

Chap. 4 is dedicated to the presentation of the experimental research completed at AECL-Research, Whiteshell Laboratory, where the multi-point ignition effects for constant volume and for vented combustion of dry hydrogen-air mixtures in various geometries have been investigated.

Various aspects of modelling and simulation for the hydrogen burning are discussed in Chap. 5. The adaptations and the new models implemented in the codes VENT and CONTAIN, aimed to broaden the simulation capabilities of their hydrogen combustion models are described. The capabilities and the limits of the modelling assumptions of these two codes are also evaluated.

This report is submitted in partial fulfillment of the requirements for a Ph.D. degree at the Technical University of Denmark. The supervisors were Prof. P.L. Ølgaard at the Technical University of Denmark and Dr. P.B. Fynbo at Risø National Laboratory

ISBN 87-550-1925-0
ISSN 0106-2840

Grafisk Service, Risø, 1993

Dansk Resumé. Brintforbrænding er ledsaget af tryk og temperaturer, der introducerer ekstra belastninger på containments struktur og på sikkerhedssystemerne. I særlige tilfælde kan de beskadige sikkerhedssystemerne og nedsætte containments evne til at begrænse det radioaktive udslip.

Mekanismerne for de kemiske reaktioner, der er specifikke for systemet brint-ilt er præsenteret i kap. 2. Betingelserne, hvorunder en brintforbrænding kan ske, og de forskellige måder en forbrænding kan foregå på, er også beskrevet.

I kap. 3 diskuteres de specifikke reaktorsikkerhedsaspekter og konsekvensbegrænsningsmetoder. Forskellige eksempler på anvendelse og sikkerheds fremgangsmåder ved visse typer af reaktorer er også givet. De nye konsekvensbegrænsningsmetoder, der bliver aktuelle for de avancerede reaktorer, er nævnt i sammenhæng med den nye transparente sikkerheds fremgangsmåde.

Kap. 4 er viet til beskrivelsen af eksperimenter udført i AECL-Research, Whiteshell Laboratory, hvor effekterne ved flerepunktsantændelse ved forbrænding med eller uden udluftning af tørre brint-luft blandinger har været undersøgt. De målte resultater for trykudvikling, maksimum forbrændingstryk og for flammens hastigheder, samt indflydelsen af de geometriske forhold er analyseret.

De forskellige modellerings- og simuleringsaspekter til brintforbrænding er diskuteret i kap. 5. I forbindelse hermed, blev de muligheder og begrænsninger, der ligger i modelleringstilnærmelserne vurderet for to koder, en en-dimensional forbrændingskode, VENT, og en integreret lumped-parameter kode for containmentanalyser, CONTAIN. Beskrivelser af de nye tilpasninger og simuleringsmodeller, der er udviklet for at forøge brugbarheden af disse koder, er også inkluderet.

Contents

1 Introduction

One of the potential threaths to the inegrity of the reactor containment, seen as a barrier against the release of radioactive products at severe accidents, comes from the supplementary pressure and temperature loads developed under the combustion of flammable gases - mainly hydrogen and, under special conditions, carbon monoxide.

As the accident at the Three Miles Island has shown, the combustion of hydrogen can occur. Since then, this issue has been given a continuous attention by all the factors responsible with the safety of nuclear power plants and by the scientific community related to the nuclear industry. The results of the research work conducted in this area are employed for devising mitigation techniques in order to minimize the hazards associated with the presence of hydrogen during the accidents and to insure an acceptable level of safety of the reactors.

The accident analyses included in the safety reports consider accidents up to the level of the design basis accident (DBA), for which the generation of hydrogen is limited to metal-water reactions in the core and to radiolysis, /7/, /8/, /9/.

The metal-water reactions are exothermic reactions of oxidation of the fuel cladding material by the oxygen existing in the molecule of steam. The reaction takes place when substantial degradation of the core cooling occurs with the fuel rods at high temperature being surrounded by saturated or superheated steam. The oxidation involves the diffusion of the steam molecules through a thin hydrogen layer at the clad surface, then the decomposition of the steam molecule, the diffusion of oxygen through zirconium dioxide, and finally, the oxidation. In the short term, the energy released by the zirconium oxidation can produce local overheated points (hot spots) on the clad which can cause a premature fuel failure.

The radiolysis is a long term mechanism which consists in the decomposition of the water molecule by radiation (α, β, γ, or neutrons) producing various radicals as OH, H, and HO_2 and, as a final result, hydrogen and oxygen in stoichiometric ratio.

Under the emphasis put in the last years on the analysis of severe accidents it has been shown that an ex-vessel phase of combustible gas production should be considered. When the molten core debris escapes into the reactor cavity, chemical reactions between the molten core and concrete (molten-core-concrete interaction, MCCI) and between the core debris and the atmosphere occur, having as result the production of hydrogen and carbon monoxide. The high temperature in the atmosphere favorises further reactions of oxidation and corrosion of various materials existing in the containment (aluminum surfaces, zinc, steel) by the steam. At direct contact, the metallic uranium reacts with the steam to UO_2 having as result a supplementary generation of hydrogen. Though still a slow process, the radiolytical decomposition of the steam molecules is enhanced, due to a higher radiation flux.

The quantity and rate of production, the place of generation, and the distribution pathways of the hydrogen are strongly dependent on the particular accident scenario and on the containment geometry, /10/.

Following the in-core metal-water reaction, the hydrogen is introduced into the containment in a strong jet, which contributes to an enhanced mixing in the injection compartment, though gradients in the near jet region can occur. The mixing is also favorized by the natural and forced convection and by the water spray as well.

The heterogeneous injection of the steam and hydrogen and the momentum sources due to the jets and forced convection sources (fans) can produce large

pressure gradients. The intercompartment flow is another factor which promotes the transport and mixing of hydrogen in containment.

Other mechanisms for distribution and mixing are the atmospheric agitation due to natural convection and turbulence and the diffusion. However, since the time to mix a volume only by diffusion is proportional to the square of the length scale, it is expected that the diffusion will only be important for slow release rates and large time scale available for mixing (days), /4/.

As the hydrogen is released, it accumulates in the containment atmosphere where it can form flammable mixtures and ignite. The combustion produces supplementary pressure and temperature loads at possible dangerous levels for the integrity of the containment and for the operability of other safety systems and mitigation systems. The combustion behaviour is strongly influenced by the composition of the atmosphere (concentration of fuel, oxygen, and diluents), thermodynamic processes (local turbulence, convective flows, various heat and mass transfer mechanisms), geometry, operation of the safety and mitigation systems (fans, sprays) and by the presence of ignition sources.

The oxidation of hydrogen, the flammability limits and the combustion modes are presented in Chap. 2.

A short description of various safety philosophies and mitigation techniques is given in Chap. 3.

In Chap. 4 there are presented the intermediate scale hydrogen combustion experiments with simultaneous multipoint ignition, performed at AECL-Research, Whiteshell Laboratory, and in Chap. 5 the adaptations, developments, and evaluation of the hydrogen combustion models in the computer codes VENT and CONTAIN, are described.

2 Hydrogen Combustion

2.1 Oxidation of Hydrogen

The oxidation of hydrogen takes place via a complex system of elementary chemical reactions where various active radicals and oxygen-hydrogen compounds are involved. A complete scheme of these reactions as it is given in literature, /12/, is included in Appendix 1.

The hydrogen-oxygen system undergoes a chain reaction which takes place in three stages:

- initiation
- propagation or chain branching
- destruction or chain breaking

Retaining the most significant reactions from the list given in Appendix 1, a simplified scheme is described below.

Since the dissociation of hydrogen is less than that of oxygen, /13/, the initiation can be related to hydrogen dissociation. Active radicals of H and OH are produced with the endothermic reactions

$$H_2 + M \rightarrow 2H + M \qquad (1)$$

$$M + H_2 + O_2 \rightarrow H_2O_2 + M \quad (2)$$

$$H_2O_2 \rightarrow 2OH \quad (3)$$

where M represents a third body molecule which facilitates the reactions.

The reactions for chain branching are reactions where the radicals react with the molecules of H_2 and O_2 generating the combustion product and other new radicals which will contribute to chain propagation

$$OH + H_2 \rightarrow H_2O + H \quad (4)$$

$$H + O_2 \rightarrow OH + O \quad (5)$$

$$O + H_2 \rightarrow OH + H \quad (6)$$

The destruction stage or chain breaking consists of recombinations of the radicals with the formation of stable molecules.

At normal conditions, spontaneous slow reactions occur, due to the nonuniform distribution of the energy of the molecules. However, in order to have a fast reaction, the rate of chain branching must exceed the rate of chain breaking. Therefore, a source of energy is required for enhancing the initial formation of radicals with the reactions (1)-(3). For a temperature above 400°C only few radicals are required to initiate a fast reaction. Represented in coordinates (p, T) the boundaries between the slow reactions and the fast reactions, named also "explosion limits", are given in Fig. 1.

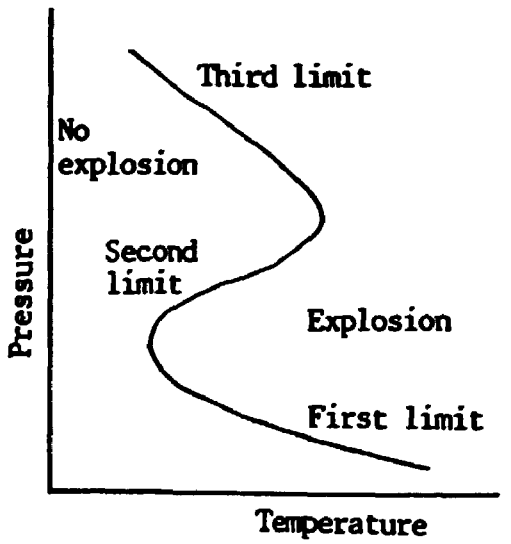

Figure 1. Explosion limits for a chain branching reaction.

At the first limit, the increase of pressure leads to an increase of the concentration of O_2 molecules such that the frequency of the reaction (5) increases. Since (5) is a chain branching reaction, the rate of chain branching increases and a lower temperature is required for a fast reaction to occur.

For a further increase of pressure, the reaction

$$H + O_2 + M \rightarrow HO_2 + M \quad (7)$$

becomes dominant since its frequency increases faster (with p^3) than the frequency of (5) which is proportional with p. The HO_2 molecule is unreactive, it diffuses to the walls where destruction reactions occur.

$$HO_2 \rightarrow \tfrac{1}{2} H_2 + O_2$$
$$HO_2 \rightarrow H_2O + \tfrac{1}{2}O_2 \quad (8)$$

Since (7) and (8) are chain breaking reactions, an increase of the pressure will require a higher temperature for a fast reaction - second explosion limit, Fig. 1.

For a further increase of pressure, the stability of HO_2 is overtaken by reactions producing active radicals.

$$HO_2 + H_2 \rightarrow H_2O_2 + H \quad (9)$$

followed by

$$H + O_2 \rightarrow OH + O \quad (10)$$

At the third limit (Fig. 1) the probability of (9) increases relative to the probability of diffusion of HO_2 molecules to the wall for destruction. At temperatures well above 600°C, a stoichiometric H_2-O_2 mixture is undergoing a fast reaction at all pressures of interest. The chain is not necessarily terminated, though recombinations of the radicals occur:

$$H + OH + M \rightarrow H_2O + M \quad (11)$$

$$H + H + M \rightarrow H_2 + M \quad (12)$$

$$O + O + M \rightarrow O_2 + M \quad (13)$$

Thus, a fast reaction can be obtained by bringing the mixture inside the "explosion limits". This can be done by raising the pressure and/or the temperature to appropriate values. For a given initial pressure, a local heating of the gas by a source of energy (spark, hot surface) is sufficient.

Though in the above discussion only the thermal mechanisms have been considered, the production of radicals by the dissociation of stable species (O_2, H_2, steam) under the influence of the radiation field associated with the power reactors has been studied, /14/, /15/, for an ionizing radiation field can essentially yield all the radicals that are normally present in the flame. Over the range of γ radiation fields which are significant for the power reactors, however, this effect is small - the reduction in the minimum hot surface ignition temperature is below 10°C, /15/.

2.2 Flammability Limits

The flammability limits specify the lean and rich fuel concentrations beyond which no flame will propagate. The explosion limits are not the flammability limits. One must have a fast reaction for a flame to propagate. Therefore, in order to have a propagating flame in a premixed atmosphere, a source of energy is required for creating the active radicals and initiate the chain reaction, and the

mixture must be inside the flammability limits.

The energy required to ignite a H_2 mixture is relatively low, with an order of magnitude of tenth of millijoules. In Fig. 2, /4/, the spark ignition energy for H_2-air mixtures is given. The ignition energy increases as the mixture approaches the flammability limits. Addition of a diluent (CO_2, steam) has also as effect an increase of the energy for ignition. In a post accident containment this energy can be provided by electrical or mechanical sparks from various equipments or by the ignition system used for mitigation.

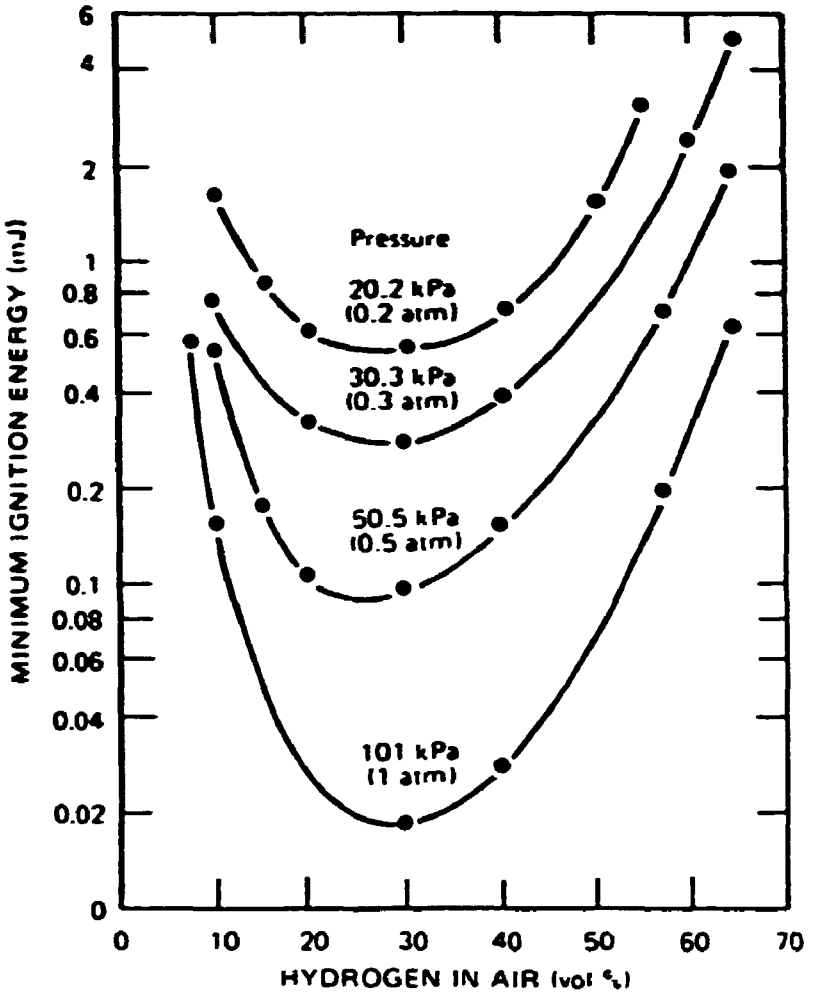

Figure 2. Spark ignition energy for dry H_2-air mixtures, /4/.

Hot surfaces are also able to ignite a mixture by a local heating of the gas up to autoignition temperature, which is the temperature that allow the chemical reactions to occur. If the mixture is brought quickly at the autoignition temperature, the ignition will occur after a certain time interval named "induction time", needed for building up the required concentration of radicals by the initiation and chain branching reactions. The induction time is proportional to the global reaction rate, $w = Z \exp(-E/RT)$, where Z is the frequency factor, E is the activation energy and T is the local temperature of the mixture. Measurements of the minimum surface temperature for ignition and its dependency with the composition of the mixture and with the initial conditions are reported. In Fig. 3, /16/, some experimental values for the minimum hot surface ignition temperature for dry H_2-air mixtures are given. At severe accidents, the hot surface of the molten core escaped in the reactor cavity can be an effective source of ignition.

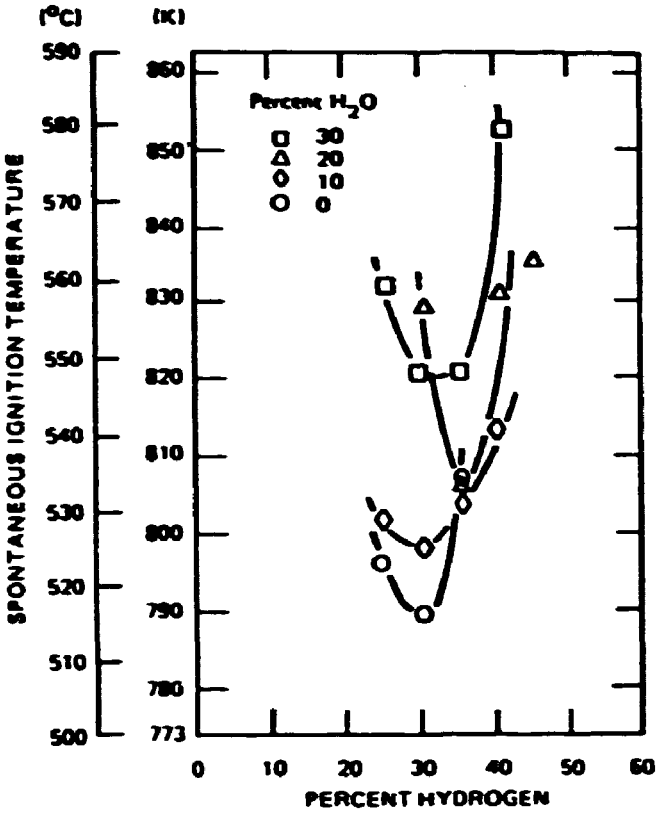

Figure 3. Minimum spontaneous ignition temperature for hydrogen-air-steam mixtures at 7.8 atm. /5/.

Inside the flammability limits the flame is able to propagate. The propagation of the flame is controlled by factors as flame stretch, buoyant convection, preferential diffusion and heat transfer to the adjacent walls and gas molecules. Due to the natural convection flow produced by burning, the upward, horizontal and downward propagation limits will differ. Since the buoyant upward flow is opposed to the dawnward flame motion, the lean downward propagation limits are slightly higher than those for upward propagation. The preferential diffusion of the radicals from the surrounding mixture into the flame is the dominant mechanism near the lean upward propagation limits, /17/. Without preferential diffusion the temperature will be too low and the heat losses will quench the flame, since a minimum temperature is required for the propagation to occur. Near the lean downward propagation limit, however, the preferential diffusion appears to play a less important role.

The hydrogen flammability limits in steam-saturated air are given in Tab. 1, /4/. These values are valid for the conditions expected to occur in a post accident reactor containment.

When more than one combustible gas are present, the lean flammability limits can be calculated with Le Chatelier formula, /18/, /19/, /20/. For the system H_2-CO

$$x_H + F \cdot x_{CO} \geq x_f^{lim}$$

Table 1. Hydrogen flammability limits in steam-saturated air, /4/

	Lower limit (vol.%)	Upper limit (vol.%)
Upward propagation	4.1	74.0
Horizontal propagation	6.0	74.0
Downward propagation	9.0	74.0

with

x_H = mole fraction of hydrogen
x_{CO} = mole fraction of carbon monoxide
F = empirical coefficient
x_f^{cri} = threshold (critical) mole fraction for ignition

The appropriate values for upward, horizontal and downward propagation are given in Tab. 2.

Table 2. Coefficients in Le Chatelier formula for lean flammability limits for H_2-CO

	F	x_f^{cri} (vol.%)
Upward propagation	0.328	4.1
Horizontal propagation	0.435	6.0
Downward propagation	0.600	9.0

The rich propagation limit (upper limit) is essentially given by the minimum volumetric concentration of oxygen required for ignition, which is 5%.

The diluents present in the containment atmosphere - steam and CO_2 -have as effect a narrowing of the domain between the flammability limits, until the lower and upper limits meet. Thus, for a diluent concentration x_d, higher than 55%,

$$x_d = x_s + x_{CO2}$$

x_s = mole fraction of steam
x_{CO2} = mole fraction of carbon dioxide

the ignition is no longer possible. The molecules of diluent which have a large heat capacity, are cooling the flame and impair the ignition and the propagation. In Fig. 4 the triangular diagram of Shapiro and Moffette, /4/, is reproduced. It indicates the flammability limits and the detonability limits for H_2-air-steam mixtures.

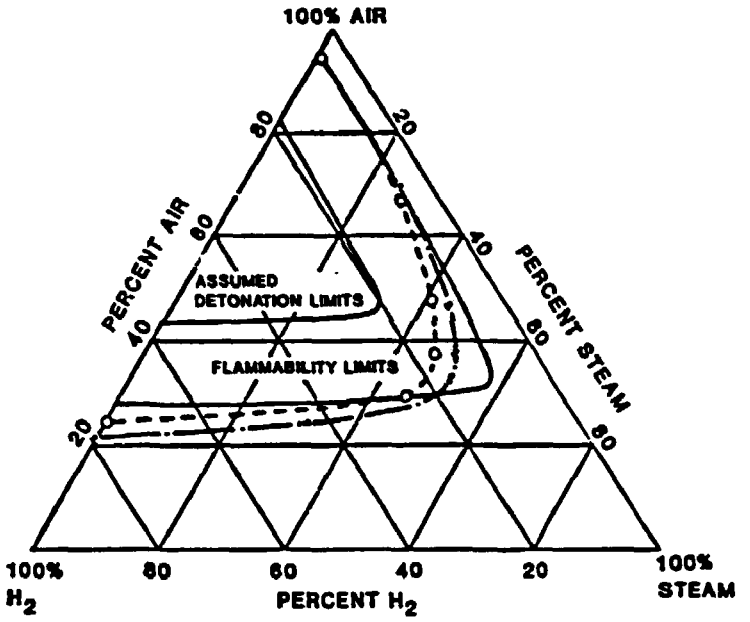

Figure 4. Flammability and detonation limits of hydrogen-air-steam mixtures.

2.3 Combustion Modes

The combustion of hydrogen is a strongly exothermic reaction with an energy yield of 1.2093 x 10^8 J/kg of hydrogen burned. The combustion, initiated in the ignition point, evolves heat, raises the temperature of the surrounding gas, and propagates. The burnt gas is separated from the unburnt gas by a layer where the burning is in progress, named "flame" or "reaction zone".

The velocity of the flame relative to the unburnt gas is named burning velocity. The flame velocity is the velocity of the flame relative to the laboratory system. The quantity of the gas which is burned in the unit of time is the burning rate. These variables are dependent upon the composition and the initial state of the mixture, the turbulence characteristics, the geometry of the compartment, the presence of convective flows, etc. For calculating the burning rate, the flame shape/surface area during combustion is needed.

In practice, for evaluating the flame velocity and the burning velocity, results of experimental measurements expressed in empirical correlations are employed. For the domain of interest of the accidents in nuclear power plants, the laminar burning velocity for rich H_2-air-steam mixtures can be calculated with the correlation Liu-MacFarlane, /21/, with correction factors for the variation of the pressure and temperature, /22/. For lean mixtures, the results reported in /23/, /24/, /25/, and /26/ can be used. For evaluating the burning velocity in a turbulent atmosphere, the knowledge of the turbulence characteristics is necessary; various correlations are given in /27/, /28/, and /29/. In /30/, /31/, and /32/ experimental measurements and empirical correlations for the flame velocity are reported. They express the dependence of the flame velocity upon the concentrations of hydrogen and diluents (steam) in the mixture, the geometrical characteristics (propagation length of the flame, positioning of the ignition points) and upon the operation of

containment systems (fans, spray).

The combustion products being at high temperature, have a lower density and expand. Thus the flame acts as a piston on the unburnt gas and an induced flow is generated. The combustion in a premixed atmosphere is thus accompanied by the motion of the gas, which results in formation of shock waves, /33/. The strength of the shock is determined by the flame speed. Reciprocally, the shock modifies the state of the gas behind, influencing in this way the characteristics of combustion: the unburnt gas is compressed and heated by the shock producing an increase of the burning velocity. A positive feedback is thus established in the direction of the accelerating the flame, effect which, however, is unsignificant for slow flames.

The structure of the flow during combustion in the planar unconfined wave approximation, /34/, is represented in Fig. 5.

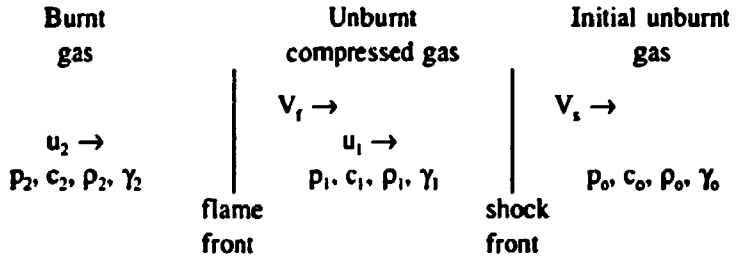

Figure 5. The structure of the flow in the planar unconfied wave approximation.

Where:

V_f = flame velocity
V_s = shock velocity
u = gas velocity
p = pressure
ρ = density
c = sound velocity, $c = (\gamma\, p/\rho)^{1/2}$
γ = ratio of the specific heats

and the indices

0 = initial unburnt gas
1 = unburnt gas behind the shock
2 = burnt gas

In Fig. 5 the velocities of the gas are represented in the laboratory system and are considered perpendicular to the shock front and to the flame front.

In the following it is assumed that the gas is ideal with constant specific heats. Since the chemical composition of the gas is not modified by the shock the adiabatic exponent of the gas ahead and behind the shock is constant,

$$\gamma_0 = \gamma_1 = \gamma$$

For shocks which are not too strong the dissociations in the burnt gas are neglected, such that γ_2 can be calculated a priori from the known composition of the burnt gas.

Under these assumptions the balance equations for mass, momentum and energy

at the flame front are

$$\rho_1(V_f-u_1) = \rho_2(V_f-u_2) \tag{14}$$

$$p_1 + \rho_1(V_f-u_1)^2 = p_2 + \rho_2(V_f-u_2)^2 \tag{15}$$

$$e_1+\frac{p_1}{\rho_1} + \frac{(V_f-u_1)^2}{2} + Q = e_2+ \frac{p_2}{\rho_2} + \frac{(V_f-u_2)^2}{2} \tag{16}$$

where

e = specific internal energy of the gas, $e = p/\rho/(\gamma-1)$

Q = reaction heat per unit mass

Eliminating $(V_f - u_1)$ and $(V_f - u_2)$ between these equations, a relation between the pressure and density for burnt gas and for the gas ahead of the flame is obtained. In this model, the following form is used, /34/,

$$(x-\alpha)(y+\alpha) = \beta \tag{17}$$

where:

$$x = \frac{\rho_1}{\rho_2} \qquad y = \frac{p_2}{p_1} \qquad \alpha = \frac{\gamma_2-1}{\gamma_2+1}$$

$$\beta = \frac{\gamma_2-1}{\gamma_2+1}\left[\frac{\gamma+1}{\gamma-1} + \frac{2\gamma Q}{c_1^2} - \frac{\gamma_2-1}{\gamma_2+1}\right]$$

The relation (17) represents the equation of the Hugoniot curve, which contains in the x-y-plane the points corresponding to all the possible states of the burnt gas expressed with respect to the state of the unburnt gas compressed by the shock.

A similar equation can be derived for the adiabatic shock (Q=0) preceding the flame, defining the Hugoniot curve for the adiabatic shock.

For determining the state of the compressed gas behind the shock as function of the shock strength and of the initial state, the relations Rankine - Hugoniot are used, /34/, /35/, derived from the balance equations at the shock front,

$$\frac{p_1}{p_0} = \frac{2\gamma}{\gamma+1}\frac{1}{\eta} - \frac{\gamma-1}{\gamma+1} \tag{18}$$

$$\frac{\rho_1}{\rho_0} = \frac{\gamma+1}{\gamma-1+2\eta} \tag{19}$$

$$\frac{u_1}{u_0} = \frac{V_s(\rho_1-\rho_0) + \rho_0 u_0}{\rho_1} \tag{20}$$

or, for quiescent initial atmosphere ($u_0 = 0$),

$$\frac{u_1}{c_0} = \frac{2(1-\eta)}{\gamma+1}\eta^{-1/2} \tag{21}$$

with

$$\eta = \frac{1}{M_0^2}$$

and

$$M_0 = \frac{V_s - u_0}{c_0}: \textit{ Mach number for the shock front.}$$

Another important equation is obtained from the definition of the Mach number for the velocity of the flame relative to the unburnt compressed gas,

$$M_1 = \frac{V_f - u_1}{c_1} \tag{22}$$

If $(V_f - u_2)$ is eliminated between (14) and (15), it results in

$$(V_f - u_1)^2 = \frac{p_1}{\rho_1}\left(\frac{p_2/p_1 - 1}{1 - \rho_1/\rho_2}\right) \tag{23}$$

and (22) becomes

$$y = -\gamma M_1^2 x + \gamma M_1^2 + 1 \tag{24}$$

$$x = \frac{\rho_1}{\rho_2} \quad , \quad y = \frac{p_2}{p_1}$$

The relation (24) represents in the x-y-plane a line named "Rayleigh line" in the English literature and "Mikkel'son line" in the Russian literature, /36/, which passes through the point $x=1$, $y=1$ and through the point representing the state of the burnt gas.

The Hugoniot curve for the flame front (eq. 17), the Rayleigh line (eq. 24) and the Hugoniot curve for the adiabatic shock are represented in the x-y-plane $x = \rho_1/\rho_2$, $y = p_2/p_1$, in Fig. 6. In this figure, the point $o(x,y) = (1,1)$ represents the initial state (no burning, no shock wave, for which $\rho_1 = \rho_2 = \rho_0$ and $p_1 = p_2 = p_0$).

The intersection between the Rayleigh line and the Hugoniot curve for the flame front gives the final state of the burnt gas for various modes of combustion: combustion at constant pressure (point CP), combustion at constant volume (point CV), deflagration and detonation.

The coordinates of these points are given by the solutions of the system of equations (17) and (24),

$$x_{1,2} = \frac{(1+\gamma M_1^2)(1+\alpha)}{2\gamma M_1^2} \pm \left[\left(\frac{(1+\gamma M_1^2)(1+\alpha)}{2\gamma M_1^2}\right)^2 - \frac{\beta+\alpha^2+\alpha(1+\gamma M_1^2)}{\gamma M_1^2}\right]^{1/2} \tag{25}$$

and

$$y_{1,2} = -\gamma M_1^2 x_{1,2} + \gamma M_1^2 + 1 \tag{26}$$

The points where the two curves are tangent represent the Chapman-Jouguet states. There are two such states - the Chapman-Jouguet Deflagration (CJ Def.) situated on the deflagration branch of the Hugoniot curve (below the point CP) and the Chapman-Jouguet Detonation (CJ Det.) situated on the detonation branch (above the point CV). They are both characterized by the sonicity of the flame front relative to the burnt gas ($M_2=(V_f-u_2)/c_2=1$) while the flame is subsonic

($M_1=(V_f-u_1)/c_1<1$) or supersonic ($M_1=(V_f-u_1)/c_1>1$) relative to the unburnt compressed gas for the CJ Def and CJ Det respectively.

In these points, the second term in (25) must vanish, such that

$$\left[\frac{(1+\gamma M_1^2)(1+\alpha)}{2\gamma M_1^2}\right]^2 - \frac{\beta+\alpha^2+\alpha(1+\gamma M_1^2)}{\gamma M_1^2} = 0 \qquad (27)$$

For detonation, this equation can be put in the form

$$c_0^2(\eta-1)^2 - 2\alpha(\gamma_2-1)\eta = 0 \qquad (28)$$

with

$$\eta = \frac{1}{M_{CJDet}}$$

$$c_0 = \left(\gamma\frac{p_0}{\rho_0}\right)^{1/2}$$

The regions on the Hugoniot curve delimited by the points CV, CP, CJ Def and CJ Det correspond to various combustion modes, as it follows.

The region between CP and CJ Def corresponds to the deflagration for which $M_1 < 1$ and $M_2 < 1$. The final state is obtained along the line Rayleigh (od). The deflagration in CJ Def can be interpreted as to be the fastest deflagration. In CJ Def, the flame must necessarily be highly turbulent, /34/, with burning velocities much greater than the laminar burning velocity of the mixture. The region below CJ Def on the deflagration branch (point e) corresponds to unstable deflagrations which are not considered. The deflagration is the combustion mode for which the ignition of the unburnt gas and thus the propagation of the flame is due to the increase of the temperature by the heat transferred from the flame. The velocity of the flame is relatively low, up to the order of tenth of meters per second. The deflagration as combustion mode is characteristic to the lean hydrogen mixtures and, in absence of the turbulence and of other factors causing the transition to detonation, to the mixtures with up to about 25% molar volumetric fraction of hydrogen in dry air. The maximum combustion pressure at deflagration is a property of the mixture; for an adiabatic and isochoric complete combustion of various H_2-air mixtures the maximum combustion pressure (P_{AICC}) and temperatures are given in Fig. 7 and respectively in Fig. 8, /4/. In reality, however, since the burning is not complete for lean mixtures and due to the dissipation mechanisms (cooling of the flame due to the heat transferred to the walls and structures in compartment), the maximum combustion pressures is up to 20% - 40% lower than P_{AICC}. For the size of the compartments in containment, the burning time at deflagration is long enough such that the pressure transient is in the range of the static loads on the containments structures.

Above CJ Det is the overdriven detonation. These states are obtained following an adiabatic compression along the adiabatic shock (oa) and an expansion along the Rayleigh line. In this region $M_1 > 1$ and $M_2 < 1$.

The weak detonation corresponds to the region CV-CJ Det. In this case, an ignition with a high energy source is needed. The final state is obtained by a fast compression along the Rayleigh line (oc, Fig. 6). In this region $M_1 > 1$ and $M_2 > 1$.

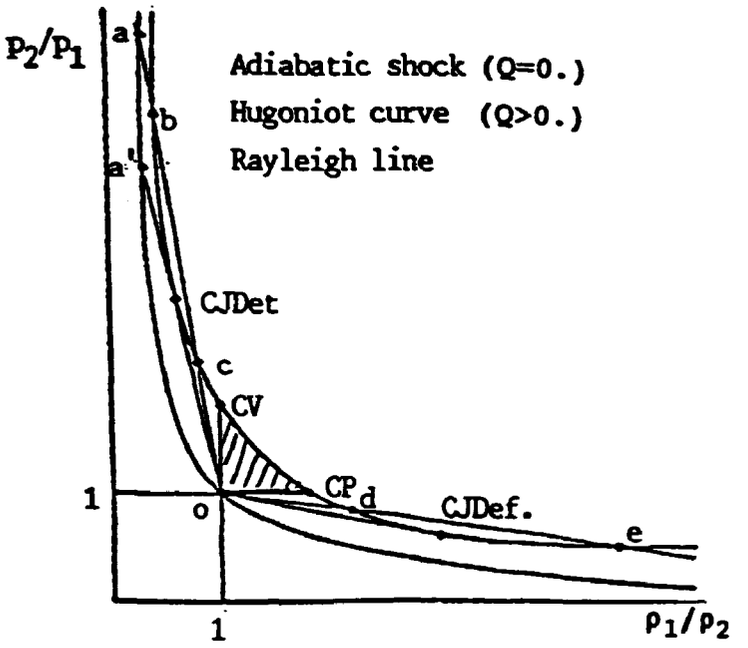

Figure 6. The diagram of the combustion modes.

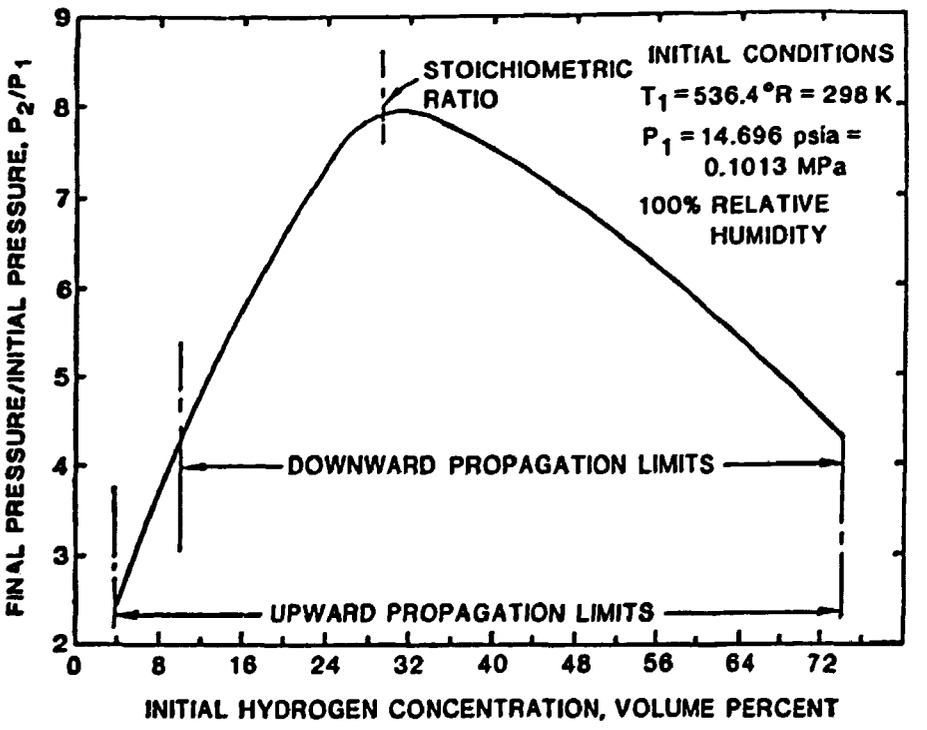

Figure 7. Theoretical adiabatic, constant-volume combustion pressure for hydrogen-air mixtures, /4/.

At detonation the continuity of the burning is insured by the compression of the unburnt gas behind the shock wave to the autoignition temperature. The flame front coalesces with the shock wave and in the region delimited by these two surfaces, the unburnt gas is compressed at elevated pressures. They are much higher than the deflagration pressures and therefore are a special concern for integrity of the containment. In Fig. 9, /4/, the theoretical detonation pressure and the pressure in the normal reflected detonation wave for various hydrogen-air mixtures are presented. The experiments have shown that the detonation occurs near the CJ Det point, such that the calculation of this state leads to acceptable results for characterizing a detonative combustion.

The structure of the shock waves generated at detonation shows a cellular pattern, as in Fig. 10, /36/. The transversal dimension of the cells, named detonation cell size, is a characteristic of the mixture being proportional to the post shock gas velocity and to the induction time. In Fig. 11, /37/, the detonation cell sizes, λ, for various H_2-air-steam mixtures are given. It can be seen that for mixtures far from stoichiometry λ increases to relatively large values; this has an important significance since the cell size is directly influencing the capacity of a detonation to propagate. The characteristic dimensions for various geometries below which a detonation with a cell size equal to λ cannot propagate, are shown in Fig. 12, /5/.

The significance of the detonation cell size as measure for evaluating the propagation of detonation and its relatively large values toward lean and rich hydrogen-mixtures, renders the scale effects important. Thus, any extrapolation of the experimental results usually performed in low or medium scale facilities, should be done carefully.

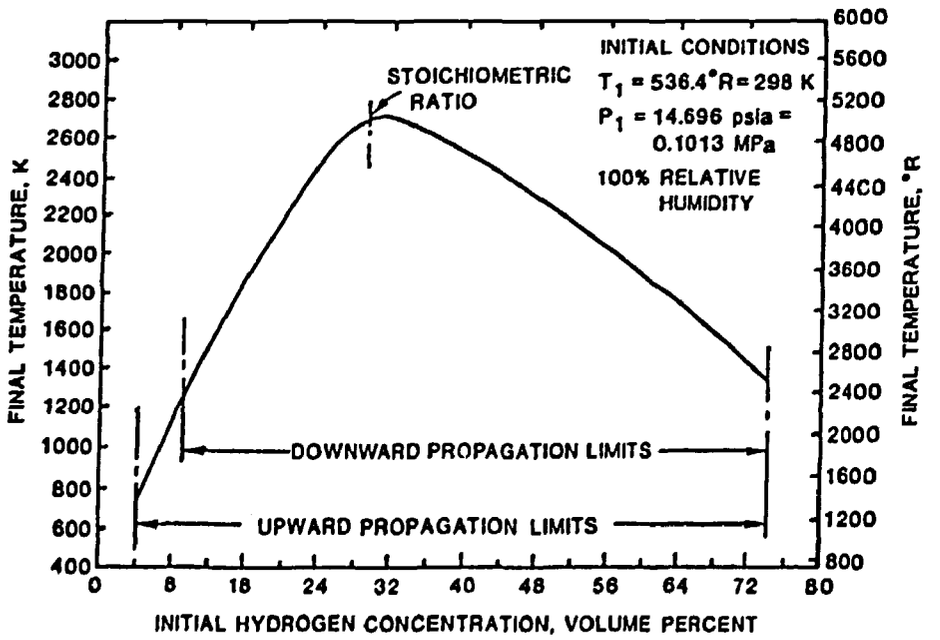

Figure 8. Theoretical adiabatic, constant-volume combustion temperature for hydrogen-air mixtures, /4/.

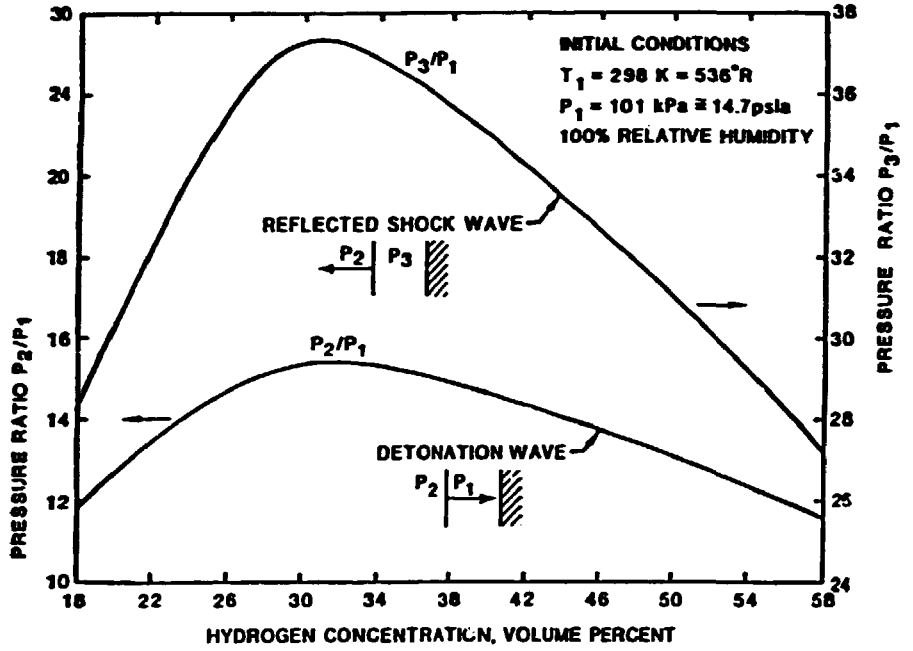

Figure 9. Theoretical detonation pressure and normally reflected detonation pressure for hydrogen-air mixtures, /4/.

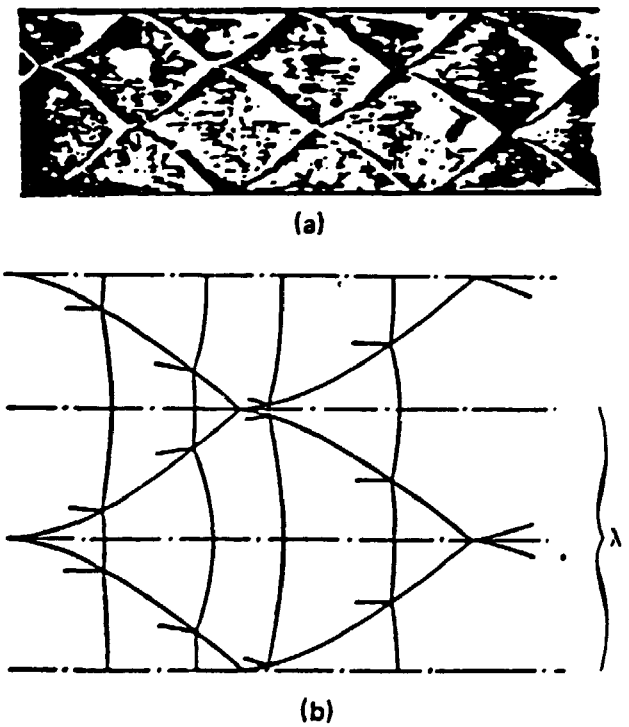

Figure 10. Detonation cells (a) and cell width (b), /36/.

In the region between CP and CV, two simultaneous conditions should be satisfied,

$$p_2 > p_1 \quad \text{and} \quad \rho_2 < \rho_1$$

which is physically unacceptable. In this region the slope of the Rayleigh line should be positive which again is impossible (eq. 24) because always $\gamma > 0$ and $M_1^2 > 0$.

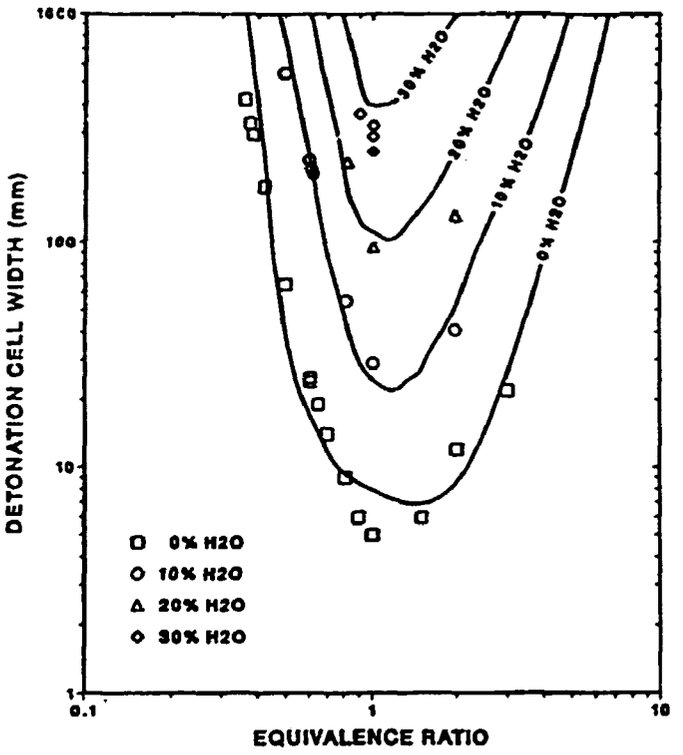

Figure 11. The effect of steam dilution on the detonation cell width as a function of the equivalence ratio for hydrogen-air-steam mixtures at 100°C initial temperature and an air density of 41.6 moles/m³, 137l.

2.4 Flame Acceleration and Transition to Detonation

The burning rate representing the quantity of gas (fuel) burned in the unit of time is directly dependent on the burning velocity and on the flame surface area. The compounded parameter expressed as the product of the burning velocity and the flame surface area is named the effective burning velocity. Any gradient in the effective burning velocity is referred as flame acceleration. Thus, the mechanisms for flame acceleration will be found among those which will affect the burning velocity and the flame surface area.

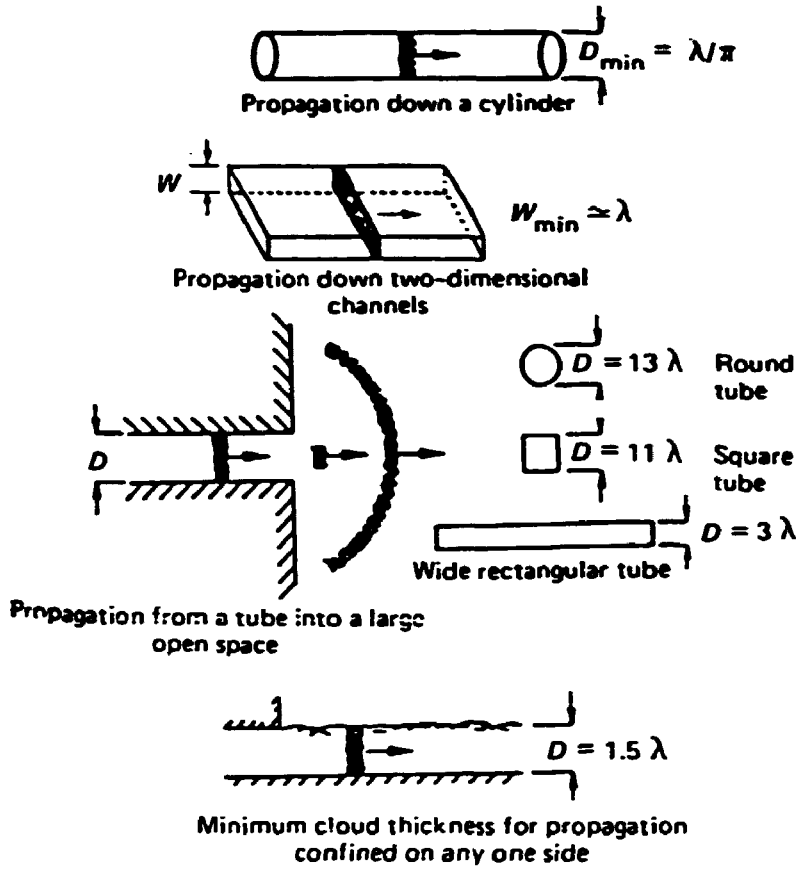

Figure 12. Schematic illustration of the effects of geometry and scale on detonation propagation, /5/.

As mentioned in Chap. 2.2 the laminar burning velocity is a characteristic of the mixture being determined by the concentration of fuel and diluent, respectively. The dependence of the laminar burning velocity on the physical and kinetic parameters can be written as

$$S \sim (\alpha w)^{\frac{1}{2}}$$

where

$$\alpha = \frac{K}{\rho c_p}$$

is the thermal diffusivity of the mixture, and w is the global reaction rate, $w = Z \exp(-E/RT)$ with being the activation energy and Z the frequency factor. Therefore at burning in closed volume the increase of the pressure and temperature of the unburnt gas during the transient will result in an increase of the laminar burning velocity. This dependence is accounted for in correlations for the laminar burning velocity with correction factors for variation of the pressure and temperature, respectively.

Under turbulent conditions, the small scale motion of the molecules is intensified. Thus, the rate of penetration of fuel molecules in the reaction zone is enhanced and the burning velocity is increased. The turbulent burning velocity (S_t) depends on the laminar burning velocity (S_u) and on the characteristics of turbulence, a dependence which is expressed with various empirical correlations, /27/,

/28/, /29/. It is also important to note an opposite effect of the turbulence on the propagation of the flame: that is, the cold molecules, whose penetration in the reaction zone is enhanced, will cool the flame. For a sufficiently intense turbulence, the effect of cooling of the flame by fresh particles (including the molecules of diluent) can be so important that the temperature in the reaction zone will drop below the autoignition temperature and the flame will quench. Thus, the turbulence can contribute not only to the acceleration but also to the quenching of the flame. Though quantitative prediction of this effect is not yet possible, both experiments and theoretical work are under way, /38/. The quenching of the flame is particularly important for lean mixtures with a significant quantity of diluent, as is the hydrogen containing atmosphere in a post-accident containment.

The presence of the walls and of other solid surfaces are also important by the turbulence generated by the near-wall gradient of the velocity of the main flow. At the same time, however, they contribute to the cooling of the flame by heat transfer; also the behaviour of the walls as a third body which promotes the recombination of the radicals wia the reactions (7) and (8) should be noted.

The increase of the flame surface area is an effective mechanism for flame acceleration. This is produced by the stretching and folding of the flame surface due to the presence of obstacles, convective flows and local pressure or velocity gradients (hydrodynamic instabilities) and due to the interaction of the flame with pressure/shock waves and with oscillating solid surfaces. In these cases, not only the surface of the leading flame is increased, but also pockets of unburnt gas may form in the volume of the hot combustion products. The burning of the gas in these pockets will substantially add to the burning rate.

Apart from the above, turbulence effects can cause a selective diffusion instability and thus, a further increase of the flame surface area. If an initially planar flame is slightly distorted, the resultant curvature will produce a gradient of the local concentration of fuel and thus, the variation of the burning velocity along the flame surface, causing a cellular structure, /34/, with the area of the flame surface larger than in the ideal planar case.

Due to the large number of factors involved, the complete calculation of the flame pattern in the particularly complex geometry and environment in a post accident reactor containment, is still a far from accessible task, /1/. Therefore, as mentioned above, various empirical correlations for the laminar and turbulent burning velocity are used. Regarding the flame shape, in the existing unidimensional or lumped parameter codes, simple geometrical forms (plane, spherical) are usually encountered.

A strong acceleration of the flame can result, under certain conditions, in a change of the combustion mode, that is to the transition from deflagration to detonation (DDT). This transition is accompanied by a significant increase of the pressure loads, since a relatively slow transient of pressure raise to a maximum value of the adiabatic isochoric complete combustion at deflagration, is replaced by a regime characterized by high pressure shocks in the shock waves at detonation. Due to the high values of the pressure spike for the direct wave and for the reflected shocks, the detonant burning and the DDT in containment must be avoided.

Though a complete qualitative and quantitative description of the DDT is not yet available, some aspects and mechanisms conditioning the occurrence of the DDT are outlined in the followings.

For a detonation to occur, a detonable mixture and a geometry which should allow the propagation of the detonation must be present. It is generally accepted that a strong ignition is required for detonation, /40/. As potential mechanisms for strong ignition, the shock focussing by multiple reflections in specific geometries (ex. corners) and the presence of hot spots in the unburnt gas where local

explosions occur, are considered. In this case, by "local explosion" a simultaneous initiation of a fast reaction in all the points of a volume of flammable mixture heated up to or above the autoignition temperature, is understood. Such a situation can occur when pockets of unburnt gas included in the volume of hot burnt gases are created. These pockets can be formed by various mechanisms which cause an accentuated folding of the flame surface, as: action of jets, interaction between the flame and the shock waves, presence of obstacles and intense turbulence fields where vortex sheets are present, /41/.

The problem of calculating the strength of the shock waves generated by an instantaneous energy release have been solved by Taylor and Lin for spherical and cylindrical geometries, /35/, and consequently, a criterion for the minimum energy which should be contained in a volume of hydrogen mixture undergoing a local explosion required for a DDT, has been developed, /40/. Since this criterion is, however, too restrictive, an amplification of the shocks resulting from several local explosions is necessary for explaining the DDT. In this case, the detonation appears as a result of amplification by coalescence of the shocks induced in several local explosions.

Following the SWACER model (Shock Wave Amplification by Coherent Energy Release), /49/, an amplification of the shock wave can also occur if the gradient in the induction time of the unburnt mixture in the path of the shock is such that the chemical energy release is coherent with the arrival of the shock and causes the strengthening of the shock. Since the induction time depends on the local temperature and concentration of active radicals, turbulent mixing, shock heating and photo-dissociation can lead to appropriate conditions for shock wave amplification. If these conditions reside along a minimum propagation length named coherence length, having the order of magnitude of the detonation cell size specific to the mixture, the shock wave becomes strong enough to produce by itself the ignition and thus, the detonation.

3 Mitigation Methods and Safety Aspects

The potential problems associated with the hydrogen at reactor accidents have been recognized from the early stages of development of commercial nuclear power reactors. However, the engineered safety measures and the high quality standards for design and execution have for a long time been believed to be sufficient to terminate any accident causing the formation of flammable mixtures in containment.

The accident at the Harrisburg station in 1979 has shown, however, that accident sequences leading to significant degradation of the core can practically develop, and that the combustion of hydrogen can occur. The recorded spike of the containment pressure was a clear indication of a hydrogen burn. It has shown that the combustion pressure might have the potential for damaging the containment and impair its ability to retain the radioactive products.

Therefore, the main safety objectives are to prevent the formation of flammable mixtures or, in the case where a burn occurs, to mitigate the combustion threats - pressure and temperature loads - to the containment and to the safety systems. High local concentrations of hydrogen which could cause local detonation, as well as global deflagrations and global detonations must be avoided.

As a result of the safety concerns and of the increasingly demanding regulation

requirements, several mitigation methods have been developed, /42/ - /54/. They are intended to reduce the hydrogen hazards for different reactors and containment designs during the various anticipated accident scenarios. In the following, an outlook on the problems related to these mitigation techniques is given. The objective of this section is not only briefly to present these methods, but rather to show the issues to be considered when making judgements for addressing safety aspects.

By pre-inerting or partial inerting, the combustion of hydrogen is controlled by limiting the quantity of the oxygen available. In normal operation, the atmosphere in containment is depleted in oxygen such that when an accident occurs, the atmosphere is beyond the flammability limits regardless the quantity and the rate of hydrogen produced. In the long term, however, an important quantity of oxygen is generated by radiolysis of water such that the atmosphere in containment might approach the flammability limits from the rich side. Therefore, a pre-inerted containment must be equipped with supplementary mitigation devices, usually with catalytic recombiners, to promote the consumption of the hydrogen and oxygen before the flammability limits are reached. This method is widely used in the BWRs usually having small size containments (type Mark I and Mark II in USA), which would otherwise present the risk of formation of rich hydrogen mixtures. For large containments specific to the PWRs, for example, where a large amount of surveillance and maintenance work involving the presence of personnel in containment during operation is needed, the pre-inerting is not considered for it presents supplementary hazards to the health of the workers.

Though not yet used in nuclear power plants, the inerting of the containment during the accident (post inerting) is under study in various organizations. It involves a fast injection of non-combustible or combustion inhibiting gases in the containment atmosphere when the evolution of accident shows that conditions for generation of hydrogen are present. Since the suppressing of the flame by dilution assumes that the diluent is intimately mixed with the fuel, a uniform distribution of the injected diluent must rapidly be obtained. Since the diluent would normally be stored in high pressure tanks, eventually under liquefied form, special provisions should be made for avoiding the pressure shocks at injection. The volume of the diluent introduced should be such that, the diluted atmosphere will be outside the flammability limits. However, the partial pressure of the diluent will add to the pressure developed under the accident, increasing the loads on the containment. Moreover, on long term, the containment will remain in a pressurized state, up to 60% above the atmospheric pressure in the case when non combustible gases N_2 or CO_2 are used, /58/. If combustion inhibitors as CF_3B_2 are injected, significantly smaller quantities are required, but, in this case the corrosion on long term could be harmful, /2/. Another disadvantage is that post inerting requires safety grade equipment (containment penetrations,valves, pipes,tanks, monitoring equipment and actuation chains) available for operation in conditions of accident.

The deliberate ignition is currently used for mitigation in containments where the low combustion pressures characteristic for the lean mixtures near the flammability limits are allowed. Using various types of ignitors (spark plugs, glow plugs) placed in strategic locations, an early burn is promoted, preventing the accumulation of hydrogen and the formation of dangerous rich mixtures. This method is consistent with the conservative approach that a flammable mixture can ignite in a post accident containment due to the presence of other random ignition sources.

The critics of this method /53/, and the separate opinion of Prof. Oppenheim /1/ argue however, that, while the main safety goal is to avoid the burning and its effects, the ignitors will actually promote the combustion. The degree of control over the type of combustion is also questioned due to the large uncertainties in

predicting the patterns of the distribution of hydrogen and, consequently, to the criteria for positioning the ignitors such that the large variety of accident scenarios is appropriately covered.

Other problems are related to ensuring the survivability of the ignitors in adverse accident conditions and their effectiveness in a steam inerted atmosphere. Moreover, the difference between the explosion limits and the flammability limits makes possible the initiation of a fast reaction in the gas surrounding the ignitor before the flammability limits are reached. The atmosphere in the near vicinity of the ignitor remains depleted in hydrogen and, in the absence of a fast local mixing mechanism, the ignitor might fail in generating a flame, while hydrogen continues to accumulate in the compartment producing a rich flammable mixture. An appropriate placement and level of redundancy is therefore required. In practice the solution adopted is the result of engineering judgements taking into account the type and particularities of the containment, the accident scenarios considered, the safety regulation requirements, etc.

A particular case of mitigation by controlled combustion is the combustion in cooling ducts. This method involves the installation of a combustor in the path of circulation of the air in containment (e.g. in vault-cooler ducts) where the steam condenses and the mixture becomes flammable, /43/, /59/. The effectiveness of this method is ensured by the continuous circulation of the gas through the combustor. It has the advantages of removing the hydrogen from lean mixtures with high steam content and of confining the combustion into a well defined zone. Since the exhaust gases can be condensed, the system can operate for a long time without causing an increase in containment pressure.

When deliberate combustion is employed as mitigation measure, a good mixing of the atmosphere is a pre-requisite for avoiding dangerous effects arising from burning of rich mixtures. For some designs (e.g. the large dry CANDU-6 containment), the combustion of hydrogen can even be avoided if an efficient mixing is ensured: due to the large volume of the containment and for the expected quantity of hydrogen released during the considered accident sequences, the maximum concentration of hydrogen attainable in a homogeneous atmosphere cannot reach the flammability limits.

Venting can be another effective means for reducing the combustion pressure in a compartment, if the blowdown volume does not contain hydrogen. It is the case e.g. of multi-unit CANDU stations for which the vacuum building is the volume for relief of the overpressures from the individual reactor containments.

If the downstream compartment, however, contains a flammable mixture, the vented jet creates an intense turbulence and the hot burnt vented gas will ignite the mixture in the second compartment. Due to the strong turbulence the combustion becomes more violent accompanied by a higher pressure. If several series volumes are present, this effect is further amplified and can lead to the damaging of the containment structures even for relatively modest concentrations of hydrogen. Therefore, considering venting as a mitigation measure is strongly dependent on the type of containment, on the expected distribution of hydrogen and on the sequence in which the combustion in various compartments takes place.

Continuous removal of the hydrogen using devices to promote the chemical recombination with the oxygen in a non-combustible manner is possible if catalytic recombiners are used. The recombiners present a large active surface coated with various materials, where the hydrogen-oxygen reaction takes place. They are passive systems without requirements for remote control and actuation. They have the advantage of being effective even for low concentrations of hydrogen (as low as 1 vol %) under steam inerted conditions (up to 90 vol % steam). They cope best with slow transients and can accommodate the long term radiolytic generation of hydrogen and oxygen.

Since only the H_2 and O_2 in the flow of air passing through are recombined, the placement in containment is very important; in exchange, the reaction heat enhances the natural circulation leading to a better mixing of the atmosphere. The rate of reaction is however low and therefore, given the quantity of hydrogen expected to be released, large active surface areas should be provided. Even in this case, the catalytic recombiners cannot accommodate large fast release rates of hydrogen as resulting from MCCI at severe accidents. In mixtures inside the flammability limits they become ignition sources and therefore their efficiency is limited in this domain.

It is therefore recommended, /54/, to couple the recombination with the deliberate ignition - dual approach. In this case, the earlier released hydrogen is recombined and, since accidential ignition with unpredictable effects cannot be ruled out, a system of ignitors will start the combustion at the flammability limits. Engineering judgements based on data from design and from deterministic accident analysis will be employed for determining the surface of recombiners and for defining criteria for establishing the level of redundancy and the placement of the ignitors.

The above considerations show that several mitigation techniques at different stages of maturity are available. The particular characteristics of these methods in the context of the relatively large number of reactor and containment designs and accidents scenarios, and of the uncertainties in predicting the source term of hydrogen, the distribution patterns and the local distribution of thermodynamic parameters and composition of the post-accident containment atmosphere, render no unique solution for dealing with the hydrogen problems. In a broader frame, the rationales for choice between different mitigation techniques are dictated by regulatory requirements, standard practices and, last but not least, by sound engineering judgements.

As a general rule, the policy for hydrogen management, including the defining of the objectives and of the safety requirements, the setting of the control instrumentation and mitigation measures and the implementation of the decision process concerning the use of these systems under accident conditions, /43/, is well defined for the accidents bounded by the design basis accidents (DBA).

For dealing with severe accidents, however, the approaches considered are significantly different. They range from disregarding this category of accidents under the principle of ensuring the safety at a level according to the design requirements (provided that the regulation authorities do not formulate licensing requirements for severe accidents), to the employing of back-up measures (e.g. use of deliberate ignition or post-inerting as supplements to the recombiners designed to cope for DBA) for diminishing the risk. In most cases, however, the mitigation systems as designed for DBA are provided to be available during severe accidents as well, /43/.

The necessity to improve and demonstrate the safety level has in the latest years led to new approaches. Since the ultimate judges of the safety are in an increasing measure the public and other factors without professional competence, a trend to replace the sophisticated concepts and complex safety features with simpler and more transparent ones has appeared, /57/. In this way it is claimed a more direct understanding of the safety, instead of making appeal to a closed group of experts who might or might not be trusted. A consequence is that the new advanced reactors promote simpler principles, in which well-known and easy acceptable phenomena (as for example the natural circulation and the gravity) are increasingly at the base of the design for safety.

In this context an improved containment, designed to withstand the worst case core melt accidents has been proposed. It will also cope with the maximum loads associated with a hydrogen burn, including the detonation, /55/, /56/.

Various methods for mitigation of hydrogen, which cannot be implemented in the existing plants are considered in the new designs. Limiting the hydrogen generation rates is sought by using new alloy compositions in the core. New techniques for removing the hydrogen released by diffusion, absorption and other chemical means are under study, while the elimination of the random ignition sources by using electrostatic charge neutralizers and intrinsically safe electrical equipment is envisaged for decreasing the risk of an uncontrolled burn. Other measures are also including the use of new filtering and venting schemes.

4 Multipoint Ignition Experiments

4.1 Scope of the Study

Mitigation by deliberate ignition involves the use of ignitors to initiate the burning near the flammability limits, where the combustion pressure is low. In order to ensure the effectiveness of the ignition system in the adverse accident conditions, an adequate redundancy level is required. On the other hand, due to uncertainties in ensuring a uniform distribution of hydrogen and the necessity to avoid the formation of regions with rich mixtures where accelerated flames or detonations could occur, several ignitors must be placed in a volume.

However, an increase of the number of ignition points will raise the likelihood that ignition will simultaneously occur in more than one point inside a volume, such that several flame fronts will coexist. Since the burning rate is proportional with the flame surface area, it will increase with increasing the number of flame fronts. Therefore, at multiple ignition, the duration of burning is expected to decrease and thus, the time available for cooling the flame and for dissipation of energy. Therefore, the concern of facing larger combustion peak pressures, closer to the AICC values is raised.

A formal literature search resulted in an unsignificant volume of data on the issue of multiple ignition/simultaneous flames, /60/, and no large-scale data at all. Therefore, a general experimental study was considered necessary for the identification and the evaluation of the specific processes and effects involved. Beyond the simplified picture presented above, other questions had to be clarified through experiments. First, the qualitative and quantitative differences between the combustion pressures resulting from multipoint ignition and those from single points ignition had to be evaluated. The dependence of the combustion pressure upon the number and location of the ignition points and the effect of the geometry of the enclosure had also to be determined. Finally, the influence of the sensitivity of the mixture (concentration of hydrogen) on the multiple ignition effects had to be investigated.

In this frame, several experiments for combustion with simultaneous multipoint ignition of dry H_2-air mixtures for various numbers and placements of the ignition points, in cylindrical and spherical vessels, with and without venting, have been performed. The work has been carried out at the Containment Test Facility (CTF) at Atomic Energy of Canada Limited Research, Whiteshell Laboratories, /32/, /61/, /62/, /81/, /82/.

4.2 Description of the Experimental Facilities, Instrumentation and Data Acquisition

The experimental set-up consisted of two instrumented vessels, one cylindrical and one spherical, named in the followings CTF-Pipe and respectively CTF-Sphere.

The CTF-Pipe is a horizontal cylinder 6.6 meters in length and 0.29 meters in diameter, designed to withstand pressures up to 10 MPa. The ignition system consisted of non-resistive CHAMPION spark plugs powered from a PRATT & WITNEY driver box. The plugs were placed along the pipe at locations denoted *I1, I2, I3, I4* (*Fig. 13*) with the sparks closed to the centerline of the vessel. The pressure was measured with three piezoelectric transducers PCB 119, (PCB1, PCB4, and PCB5) and a kulite-type transducer HEM-375/500a (K), placed at the wall surface level, Fig. 13. A kulite transducer mainly consists of a resistive bridge situated under a thin metallic sheet on which the external pressure is applied. Under operation, the bridge becomes unbalanced such that the output voltage

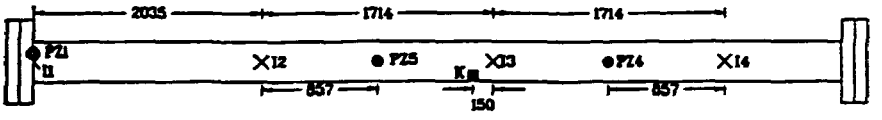

Figure 13. Geometrical dimensions and placement of the ignitors and of the pressure transducers in CTF-Pipe.

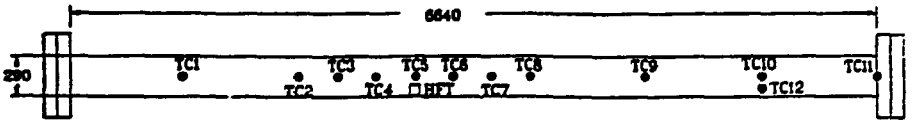

Figure 14. Placement of the thermocouples and of the heat flux transducer in CTF-Pipe.

is proportional with the pressure applied. The analog electric signals from the pressure transducers were amplified and temporarily stored on two, two-channels NICOLET oscilloscopes. The oscilloscopes have a memory of 4000 points per channel which determined the limit in the frequency of data acquisition.

In the series of experiments in CTF-Pipe where temperature and heat flux measurements were required, the instrumentation included twelve Platinum-Rhodium bare, fine-wire thermocouples and a MEDTHERM heat flux transducer. Due to the limited number of penetrations available, the thermocouples were placed on a support inside the pipe and the heat flux transducer was mounted in the place of PZ5 (Fig. 14). For the acquisition of data from the pressure transducers and from the heat flux gauge, the two NICOLET oscilloscopes were used, while for processing and permanent storage, the ASYSTANT-GPIB software package has been employed. The signals from the thermocouples, after amplification with ECTRON

amplifiers, were recorded using the High-Speed-Recorder option in the ASYSTANT-PLUS package, via a seven channels input-output board. The maximum number of channels available on the board (7) and the frequency and number of points per channel available with the High Speed Recorder (1000 Hz and respectively 2600 points/channel) provided the limits of accuracy of measuring the arrival time of the flame.

For the combustion tests in spherical geometry, the CTF-Sphere, a 6.6 m^3 vessel was used. The ignition system was based on a high voltage source which powered one or four spark ignitors. The configurations of the ignition points are shown in Fig. 15. The single ignitor was located in a central position in the sphere (referred to as 1C), while the four ignitors were placed in a horizontal plane through the center of the vessel. Two configurations were used - one for which the ignitors were placed in a relatively central position (referred to as 4C) and one for which the ignitors were near the walls (4W). CTF-Sphere was instrumented for pressure measurements with two HEM-375/250g kulite transducers (K1, K2) and three PCB-112A/300g piezoelectric transducers (PCB1, PCB2, PCB3), Fig. 15. The two kulites, K1 and K2 and the piezoelectric transducer PCB2 were located in a particular position at the closed end of a cylindrical penetration in the vessel, 14.6 cm diameter and 33 cm height. The output from the transducers was first amplified and then entered a digital data acquisition system with discrete channels for digitalization and intermediate storage. For processing and permanent storage, the software package ASYST-3.1 was used. The data acquisition system provided a maximum number of 8000 data points per channel.

For venting, a 3 m long, 45 cm diameter pipe was attached to CTF-Sphere, connecting the vessel with the outside atmosphere (Fig. 16). The vent, initially closed, opened at a differential pressure of about 10 kPa. The moment of the opening was recorded with an electrical contact. The ignition system, the instrumentation and the data acquisition system for the vented combustion experiments were identical to those used for constant volume combustion in CTF-sphere.

For all the experiments, the surfaces of the piezoelectric transducers were protected against the high temperature of the flames with a 0.5 mm layer of silicone compound RTV-108.

4.3 Experimental Procedures

For the constant volume experiments, the desired mixture was prepared with the partial pressures method. The experimental vessel was initially evacuated with the local vacuum pump and the desired partial pressure of air and then hydrogen are admitted into the vessel via remote controlled valves. An exception was made for the case of rich mixtures with 60-65% hydrogen, where the hydrogen was first added in order to avoid the formation of intermediate detonable mixtures. The gases were then mixed using one circulation pump (in CTF-Pipe) and two internal fans (in CTF-Sphere), after which the mixture was ignited.

The combustion took place in an initially quiescent atmosphere (the recirculation pump/fans were turned off before ignition), in the absence of other perturbing factors as fans, sprays, obstacles, etc. In CTF-Pipe a potential source of experimental errors arose from the real geometry of the vessel which could have a negative influence on the homogeneity of the mixture. First, it was difficult to ensure a uniform mixing in the terminal regions of the different pipes connected to the main vessel (lines for feed of hydrogen, air, steam, etc.) where, delayed burns could occur. A second concern came from the relatively small distance (about 4 m) between the connections with CTF-Pipe of the inlet and outlet lines

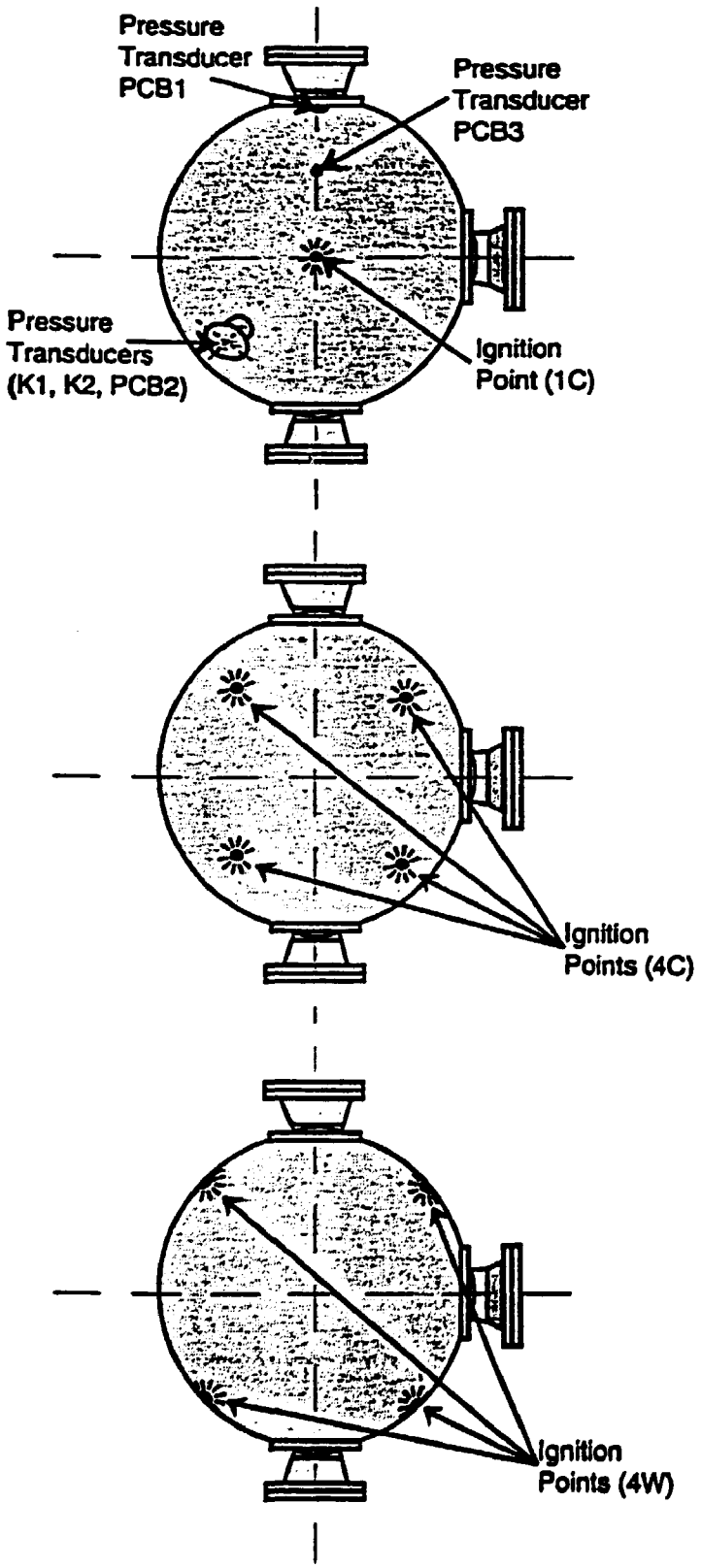

Figure 15. Scheme of the configuration of the ignition points in the CTF-Sphere (top view).

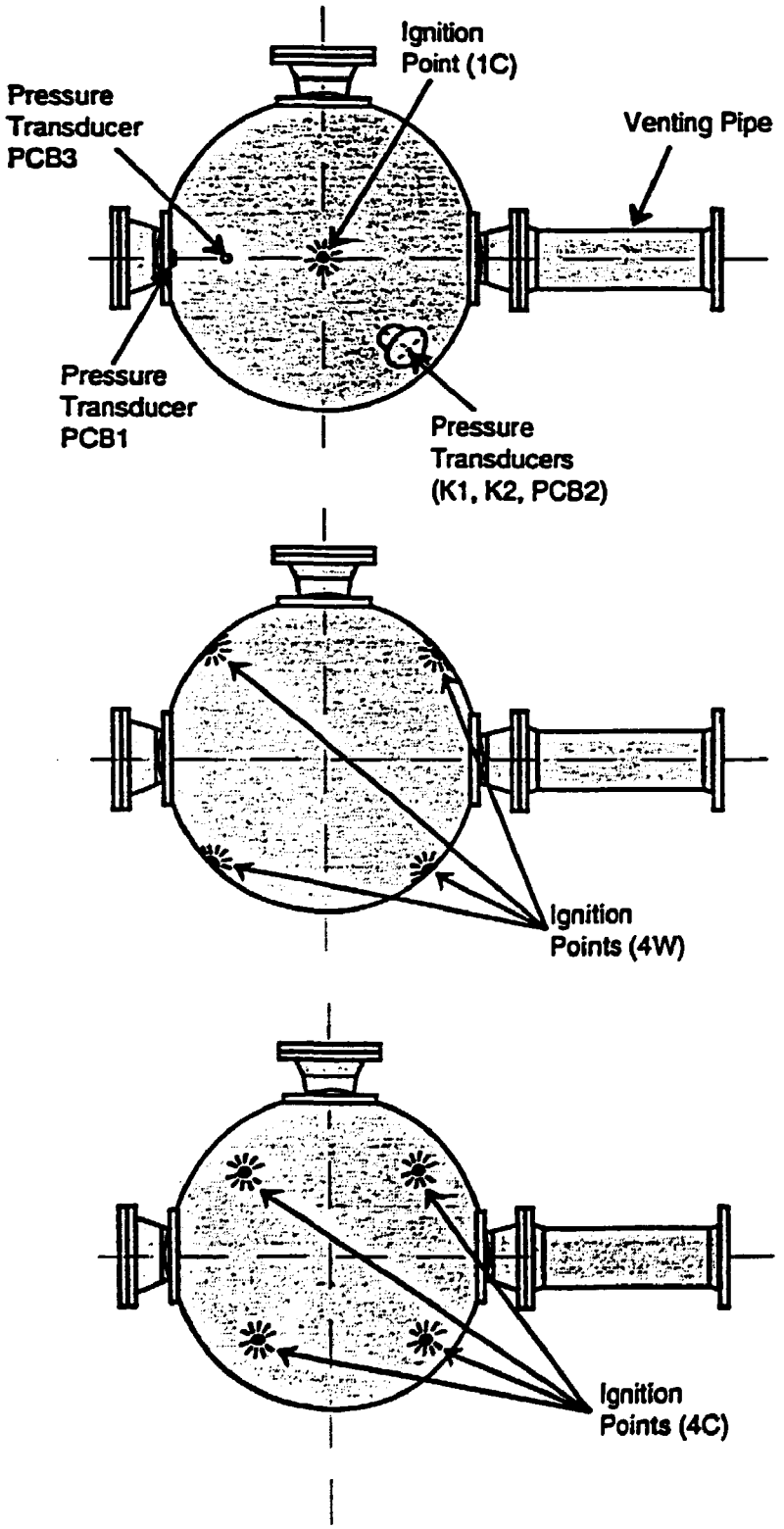

Figure 16. Schematic drawing of the 6.6 m³ CTF-Sphere for vented combustion.

of the recirculation pump, such that dead ends outside the path of the gas flow were created.

For the vented combustion experiments, the test mixtures were obtained by continuous addition of hydrogen and purge of the mixture, with the vent closed, at a pressure slightly below the ambient pressure. Simultaneously, the concentration of hydrogen was measured with a NOVA-340 H_2 analyzer. For ensuring a good homogeneity, the mixing fans were continuously "on" during the preparation of the mixture, and they were turned off just before ignition. All the experiments have started with the mixture being at atmospheric pressure and room temperature.

4.4 Constant Volume Combustion Experiments. Results and Comments

Several experiments have been performed for various mixtures and number and position of the ignition points. In CTF-Pipe we have used mixtures of 10%, 12%, 15%, 20%, and 65% H_2-air and the following combinations of ignitors (Fig. 13): I1, I3, I2+I3, I2+I3+I4, I1+I2+I3+I4, I2+I4, I1+I4. In CTF-Sphere, the ignitor configurations 1C, 4C, and 4W were used (Fig. 15), for 10%, 12%, 16%, 20%, and 60% H_2-air mixtures.

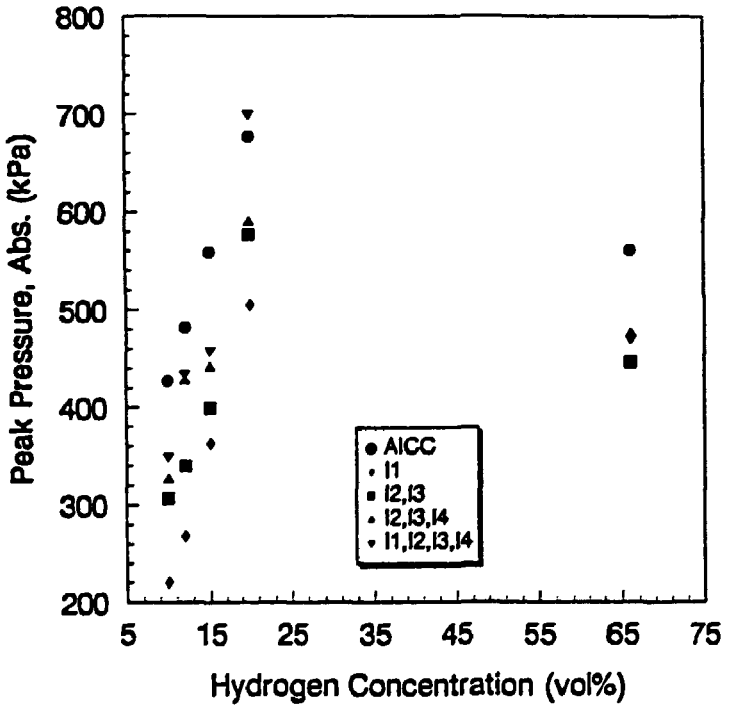

Figure 17. Combustion peak pressures in CTF-Pipe.

4.4.1 Pressure Histories

The maximum combustion pressures in CTF-Pipe for various ignition points and hydrogen concentrations are given in Fig. 17 where the calculated adiabatic isochoric complete combustion pressure (P_{AICC}) is also represented. For one speci-

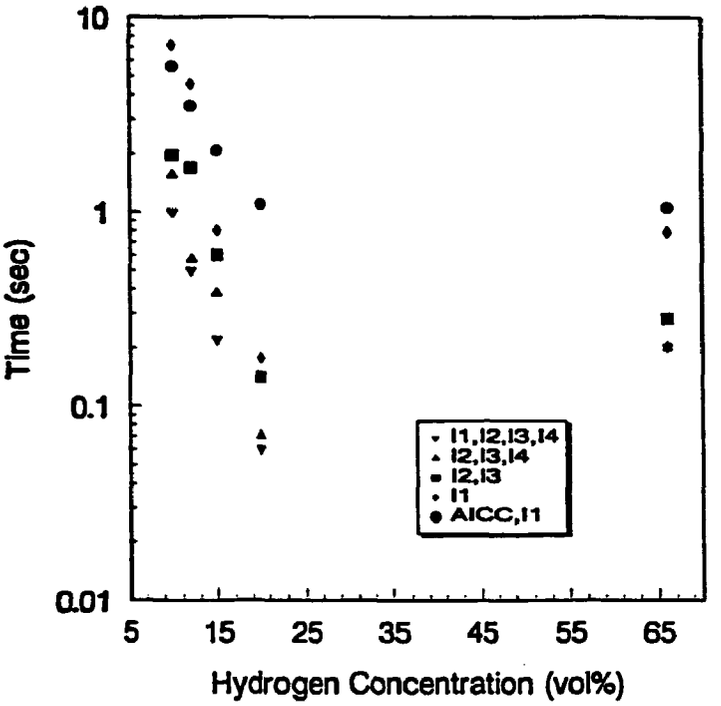

Figure 18. Time to maximum pressure in CTF-Pipe.

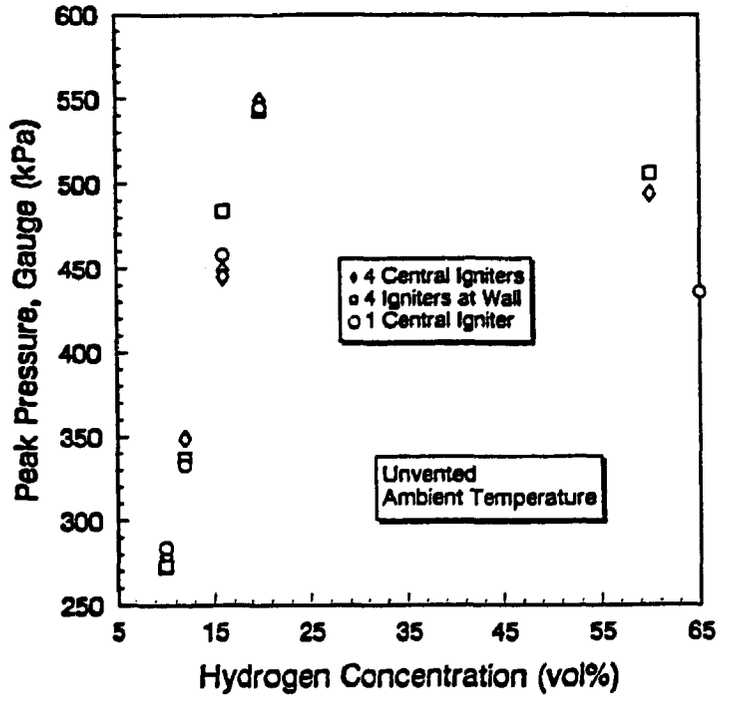

Figure 19. Measured peak pressures in CTF-Sphere.

fic mixture, the measured maximum pressure increases with increasing the number of ignitors. This correlates with the time to maximum pressure (Fig. 18) which decreases with the number of ignition points, qualitatively corresponding to the decrease of the distance the flames must travel until the completion of burning. For a lower burning time, the energy lost during combustion is smaller and thus the increase of the pressure in the vessel is justified.

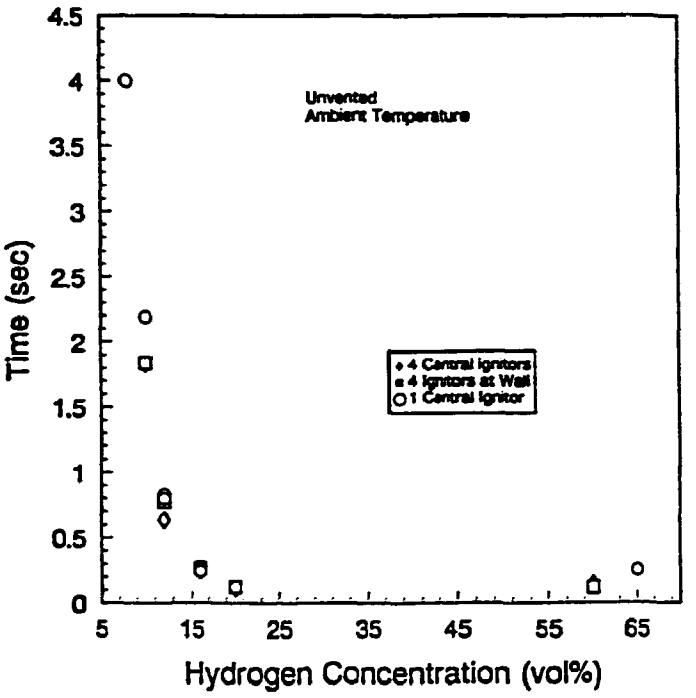

Figure 20. Time to maximum pressure in CTF-Sphere.

Significant differences appear, however, in the general shape of the evolution of the pressure during combustion. Typical shapes are presented in Fig. 21, for 10% H_2-air, case 1C and case 4C. The shape of variation for these two cases are interpreted as it follows. When several ignitors are used, the flames develop simultaneously in a spherical shape until they coalesce. For the configuration of ignitors used in experiments, the gas first burns in a central zone with a height smaller than the sphere radius, leaving two regions of unburnt gas in the upper and lower parts of the vessel. In the first phase, the rate of increase of pressure is high because several flames coexist, with a total surface area much larger than for a single flame. After the flames coalesce, the gas in the two regions in the top and bottom of the sphere will burn. The much lower surface area will, in this case, produce a burning rate, and thus a rate of pressure rise, lower than in the first period (curve 4C, Fig. 21).

With single points central ignition (curve 1C, Fig. 21), the flame develops continuously with a corresponding continuous increase of the surface area. Therefore, the rate of pressure rise will be maximum just before the end of combustion where the flame surface area has a maximum value.

Though the real situation is slightly different (the flames are not perfectly spherical and, for lean mixtures, differences between the upward and downward propagation patterns might occur), the above simplified picture seems to provide an appropriate explanation to the observed data.

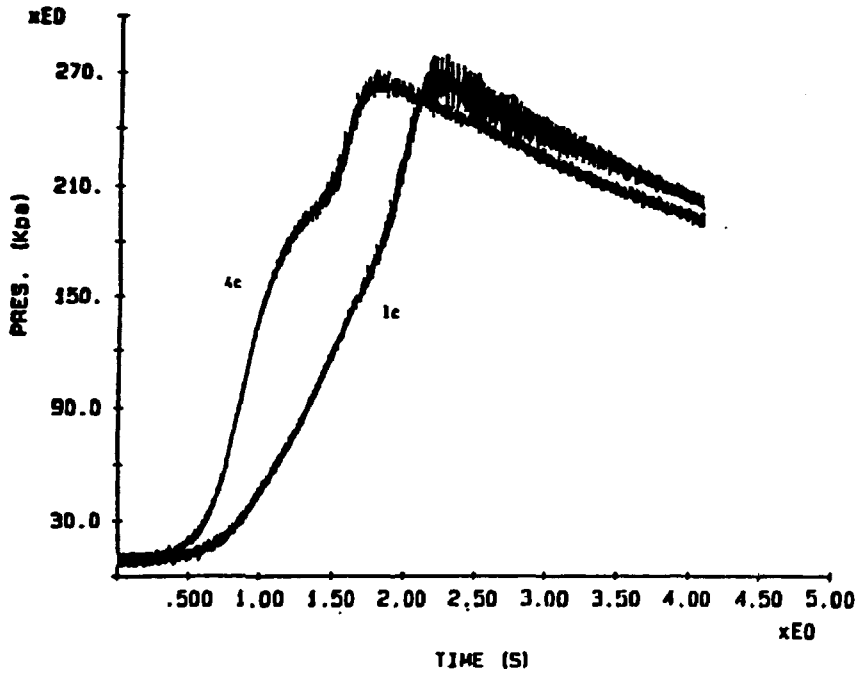

Figure 21. Pressure histories for 10% H_2-air in CTF-Sphere, case 1C and case 4C.

4.4.2 Oscillatory Regimes

As observed in Fig. 17, the maximum combustion pressure with multiple ignition can have high values, sometimes higher than the corresponding P_{AICC}. These large peak pressures appear as a consequence of establishing enhanced oscillations of the pressure during and after the combustion is completed. Two typical shapes for the evolution of the pressure, as measured with PZ1, are given in Fig. 22 (20% H_2-air, ignitors I2, I3, and I4 in CTF-Pipe) and in Fig. 23 (20% H_2-air, ignitors I1, I2, I3, and I4, in CTF-Pipe).

The Fourier analysis of the experimental data showed that the frequency of the oscillations are between 48 and 58 Hz. The broadness of this interval is due to the different frequencies for the different mixtures, during and after combustion. In Fig. 24 the maximum amplitude of the oscillations are represented. The dependence of the amplitude with the number and location of the ignition points suggests that the pressure waves originate in the flames. They are longitudinal waves having a pressure antinode (the amplitude is maximum) and a velocity node (the amplitude is zero) at the closed end of the vessel. Our results confirm the observations of other researchers, /63/, /64/, /65/, who also observed acoustic effects at combustion.

From the temperature measurements we have also been able to record the evolution of the temperature in the burnt gas. Remarkable results have been obtained with the thermocouples TC1 and TC3 (Fig. 14) whose output present an oscillatory pattern. In these locations, the oscillations of temperature are in phase with the oscillations of pressure, Fig. 25. We have also to mention that the shape of time variation of the output signals differs for various transducers; only TC1 and TC3 showed an oscillatory pattern, while all the other thermocouples had a smooth output. These facts suggest the existence of nonuniform fields of pressure and temperature inside the vessel, similar to the observations by Kordilewski and

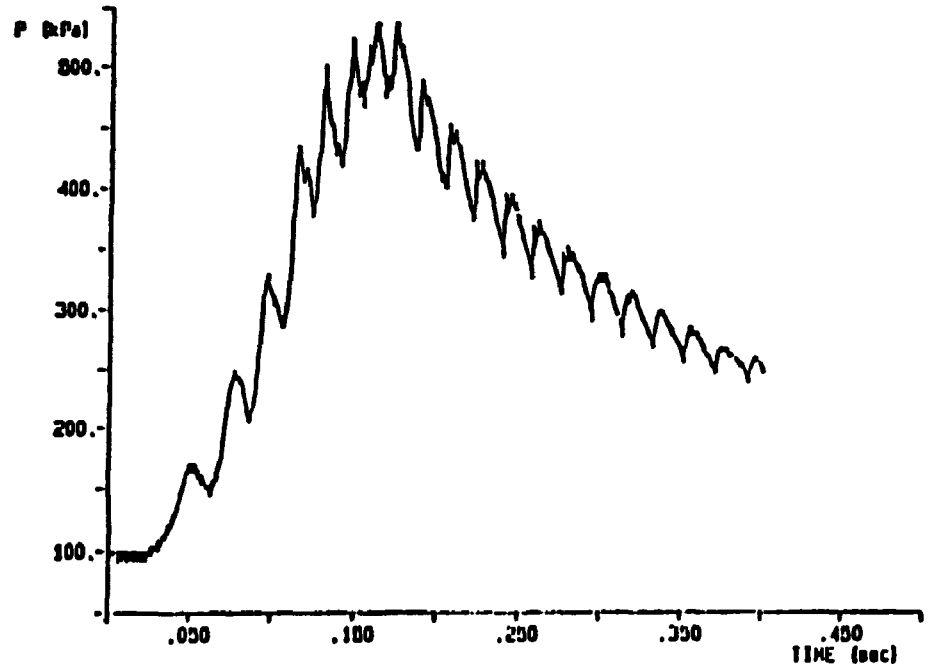

Figure 22. Pressure evolution for 20% H_2-air, ignitors I2, I3, and I4.

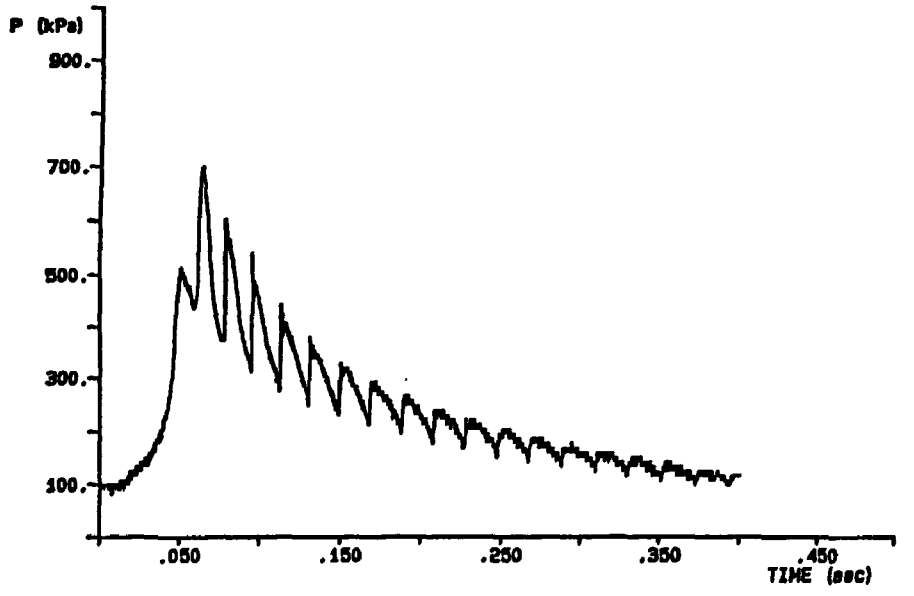

Figure 23. Pressure evolution for 20% H_2-air, ignitors I1, I2, and I4.

Wach, /63/. For further tests, a more careful placement of the transducers and a more sensitive instrumentation for pressure and temperature measurement are recommended.

Similar behaviour for the evolution of pressure has been observed in CTF-Sphere. Oscillations with a frequency of about 500 Hz were recorded in the particular location where K1, K2, and PCB2 were situated (Fig. 15). In Fig. 26, the

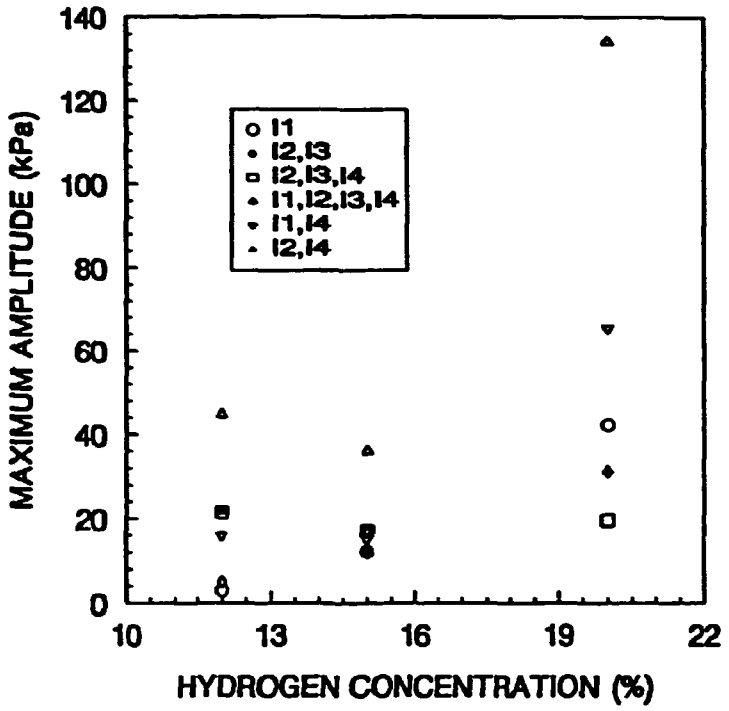

Figure 24. Maximum amplitudes of the combustion generated pressure oscillations.

recorded pressure evolution for 16% H_2-air, ignitors 4W, is given, with details for two periods, during and at the end of combustion. The continuous increase of the frequency and of the amplitude of the oscillations during burning can easily be noticed.

Again, the coupling between the combustion and the acoustic characteristics of the geometry of the vessel has to be emphasized. It generates local effects in terms of oscillatory regimes of pressure and temperature by formation of standing waves and resonance phenomena, which are enhanced when several flames are simultaneously present. According to /66/, spatial discontinuities in gas composition, flame velocity, turbulence characteristics, etc., induce step variations of the pressure in the reaction zone, which propagate into the volume. When such phenomena occur, a wave will propagate ahead of the flame in the unburnt gas. This wave is reflected by the walls and interacts with the flame by modifying the local burning conditions - feedback effect. The flame surface constitutes a discontinuity boundary for temperature and density between the unburnt gas and the combustion products, and here reflection and refraction processes occur. When several flames are simultaneously present, the propagation of the pressure waves is more complex. The complexity arises from the moving character of the waves sources (the flames) and from the highly inhomogeneous properties of the atmosphere inside the vessel, where regions of variable size containing burnt gas alternate with zones of unburnt gas. The pressure waves interfere with each other and, when appropriate conditions are met, standing waves and resonance phenomena are produced.

In a double ended cylinder, the wave lengths of standing waves are related to the geometrical length of the vessel with

$$L = k\frac{\lambda_k}{2} \quad , \quad k = 1,2,\ldots,n \tag{29}$$

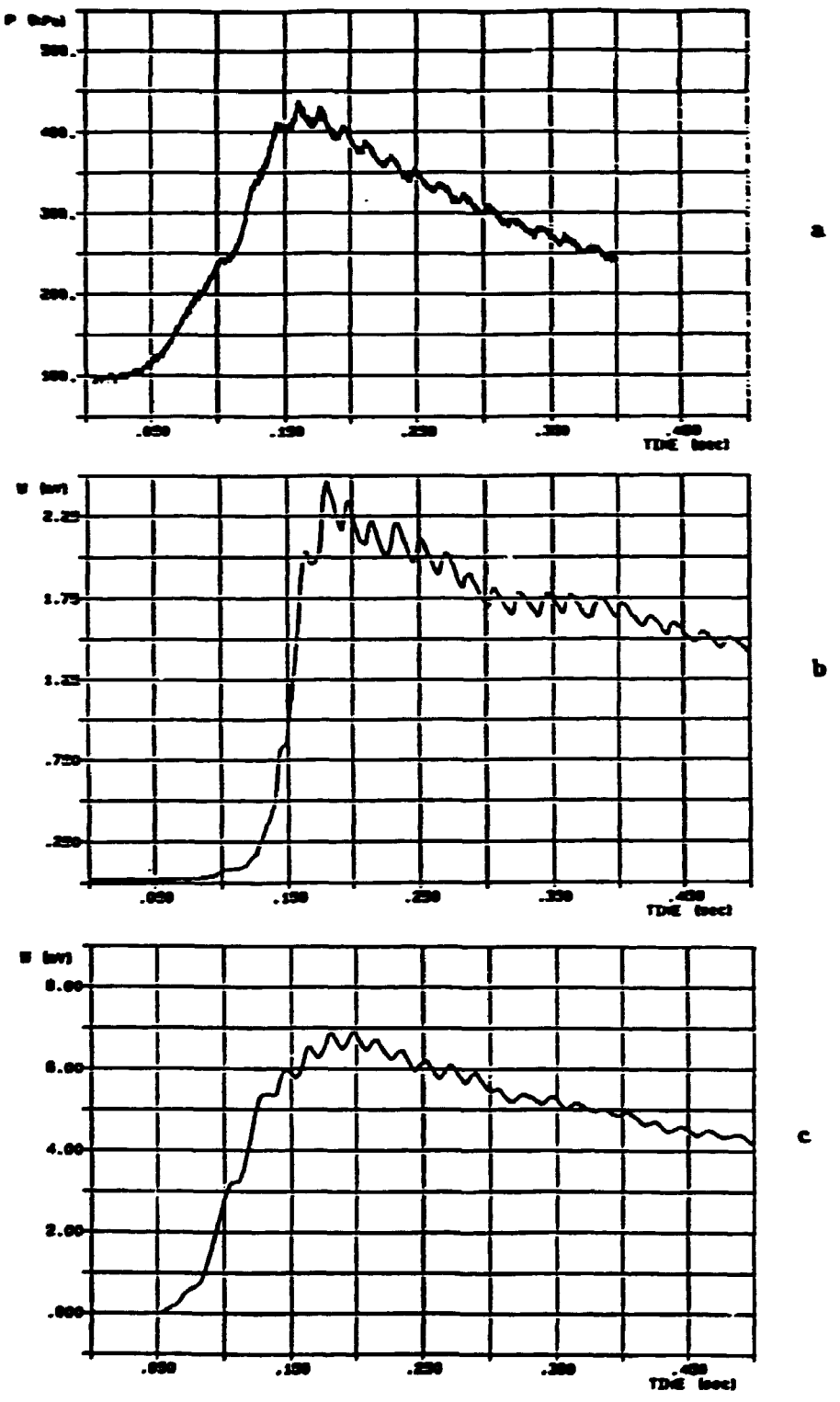

Figure 25. Pressure and temperature histories for 20% H_2-air, ignitors I2, I3, and I4, as measured with PZ1 (a), TC1 (b), and TC3 (c).

or

$$\lambda_k = \frac{2L}{k} \quad , \quad k = 1,2,\ldots,n \tag{30}$$

where:

L = length of the vessel
λ_k = length wave of harmonic of order k

For the fundamental mode, k = 1, we have

$$L = \frac{\lambda_1}{2} \quad or \quad \lambda_1 = 2L \tag{31}$$

The corresponding frequencies are

$$f_k = \frac{c}{\lambda_k} \quad , \quad k = 1,2,\ldots,n \tag{32}$$

or

$$f_k = k\frac{c}{2L} \quad , \quad k = 1,2,\ldots,n \tag{33}$$

where

c = sound velocity
f_k = frequency of the harmonic of order k

For the fundamental mode, k = 1,

$$f_1 = \frac{c}{2L}$$

With the assumption that the volume is filled with burnt gas, for which c = 700 m/sec., we obtain for the geometry of CTF-Pipe f_1 = 52.7 Hz. This is a reasonable assumption since the density of the burnt gas is significantly lower than the density of the unburnt gas, which means that the burnt gas will occupy the largest part of the volume very soon after ignition. The frequency calculated in this way is in very good agreement with the experimental observations.

In the case of a one open ended cylinder (as the cavity where K1, K2, and PCB3 are placed in CTF-Sphere), the formulae for the wave lengths and for the frequencies of the standing waves are:

$$L = (2k-1)\frac{\lambda_k}{4} \quad , \quad k = 1,2,\ldots,n \tag{34}$$

or

$$\lambda_k = \frac{4L}{2k-1} \quad , \quad k = 1,2,\ldots,n \tag{35}$$

and

$$f_k = (2k-1)\frac{c}{4L} \quad , \quad k = 1,2,\ldots,n \tag{36}$$

With the same assumption as above, for the geometry of the CTF-Sphere, the frequency of the fundamental mode is f_1 = 530 Hz, again in good agreement with the experimental observations.

For containment applications, the large amplitude pressure oscillations can be

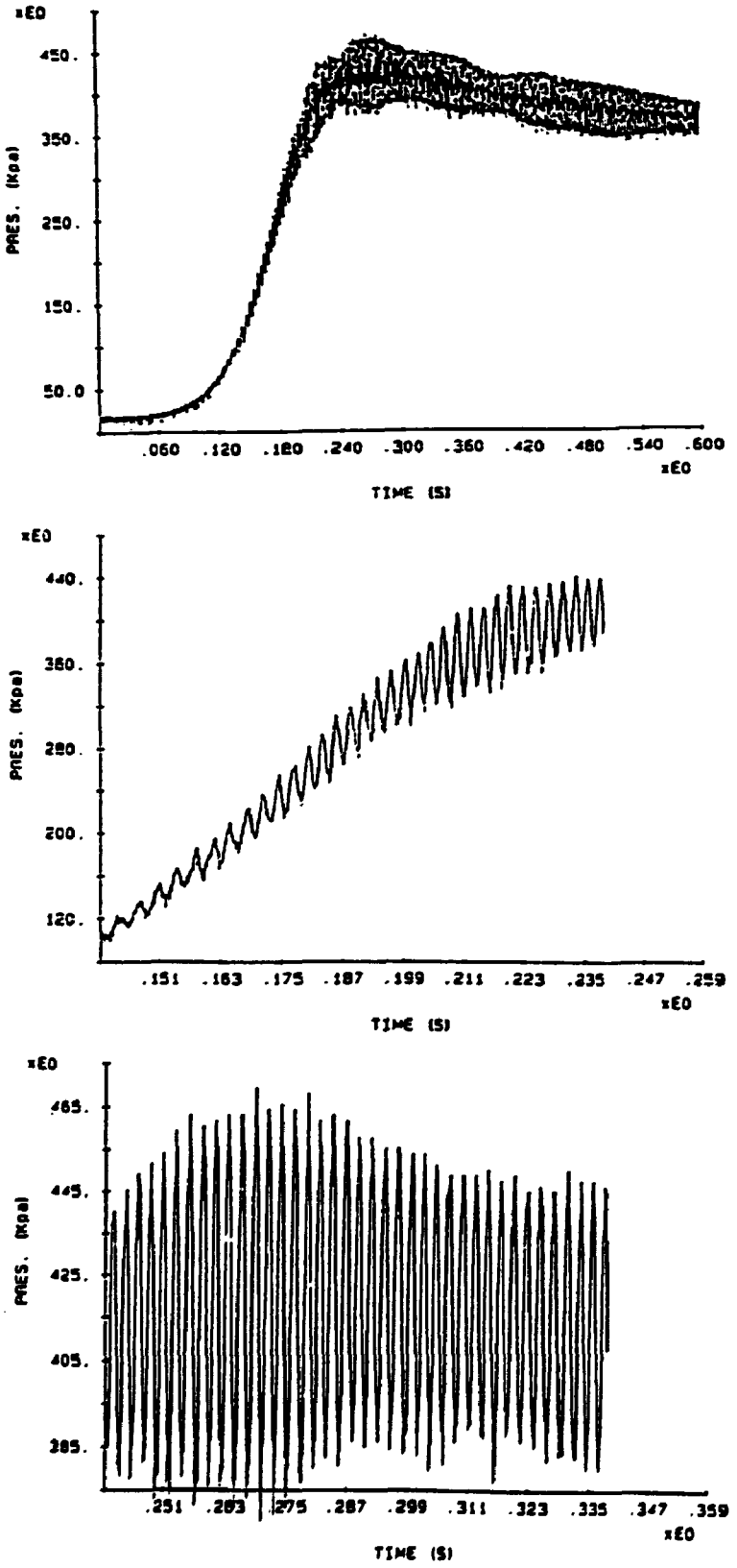

Figure 26. Pressure evolution in CTF-Sphere, as measured by K1, for 16% H_2-air, 4W.

avoided by preventing the formation of rich hydrogen mixtures and by avoiding the particular geometries where standing waves could establish.

4.4.3 Arrival Time and Flame Speeds

The thermocouples installed in the CTF-Pipe allowed determination of the arrival time of the flame at different points along the vessel. This is possible since at the arrival of the flame the output of a thermocouple shows a sudden sharp rise. For end ignition (ignitor I1) the flame arrival time is shown in Fig. 27 for various concentrations of hydrogen. In Fig. 28 the arrival times for the flames propagating in the space between ignitors I2 and I3 for a 20% H_2-air mixture and various ignition points, are shown. Fig. 29 presents the arrival time of the flames originating in I2 and I3 for various mixtures.

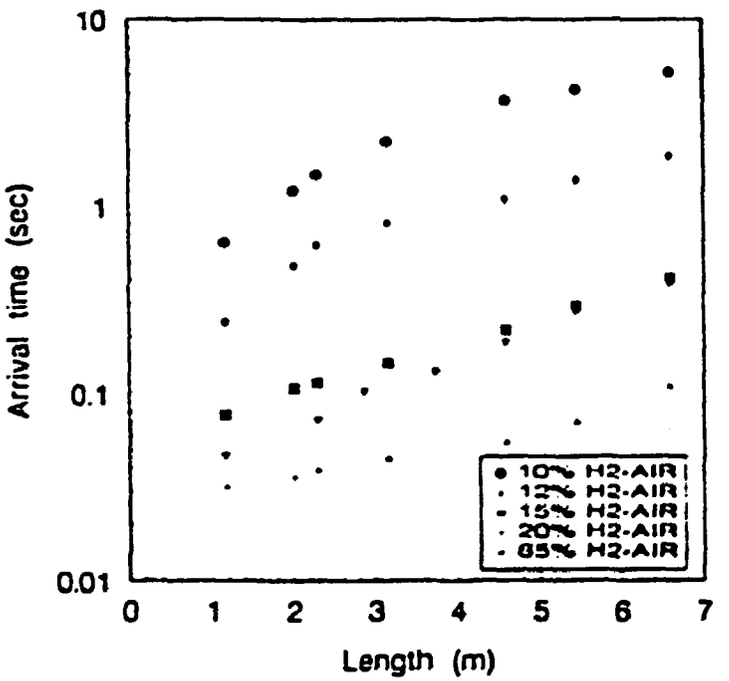

Figure 27. Flame arrival time for end ignition (I1).

The variation in time of the flame position (R_f) for end ignition various mixtures is presented in Fig. 30 and in Fig. 31. The dependence of R_f in time has an almost linear pattern for 10% and 12% H_2, representing flames which propagate with constant speed. For mixtures with higher hydrogen concentration, however, a rapid acceleration of the flame is initially present, followed by a slowing down at the end of combustion. The local values for the flame velocities derived from the experimental data at end ignition, are shown in Table 3.

With multipoint ignition, the flame position has an approximately linear variation in time, and no acceleration has been observed (Fig. 29). Thus, averaged values for the velocities of the flames could be determined. In Table 4, the velocity of the flame originating in I2 is given for various numbers and locations of the ignition points and for different mixtures.

Though the experiments carried out did not cover all the possible configurations for the ignition points, it can be concluded that, for multipoint ignition the flame speeds are lower than for the case of end ignition (Tab. 3). This is due to a lower

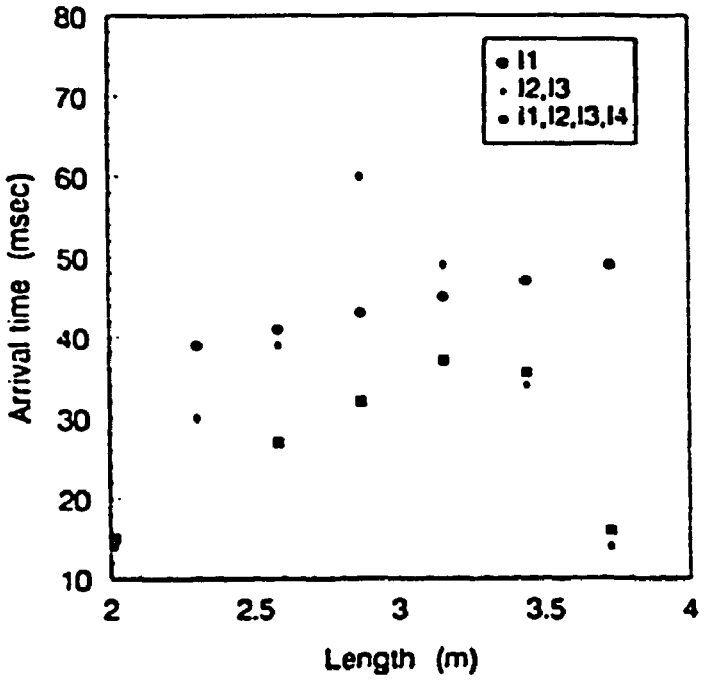

Figure 28. Propagation of the flames between I2 and I3 when different ignition points are used, for a mixture of 20% H_2-air.

distance available for the propagation of the flame which shortens the accelerating stage of the flames. It appears that this reduced propagation distance is more effective in reducing flame acceleration at higher concentrations of hydrogen. This influence is thus shown to be stronger than the expected supplementary acceleration due to the enhanced turbulence produced by the patterns of the induced flows by the several coexisting flames.

Table 3. Local values of the flame velocity V_f (m/sec) at end ignition for various mixtures

H_2-air	Axial flame position, R_f (m)							
(%)	0.4	1.157	2.015	2.30	3.157	4.586	5.443	6.6
10%	1.17	1.17	1.17	1.17	1.17	1.17	1.17	1.17
12%	3.54	3.54	3.54	3.54	3.54	3.54	3.54	3.54
15%	15.02	28.55	26.27	25.74	23.38	17.91	12.13	3.32
20%	36.15	196.3	175.6	160.8	133.6	94.84	51.94	25.5
65%	24.61	27.25	25.82	25.35	22.45	16.94	10.52	2.56

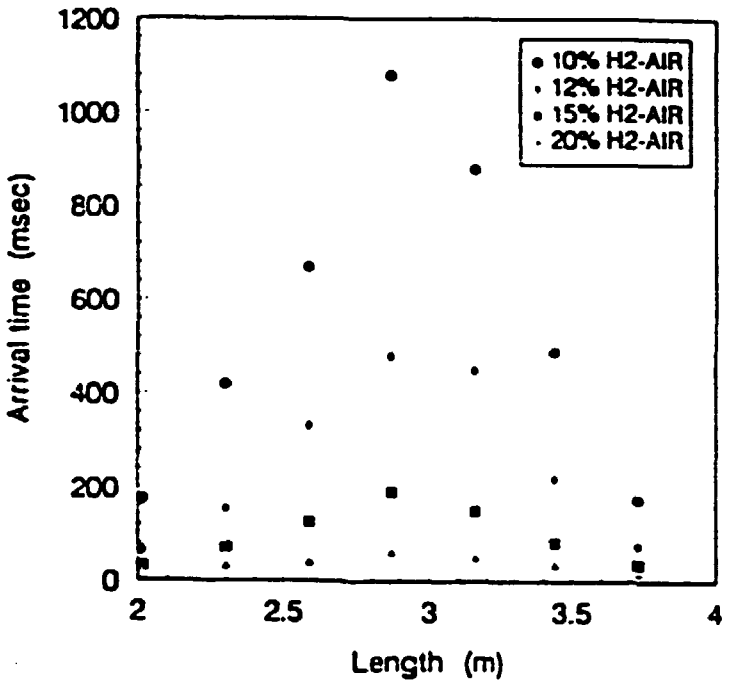

Figure 29. Arrival time the flames originating in I2 and I3 for various H_2-concentrations and ignition in I2 and I3.

Table 4. Average velocities (m/sec) for the flame originating in I2

Ignition points	Hydrogen concentrations				
	10%	12%	15%	20%	65%
I2 + I3	1.153	2.052	5.594	22.84	
I2 + I4				38.49	
I2 + I3 + I4				37.21	
I1 + I2 + I3 + I4	1.283	3.147	12.22	50.35	14.03

4.5 Vented Combustion Experiments

Tests were performed for 10%, 12%, 16%, and 20% dry hydrogen-air mixtures initially at atmospheric pressure and at room temperature.

The vent was initially covered with a steel sheet and opened when the combustion pressure in vessel was with about 10 kPa higher than the external pressure. Therefore, the elapsed time from ignition to the vent opening varies from one

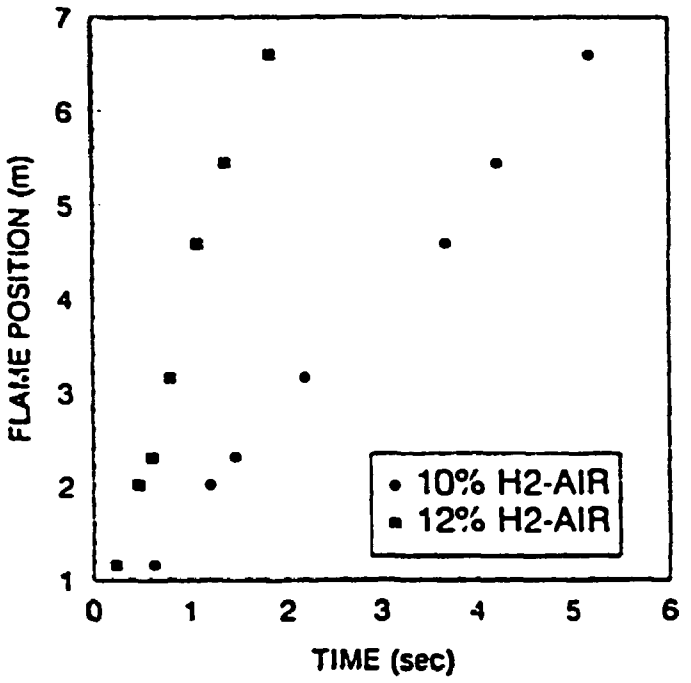

Figure 30. Evolution in time of the flame position for end ignition in 10% and 12% h_2-air mixtures.

experiment to another, Fig. 32, depending on the rate of pressure rise in the vessel.

The "initially covered vent" case slightly differs from the real situation in containment where vented combustion from one volume to another at reactor accidents, takes place with the doors or the blowout panels between compartments already open due to the pressure transients in the earlier phases of the accident. However, this was not expected to affect combustion behaviour in a significant way.

4.5.1 Pressure Development

For different mixtures and different ignition points, the maximum pressures measured for vented combustion are shown in Fig. 33. Comparing these values with the maximum pressures at constant volume combustion, Fig. 34, it can be seen that the vented combustion always produces lower pressures and therefore it can be regarded as an effective means for mitigation. Fig. 33 shows that, for all the mixtures the highest values for the pressure occurred in the case 1C, i.e. single point central ignition; the pressure is reduced if multiple ignition is used, cases 4C and 4W. The lower peak pressures with multiple ignition seem to be the consequence of the different shapes of evolution of the pressure for single point and for multipoint ignition respectively. As it is shown in Chap. 4.4.1, in a first stage of the transient (for constant volume combustion which corresponds to the period between ignition and vent opening), the rate of pressure rise is higher for multiple ignition than for the single ignition case. The higher burning rate continues also during venting, when burning is enhanced by the turbulence and the flow induced

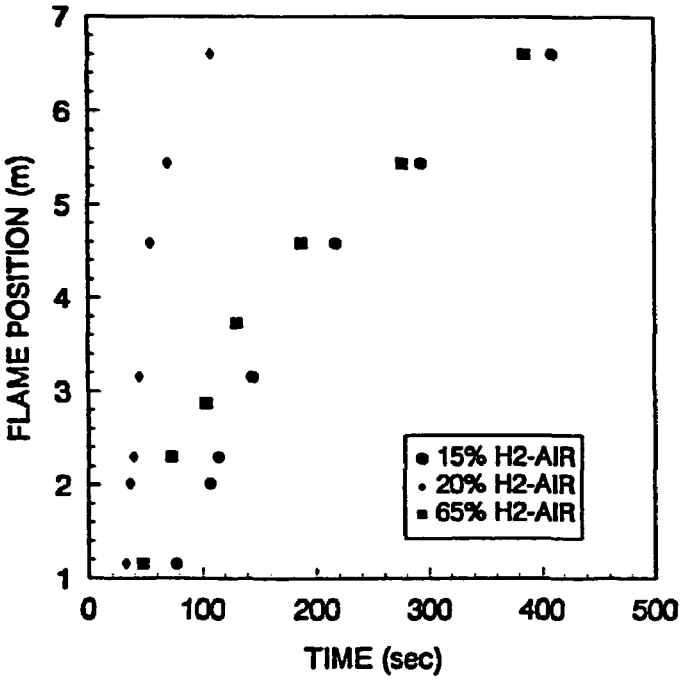

Figure 31. Evolution in time of the flame position for end ignition in 15%, 20%, and 65% H_2-air mixtures.

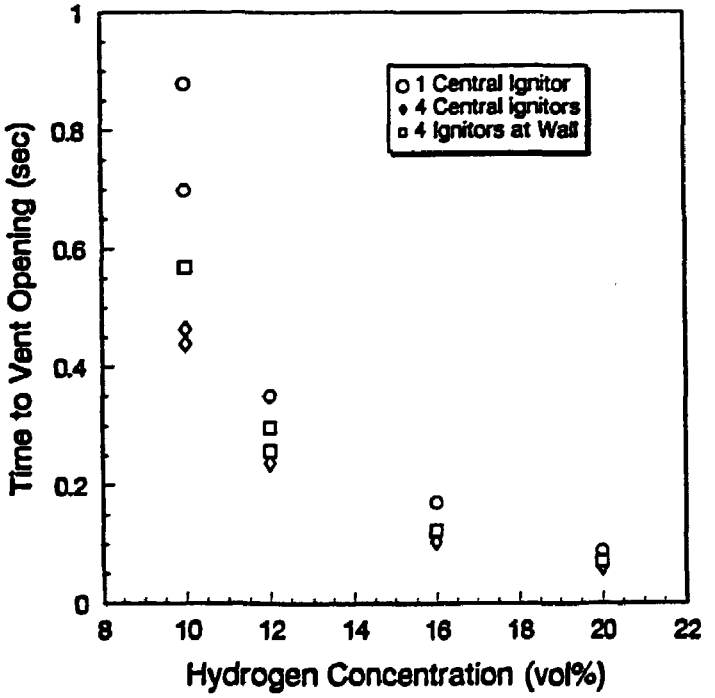

Figure 32. Time of vent opening as a function of H_2-concentration and number of ignitors.

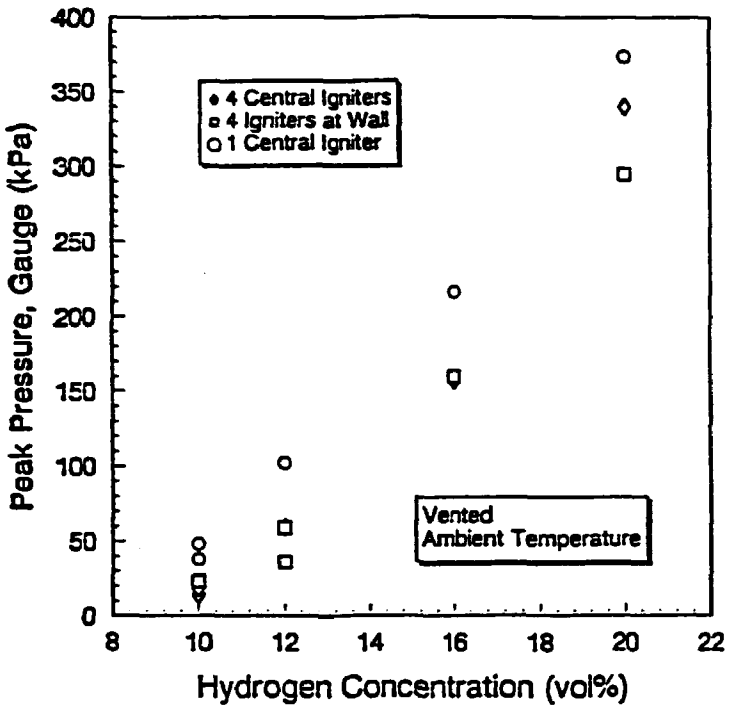

Figure 33. Maximum pressure for vented combustion for different concentrations of hydrogen and different number and location of the ignition points.

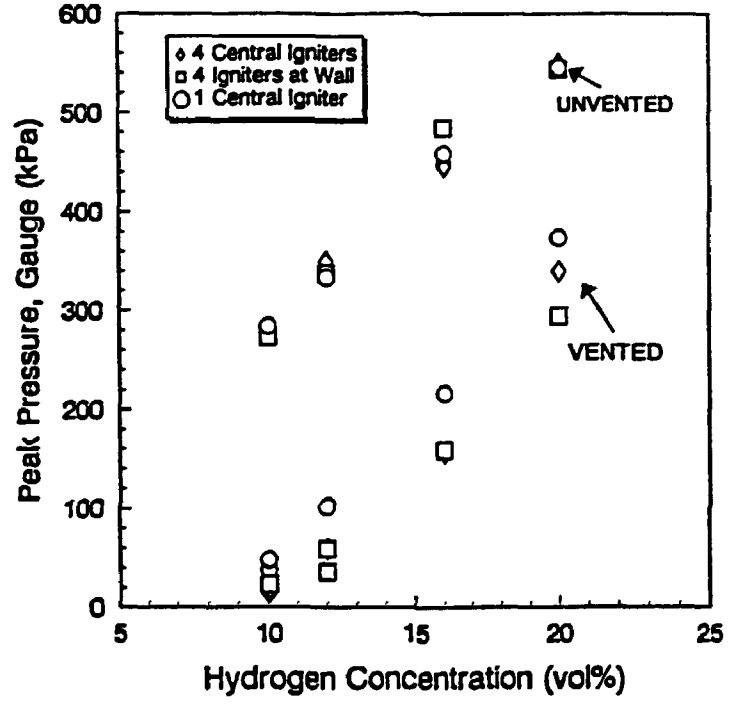

Figure 34. Maximum pressure in the CTF-Sphere during combustion, with and without venting.

by venting. As a result of the faster initial pressure rise, at multiple ignition the effectiveness of the vent is increased.

For a given geometry, it is possible to express empirical correlations for evaluating the maximum combustion pressure as a function of vent characteristics and mixture properties, /67/. Here, the vent effectiveness, ε, is defined as:

$$\varepsilon = \frac{P_a - P_v}{P_a - P_o} \tag{37}$$

where

P_a = adiabatic isochoric complete combustion pressure
P_v = maximum pressure with vented combustion
P_o = initial pressure.

It is useful to express ε as a function of the parameter $\bar{A}/S_o$, /67/, /68/, which contains information on the vessel geometry and gas composition,

$$\bar{A} = \frac{C_d A_v}{A_s} \tag{38}$$

with

C_d = discharge coefficient
A_v = venting area
A_s = area of the internal surface of the vessel

and

$$S_o = \frac{S_{uo}}{c_o}\left(\frac{\rho_{uo}}{\rho_b} - 1\right) \tag{39}$$

where

S_{uo} = laminar burning velocity
c_o = sound velocity
ρ_{uo} = density of the unburnt gas
ρ_b = density of the burnt gas

and the index "o" specifies the initial conditions.

Using the experimental results, a polynomial fit of the type

$$\varepsilon = a_0 + a_1\left(\ln\frac{\bar{A}}{S_o}\right) + a_2\left(\ln\frac{\bar{A}}{S_o}\right)^2 \tag{40}$$

was done. A good fit was obtained if the coefficients given in Tab. 5 are used.

The values calculated with (40) and the experimental data for the variation of the vent effectiveness (ε) with $\bar{A}/S_o$ are given in Tab. 6. In Tab. 6, the variation of the normalized pressure increase,

$$\frac{\Delta p}{\Delta p_a} = \frac{P_v - P_o}{P_a - P_o} = 1 - \varepsilon$$

is also represented.

The results obtained show that the vent effectiveness is higher for the multipoint ignition, when the maximum pressure is well below the value corresponding to the single point central ignition.

Table 5. Coefficients in the empirical correlation, $\varepsilon = f(\bar{A}/S_v)$

Coefficient in (40)	Number and position of the ignition points		
	1C	4C	4W
a_0	0.65	0.7675	0.7651
a_1	0.1655	0.1849	0.1511
a_2	-0.035	-0.0473	-0.0348

Table 6. Experimental and calculated values for the vent effectiveness, ε, and for the normalized pressure increase, $\Delta p/\Delta p_s$

		$\bar{A}/S_v$	ε_{exp}	ε_{calc}	$\Delta p/\Delta p_s$ exp	$\Delta p/\Delta p_s$ calc
10%	1C	13.67	0.84	0.84	0.15	0.15
	4C	13.67	0.93	0.92	0.07	0.07
	4W	13.67	0.92	0.91	0.08	0.08
12%	1C	1.71	0.72	0.72	0.27	0.27
	4C	1.71	0.83	0.85	0.16	0.14
	4W	1.71	0.83	0.83	0.16	0.16
15%	1C	0.57	0.55	0.54	0.44	0.45
	4C	0.57	0.67	0.65	0.32	0.34
	4W	0.57	0.67	0.66	0.32	0.33
20%	1C	0.25	0.35	0.35	0.64	0.64
	4C	0.25	0.40	0.42	0.59	0.57
	4W	0.25	0.48	0.48	0.51	0.51

4.5.2 Pressure Oscillations

During the experiments, the excitation of pressure fluctuation has been observed. A typical curve for the evolution of pressure for a 10% H_2-air mixture, case 4W, is given in Fig. 35. It presents an oscillatory pattern which persists during combustion and after the completion of combustion as well. Several qualitative explanations are reported, /63/, /67/, /68/, /69/, /70/ for justifying the presence of one,

two, three, or four pressure peaks during combustion. Though the explanations proposed are based on reasonable phenomenological assumptions regarding the dynamics of the flame in the vessel, their predictive capability is negligible.

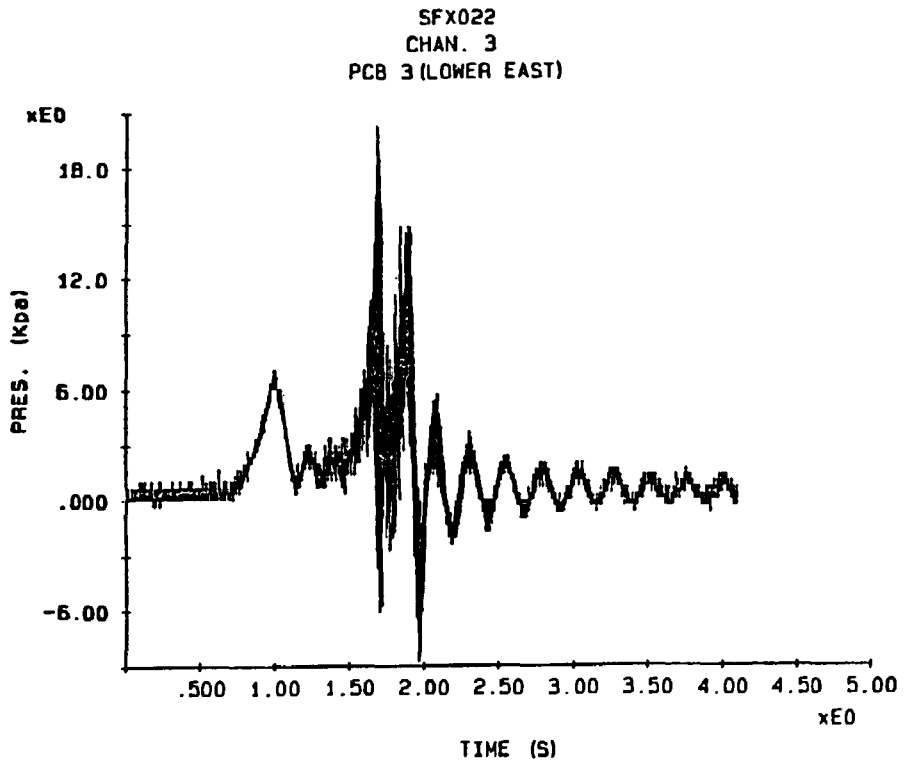

Figure 35. Combustion pressure for 4W - 10% H_2-air mixture, with venting.

We have observed in experiments that the number of pressure peaks during combustion changes dramatically with hydrogen concentration due to the change in the burning time, but it is not significantly influenced by the number and position of the ignition points. Also, in all the experiments, after the completion of burning, pressure oscillations with low frequency (about 5 Hz) have been observed. The frequency of these oscillations depends neither upon the concentration of hydrogen nor upon the number and location of the ignition points.

Considering the combustion vessel and the venting pipe as a Helmholtz resonator, /71/, the frequency of the pressure oscillations which occur due to the transient initiated by the opening of the vent, f_H, can be calculated with:

$$f_H = \frac{1}{2\pi} c \left(\frac{S}{l'V}\right)^{\frac{1}{2}} \tag{41}$$

where

c = sound velocity
S = vent area
V = volume of the enclosure
l' = equivalent length of the venting pipe connected to the vessel

$$l' = l + \frac{16R}{3\pi} \tag{42}$$

l = pipe length
R = radius of the venting area

For the geometry of CTF-Sphere, the result is a frequency, f_H = 5 Hz, in good accordance with the experimental observations.

Thus, at vent opening, the Taylor instabilities of the flame (created by the gas flow and by the turbulence induced by venting), overlap with the Helmholtz oscillations. The Helmholtz frequency, correlated with the moment of vent opening and with the duration of burning (via the sensitivity of the mixture), will determine the number of pressure peaks during combustion.

In the reactor containment, the frequency of the pressure oscillations at venting can be calculated from the known geometry and venting characteristics of the compartments. It is important to know this frequency in order to evaluate the likelihood of the occurrence of resonance phenomena at the characteristic frequency of various structures in containment.

Further, upon detailed analysis of the pressure shape, pressure oscillations of higher frequency (about 500 Hz) were observed. This frequency corresponds to that of the fundamental mode of the standing pressure waves established in the cylindrical cavity where the pressure transducers K1, K2, and PCB2 were placed. These observations offer a good confirmation on the existence of this type of local effect, as described in Chap. 4.2.2, for constant volume combustion, /32/, /62/.

5 Simulation Models

For evaluating the simulation capabilities of various existing computer programs, in different stages of the work for this project we have used two codes, VENT, /22/ and CONTAIN, /19/. As shortly described below these two codes have been subjected to several adaptations and developments as part of the present project /26/, /72/. These were addressed toward removing some simplifying assumptions, concomitant with broadening their applicability domain.

Due to very large, uneconomic computing time, the use of two or three dimensional models for simulating the combustion of hydrogen in a post-accident containment, has not been considered for this stage of the work.

5.1 Simulations with VENT

VENT is a unidimensional computer program licensed for analyzing pressure transients during the combustion of hydrogen in a post accident reactor containment, /22/. The code simulates constant volume or vented combustion for cylindrical geometry (with central ignition or with end ignition) and for spherical geometry (central ignition or ignition near the wall) in adiabatic conditions.

The mathematical model is based on the mass and energy balance equations solved for the burnt and for the unburnt gas volumes. For both gases, a homogeneous spatial distribution of the thermodynamic parameters (temperature, density) and for the concentrations of the components in the atmosphere is assumed. The burning is considered to be slow such that the pressure distribution in the volume is uniform in every moment.

The flame is assumed to be an infinitely thin smooth spherical surface centered in the ignition point. An important input parameter for the combustion model is the laminar burning velocity calculated with an empirical correlation as function

of the unburnt gas state (pressure, temperature) and composition. Based on the laminar burning velocity and on the flame surface area, the variation in time of the volume of burnt gas is calculated and thus, the burning is allowed to progress.

The version we have worked with, VENT-11, is economic, fast and user friendly. To remove some degree of conservatism efforts have been directed for re-analyzing and refining some of the modelling approximations.

5.1.1 Laminar Burning Velocity

For hydrogen-air-steam mixtures, the laminar burning velocity, S_u, is calculated in VENT-11 with the correlation of Liu - MacFarlane, /21/. This is an empirical polynomial-type correlation where S_u is expressed as a function of the concentrations of the atmosphere components, with correction factors for the variation of the pressure and temperature in the unburnt gas.

Burning velocities obtained with this correlation are generally overestimated when compared to the experimental values obtained by other workers, /23/, /24/, /25/, for lean mixtures (hydrogen concentration less than 20%), Fig. 36. Also, the applicability of this correlation in this domain is not fully justified because the experiments based on which it was developed only involve mixtures with more than 20% H_2 /21/.

Therefore, based on the experimental data reported in /22/, a new correlation was developed for dry H_2-air mixtures,

$$S_u = C_o + \sum_i C_i (X_{H_2})^i \quad , \quad i = 1\text{-}5 \tag{43}$$

where X_{H2} is the volumetric concentration of hydrogen and C_i are polynomial coefficients, with the values

$C_o = -2.69283 \times 10^{-2}$ $\quad$ $C_3 = 1.2606$
$C_1 = -4.98026$ $\quad$ $C_4 = -95.8711$
$C_2 = 89.1152$ $\quad$ $C_5 = 1.60765 \times 10^2$

5.1.2 Turbulent Burning Velocity

The calculation of the turbulent burning velocity, S_t, is a principal factor of uncertainty in VENT-11. In /22/, there are three options available to the user for considering the influence of the turbulence on the burning velocity; these are included in the input data ITURB, as it follows:

ITURB=0: laminar burning, $S_t = S_u$

ITURB=1: turbulent burning, S_t = TFC1* S_u, where TFC1 is an input parameter

ITURB=2: turbulent burning, where the input must include values for the r.m.s. turbulent velocity (u') and for the mean size of large turbulent eddies (l).

However, the user will often have no knowledge a priori of the turbulence characteristics in containment (u' and l) and the assignment of an input numerical value for TFC1 by the user can hardly be justified.

Important efforts have been made /73/ for determination, by repeated calcula-

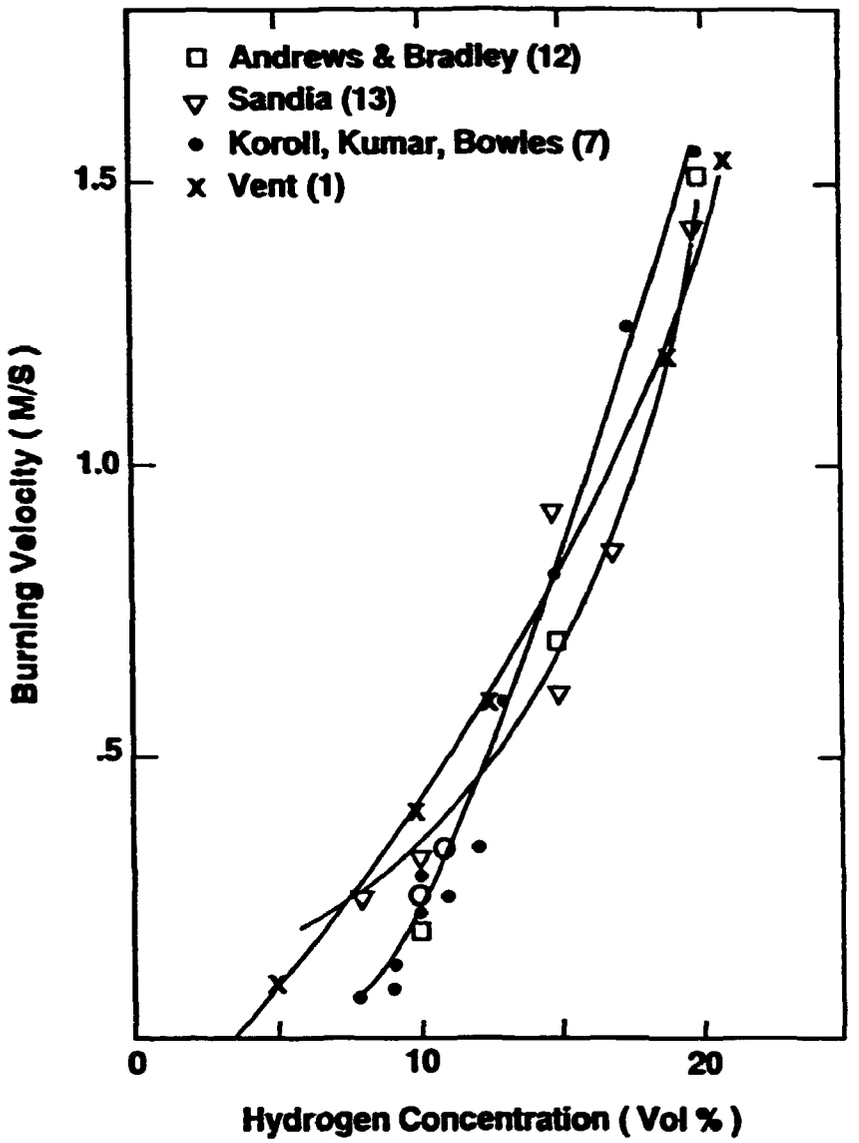

Figure 36. Laminar burning velocities for H_2-air mixtures.

tions, of a set of values for TFC1 fitted to experimental results. However, it is difficult to ensure that one input value can reflect in an appropriate manner the evolution of burning velocity during combustion. The modification of the turbulence characteristics due to the flame induced flow cannot be accounted for with this method.

In order to relax this deficiency, several correlations for expressing the influence of the flame induced turbulence on the burning velocity have been tested /27/, /28/, /29/. Following the results of test calculations, the Wohl correlation /29/ has been retained as the most appropriate.

$$\frac{S_t}{S_u} = 1 + \frac{2u'}{S_u} \qquad (44)$$

where S_u is the laminar burning velocity, and u' is the r.m.s. turbulent velocity due to the flame induced unburnt gas flow, calculated from /28/,

$$u' = u_t \cdot 0.1676\ Re^{-0.175} \quad (45)$$

with

u_t = unburnt gas flow velocity
Re = Reynolds number for the unburnt gas.

Similar to the correlation for the laminar burning velocity (Eq. (43)), the module for calculating the turbulent burning velocity due to the flame induced flow (Eqs. 44 and 45), has been implemented in the FUNCTION SU(P,T) of the code.

The above option for S_t is available to the user by assigning ITURB=3 as input data.

5.1.3 Flame Speed

In VENT-11, the flame velocity, V_f, is not calculated. While V_f is not an important parameter in calculating the combustion effects at slow deflagrations, considerations related to further development of the simulation models in VENT made necessary the determination of the flame speed.

An implicit intermediate result in the calculation is the time evolution of the position of the flame relative to the ignition point , R_f. Thus, calculating the time derivative dR_f/dt the flame speed is straightforward.

In this connection it is noted, however, that the flame velocity is also directly dependent on the burnt gas volume fraction and on the surface area of the flame. As consequence, special attention should be paid to the calculation of R_f and the significance of its time derivative if the assumptions on the flame shape are re-evaluated.

5.1.4 Heat Loss Term

In VENT-11, the energy balance equations are written without including energy losses, such that the combustion is considered to take place under adiabatic conditions. Therefore, for slow-burning mixtures the combustion pressure will always be considerably overestimated. It is recognized that, in reality, the peak pressure can be with up to 20-40% lower than the adiabatic isochoric complete combustion pressure (P_{AICC}), this difference increasing for lean mixtures.

In real systems complex processes of heat transfer occur: thermal radiation from the flame and from the hot burnt gas, conduction and convection to the walls and internal structures, and condensation of the vapour produced by burning at the cold solid surfaces. In post-accident reactor containments, the evaporation-condensation at the spray droplets, the presence of a liquid film formed by previously condensed steam and a much more complex composition of the atmosphere should also be considered.

While a comprehensive approach of this issue is desired, a more tractable model was chosen. In the equations for pressure and for the burnt gas volume fraction, a convective-equivalent heat flux, q,

$$q = h_c \cdot S_w(T_b - T_w) \quad (46)$$

from the burnt gas at the temperature T_b toward the walls at the temperature T_w (assumed to be equal with the initial temperature of the system, T_i), has been introduced. In Eq. 45, S_w is the heat transfer surface and h_c is the equivalent heat

transfer coefficient.

In the new version of the program, S_{bt} is calculated in FUNCTION AV. For the case of multiple ignition in cylindrical geometry, this value is corrected in SUBROUTINE FLAME in order to take into account the number and position of the flames and of the zones containing burnt gas during combustion.

For calculating the equivalent heat transfer coefficient, h_e, several convection type empirical correlation have been implemented.

For the convective heat transfer at high temperatures at gas-solid interfaces, Babiy /74/, recommends

$$Nu = K(2 + 0.17\ Re^{0.66}) \tag{47}$$

where Nu is the Nusselt number and Re is the Reynolds number for the burnt gas, and K is a coefficient for considering the effect of the high temperature. This correlation was developed for the heat transfer at the surface of burning coal particles, for which,

$$K = 145\ \exp(-5000/T_g) \tag{48}$$

where T_g is the gas temperature. For hydrogen combustion in dry H_2-air mixtures, we have developed a polynomial correlation for K, expressed as a function of the volumetric concentration of hydrogen, X_{H2}, /26/,

$$K = C_0 + \sum_i C_i\ (X_{H_2})^i \tag{49}$$

where the coefficients C_i are

$C_0 = -21.9947$ $\qquad$ $C_3 = 2.1089 \times 10^4$
$C_1 = 7.44927 \times 10^2$ $\qquad$ $C_4 = -1.94645 \times 10^4$
$C_2 = -6.5141 \times 10^3$

Another correlation, implemented for use in VENT, is available from Lignola et al. /75/, for the heat transfer from hot gases (at about 800°C) in a closed volume,

$$Nu = 0.39\ Re^{0.57}\ Pr^{0.33} \tag{50}$$

where, Nu, Re, and Pr are the adimensional Nusselt, Reynolds and Prandtl numbers for the gas respectively.

For the convective heat transfer in hot air furnaces, a modified Dittus-Boelter correlation is used in /76/ and in /77/,

$$Nu = 0.069\ Re^{0.8}\ Pr^{0.4} \tag{51}$$

This correlation was also implemented in VENT.

The user has access to different options regarding the heat transfer model in VENT through the input variable IHTC in NAMELIST COMB, as it follows

IHTC = 0: adiabatic combustion (default)
IHTC = 1: the equivalent heat transfer coefficient h_e is provided by the user as input data (variable ALFA in NAMELIST COMB)
IHTC = 2: h_e is calculated in the program with (50)
IHTC = 3: h_e is calculated in the program with (48) with K given by (49)
IHTC = 4: h_e is calculated in the program with (51)

In summary, the main changes in the VENT program with respect to heat loss include the following:

MAIN:	Calculation of burnt gas and of the unburnt gas parameters (temperatures, densities, velocities)
SUBROUTINE HTC:	Calculation of the equivalent heat transfer coefficient
SUBROUTINE FUNC:	Implementation of the heat loss term in the main equations of the model
FUNCTION HCOND:	Calculation of the thermal conductivity of the burnt gas, based on the data from /78/.
SUBROUTINE READ:	Implementation of the new input data, IHTC (default value = 0) and ALFA (default value = 0) in NAMELIST COMB
FUNCTION AV:	Calculation of the heat transfer surface area for single point ignition, cylindrical/spherical geometry
SUBROUTINE FLAME:	Correction of the heat transfer surface area for the case of multiple ignition in cylindrical geometry.

5.1.5 Simultaneous Multipoint Ignition

A set of modifications have been implemented which allow the use of VENT for calculating combustion transients arising from multiple ignition points in cylindrical geometry. The model is based on the following assumptions:

a. The flames are generated simultaneously and characterized by the same geometry, speed , and turbulent or laminar burning velocities.
b. An algorithm has been implemented for counting the number and type of the flames existing at every moment in the system; the flames have been classified in three categories: turbulent flames, laminar flames (for the case when two flames approaching one to the other are closer than a specified distance) and quenched flames.
c. The flames and the walls of the vessel create zones with burnt gas and zones with unburnt gas. It is considered that the burnt gas, and also the unburnt gas is characterized by the same parameters (temperature, density, velocity, etc.).
d. The pressure is uniform inside the vessel and it is calculated considering the heat released in all the existing flames. The equation for the rate of formation of burnt mass is written and solved two times, for a single turbulent and for a single laminar flame respectively.

The user has access to the model for multiple ignition by assigning the value 3 to the input variable IGEOM (in NAMELIST COMB). Other input data associated to this option are:

NI:	- number of the ignition points, in NAMELIST COMB, NI≤10; the default value is 1
DN(I), I = 1, NI+1:	- geometric distances along the cylinder for defining the position of the ignitors (m). This data is required only for NI>1, and must be placed after NAMELIST COMB, in free format. Example: for two ignitors (NI=2) situated at the two ends of the cylinder, we have

DN(1) = 0.
DN(2) = H -(vessel height-NAMELIST COMB)
DN(3) = 0.

The routines of the program which had to be modified for implementing this model are:

SUBROUTINE FUNC	-	implementation of the main equations of the model, modified as above
SUBROUTINE INI	-	defining the initial conditions
SUBROUTINE FLAME	-	defining and calculation of the number and type of the flams during the transient
SUBROUTINE READ and PROGRAM MAIN	-	Modifications for the new input/output data required by the present version.

The common deck-file VM11.INC have also been completed with a new common block containing intermediate variables transferred inside the code.

5.1.6 Test Calculations

Several calculations for the constant volume combustion experiments with simultaneous multipoint ignition in CTF-Pipe have been performed, and the results have been compared with the experimental data.

The calculated and experimental values for the maximum combustion pressure for various mixtures and different number and position of the ignition points are given in Tab. 7. For most of the cases, at low concentrations, a good agreement is obtained. However, the presence of the pressure oscillations observed in experiments, lead to an underprediction of the peak pressures for rich mixtures. The differences between the real maximum combustion pressures and the pressure calculated for the adiabatic isochoric complete combustion (P_{AICC} in Tab. 7), illustrate the need for introducing a term for considering the heat losses.

In Tab. 8 the calculated ano experimental average values for the velocities of the flame, expressed as the ratio between the propagation path length and the burning time, are presented.

For all the situations, VENT predicts slower flames than those observed in experiments. For leaner mixtures (10% and 12% H_2) the differences are minor but at higher concentrations, where the acceleration effects are more important, the underprediction are significant. This trend is more clear when looking at the maximum flame speeds at end ignition (Tab. 9). The large differences between the calculated and measured values for mixtures with 15%, 20%, and 65% H_2 suggest that implementation of models for simulating other acceleration mechanisms of the flames could be considered.

In Tab. 10 the average flame velocities as calculated with VENT for multiple ignition are given, and for comparison in Tab. 11, the average velocities of the flames originating in the ignition point I2, are given. Again, especially for rich mixtures, the calculated values are much lower, having as effect longer durations of burning.

These results are, however, not unexpected, since the model introduced in VENT for calculating the turbulent burning velocity was not originally designed to cover this type of transients. It was only intended to cover the increase of the burning velocity due to the flow induced by the flame. It does not include the acceleration mechanisms due to the presence of obstacles (the support and the

Table 7. Calculated and experimental peak pressures in the CTF-Pipe

H_2 %	P_{max}/P_o AICC	P_{max}/P_o exp	P_{max}/P_o VENT	Ignition points
10	4.269	2.20	2.28	I1
10	4.326	3.15	2.43	I3
10	4.293	3.06	2.99	I2,I3
10	4.317	3.26	3.00	I2,I3,I4
10	4.310	3.50	3.55	I1,I2,I3,I4
10	4.339	2.80	3.03	I1,I4
10	4.232	3.56	3.22	I2,I4
12	4.816	2.68	2.75	I1
12	4.882	3.25	2.95	I3
12	4.880	3.39	3.42	I2,I3
12	4.876	4.26	3.58	I2,I3,I4
12	4.875	4.34	4.01	I1,I2,I3,I4
12	4.881	3.51	3.53	I1,I4
12	4.882	3.63	3.37	I2,I4
15	5.585	3.63	3.38	I1
15	5.657	4.17	3.70	I3
15	5.635	3.99	4.19	I2,I3
15	5.628	4.40	4.36	I2,I3,I4
15	5.633	4.58	4.77	I1,I2,I3,I4
15	5.658	4.40	4.25	I1,I4
15	5.647	4.39	4.32	I2,I4
20	6.765	5.05	4.34	I1
20	6.860	5.45	4.69	I3
20	6.857	5.76	5.30	I2,I3
20	6.849	5.88	5.43	I2,I3,I4
20	6.847	7.00	5.91	I1,I2,I3,I4
20	6.845	6.11	5.29	I1,I4
20	6.859	5.41	5.43	I2,I4
65	5.607	3.27	3.70	I1
65	5.672	4.22	3.99	I3
65	5.656	4.46	4.47	I2,I3
65	5.634	4.75	4.67	I2,I3,I4
65	5.610	4.70	4.97	I1,I2,I3,I4
65	5.655	4.22	4.50	I1,I4
65	5.664	4.70	4.59	I2,I4

Table 8. Average values for the flame velocity (V_f) at end ignition (m/s)

	Hydrogen concentration				
	10%	12%	15%	20%	65%
V_f exp1,av	1.06	2.31	8.80	35.60	8.25
V_f exp2,av	1.17	3.54	16.23	61.48	17.24
V_f VENT,av	0.78	1.44	2.71	5.18	3.35

Table 9. Maximum flame speeds at end ignition (m/s)

	Hydrogen concentration				
	10%	12%	15%	20%	65%
$V_f$exp2,max	1.17	3.54	28.55	196.30	27.25
V_fVENT,max	1.38	3.34	6.49	14.25	7.99

Table 10. Average flame speeds for multiple ignition as calculated with VENT

Ignition points	Hydrogen concentration				
	10%	12%	15%	20%	65%
I2+I3	0.78	1.40	2.82	5.47	3.67
I2+I4	0.89	1.55	3.18	6.36	4.15
I2+I3+I4	0.70	1.52	2.75	5.98	3.59
I1+I2+I3+I4	0.81	1.48	2.85	5.71	3.72

Table 11. Experimental values for the average flame velocities originating in I2

Ignition points	Hydrogen concentration				
	10%	12%	15%	20%	65%
I2+I3	1.15	2.05	5.59	22.84	
I2+I4				38.49	
I2+I3+I4				37.21	
I1+I2+I3+I4	1.28	3.14	12.22	50.35	14.03

wires associated to the thermocouples in the second series of experiments in CTF-Pipe), to the interactions between the flame and the pressure waves and to the enhanced turbulence generated by the induced flow patterns at multiple ignition.

5.2 Simulations with CONTAIN

CONTAIN, /19/, /20/, is an integrated lumped-parameter multicompartment code for accident analysis in containment. It allows for the simulation in an integrated manner of the various aspects in a post-accident containment. Among other features, CONTAIN includes specific models for simulating the engineered safety features (cooler fans, containment spray, ice condenser) and for aerosol and fission products behaviour. As a lumped parameter code, the capabilities of simulating the real geometry are rather limited, possible only by introducing user-defined structures of various types and shapes.

The atmosphere thermodynamics model considers a homogeneous atmosphere. The mass and energy balance equations containing terms associated with various heat and mass transfer mechanisms (convection, radiation, evaporation and condensation), with the user defined leak or source flows, and with the sinks or sources of energy as calculated by other sections of the code (as the models for combustion of combustible gases, and, in the newer versions, for cavity phenomena and for molten core-concrete interactions) are solved for every compartment (cell). The calculation scheme of the program requires that all the above mentioned calculations should be performed with a shorter time step, named "cell time step", separately, for every cell. Then, the balancing of the pressure throughout the system and the calculation of the intercompartment flows are performed with a longer integration time step, named "system time step".

The combustion model is executed every cell time step in the cells where the conditions for burning are met, i.e. the burning is already in progress or the atmosphere is inside the flammability limits and a source of ignition is available. At system calculations, the possibility for flame propagation from one compartment (cell) to another is tested. For this, empirical sets of values for flammability limits and for flame propagation limits are used.

The burning model is based on the calculation of the velocity of the flame with empirical correlations, as function of the composition of the atmosphere at the moment of ignition. Also, empirical correlations for determining the unburnt fraction of fuel at the end of burning are included. From the flame velocity thus determined and with a user-defined characteristic length of the compartment, the burning time is calculated. Further, the burning rate, expressed as the variation in time of the number of moles of fuel during combustion, is calculated such that at the end of burning (after the burning time), the concentration of fuel (hydrogen and possibly carbon monoxide) should be equal to the unburnt fraction.

The burning rate is actually a measure of the rate with which the combustion energy is released. This value is further transferred to the other sections of the code, where the thermodynamic state of the atmosphere (pressure and temperature) is determined.

By choosing the flame velocity as main input data for the burning model, the inconveniences implied by the assumptions for calculating the laminar and turbulent burning velocities and, especially, those coming from the arbitrary definition of the flame shape, and thus the calculation of the flame surface area (as in VENT), are avoided. However, determining the velocity of the flame from experimental data is not an error-free process, due to the influence of factors difficult to control or even out of the experimentator's possibility of controlling them. Thus, if the flame speed is determined from the arrival time measured with a set of

thermocouples, which is a usual experimental method, the very presence of the measuring system influences the propagation of the flame, as our experiments in CTF-Pipe have shown, by distorting the flame and thus inducing supplementary acceleration phenomena. Another uncertainty in measuring the speed of the flame comes from the subjective definition of the point on the flame surface whose speed is measured. This is an important issue since the flame front is not plane such that the reaction zone will advance in the unburnt gas with different velocities in different points. The difficulty of this choice also appears in the cases when the flame speed is measured without introducing supplementary instrumentation in the vessel - e.g. by using a high speed camera, /31/.

On the other hand, the complex geometry given by the presence of various obstacles (pipes, grills, etc.) in the compartments where a burning is expected to occur, can require special experimental setups for reproducing in experiments, the real situation, /79/.

In any case, however, engineering judgement should always decide, for the particulary analysis (reactor containment design and geometry, accident scenario), on the empirical correlations which are going to be employed. Knowing the difficulties embodied in the models for simulating the combustion behaviour, is a necessary step toward a correct use and interpretation of the computed results.

In the following, some of the adaptations and new modelling features implemented in CONTAIN 1.12, /72/, are described. They are mainly aimed to the simulation of multiple ignition in an inhomogeneous atmosphere. Other changes refer to the optional calculation of the pressure/shock waves and of the Chapman-Jouguet detonation state. Also, the number of options available for calculating the flame velocity and for combustion completeness, /31/, has been extended.

5.2.1 Nodalization and Calculation Strategy

The present approach implies the use of a supplementary level of detail by dividing the cells, as defined in CONTAIN, into several zones named subcells. The geometry of the subcells is given by their volume and characteristic length, which have the same significance as in CONTAIN. The placement of the subcells relative to each other inside a cell and the neighbour subcells between adjacent cells are also specified as input data.

In a subcell the atmosphere is homogeneous. The concentration of various components is calculated using distribution coefficients, allowing for the simulation of the nonhomogeneity of the atmosphere in the compartment (cell) at the moment of ignition, and of the nonuniform local distribution of the gas flow sources during combustion.

For a flammable mixture, the moment of ignition can be defined with one of the following criteria:

- ignition at flammability limits
- ignition when the concentration of hydrogen is higher than a user-specified value
- ignition at a user-specified moment of time

For each of the ignitors present in a subcell, one of these criteria can be specified. A flame from an adjacent cell/subcell becomes an ignition source at the beginning of the next system/cell time step after the flame has reached the boundary of the subcell. This assumption can introduce delays in combustion behaviour in a cell; the error can be minimized by a careful strategy in calculating the time steps during combustion, /72/. In this respect we have to note that the boundaries

between subcells are fictive surfaces which do not prevent the propagation of the flames. It is therefore possible to have in a cell, or even in a subcell, at a particular moment, several flames. Inside a subcell the flames are characterized by the same burning rate and flame speed, but these values may differ from a subcell to another corresponding to the local conditions.

The combustion model preserves the capability to consider both the hydrogen and the carbon monoxide as flammable gases. It is activated when one of the ignition criteria is satisfied.

When burning starts in a cell, the composition of the atmosphere in every subcell is first determined. For every subcell, at ignition only, the flame speed is calculated and, based on the characteristic length of the subcell, an estimated burning time. Using this "estimated burning time", the unburnt fraction of fuel and the input gas flow sources integrated over this duration, an elementary burning rate is determined. This rate is defined as being equal to the burning rate which would ensure the end of combustion after the "estimated burning time" in the case of a single flame, based on the initial conditions at ignition and on the input gas flow sources. Since during combustion, however, the simultaneous existence of several flames is possible (due to multipoint ignition and to the flames propagating from neighbour subcells), the effective burning rate (in the following named burning rate) is recalculated for every subcell in every time step by multiplying the elementary burning rate with the number of flames existing in the subcell.

Knowing the burning rate the immediate calculation of the variation of the number of moles of gaseous components and of the thermal energy released by combustion in the subcells is possible. Integrated for the whole cell, these values, which are the main result of the combustion model, are transferred to the other calculation modules of the code.

In a subcell the combustion ends when the concentration of the flammable gases (H_2 and CO) decreases to the values given by combustion completeness, or when the mole fraction of oxygen decreases to 0.05, /20/.

At every time step the local composition of the atmosphere in the subcells is also calculated considering the composition at the beginning of the time step, the variation of the number of moles due to combustion, the gas flow sources as specified in the input and also the variation of the number of moles of gas due to processes calculated in other sections of CONTAIN.

5.2.2 Flame Velocity

The velocity of the flame is calculated for every subcell at the moment of ignition and, as in CONTAIN, it is considered to be constant during combustion.

In addition to the correlations existing in CONTAIN, another set of correlations is implemented. The new correlations have been developed by Wong /31/ based on hydrogen combustion experiments at Nevada Test Site (NTS). For lower hydrogen concentrations (below 18%), separate expressions are given to account for the acceleration of the flame due to the turbulence generated by the operation of sprays and fans in containment. For rich mixtures (above 18% hydrogen), the flame is considered so fast that the turbulence generated by the fans and the sprays is no longer important, /31/, and therefore a single correlation is given. The explicit dependence of the flame speed on the length of propagation is also included.

Again, we have to note that the user should be aware of the conditions for which the correlations have been developed in order to fairly evaluate the degree of applicability to the particular problem under study. The user is therefore allowed to override these correlations by specifying the flame velocity as input data.

Regarding the variation of the flame velocity during combustion in a closed compartment, some comments appear to be necessary.

First it must be recalled that the velocity of the flame is not constant during burning. In a first stage an (auto)acceleration of the flame occurs due to the turbulence generated by the flame, increase of the pressure and temperature in the system, presence of obstacles, convective flows, etc. As the flame approaches the opposite wall the velocity of the induced flow of unburnt gas pushed by the flame decreases, such that the flame velocity decreases to the local value of the burning velocity.

For a specified mixture, the maximum and the average values for the flame speed depend not only on the acceleration rate but also on the length of propagation path of the flame. As result, for the case of single ignition, the maximum and average values for the flame velocity will be lower for compartments with lower geometrical size (as long as the other conditions determining the acceleration of the flame and the dissipation mechanisms are similar). This dependence is included in the correlations /31/

$$V_f \sim L^{1/n} \quad , \quad n = 3 \tag{52}$$

where

V_f = flame velocity (m/sec)
L = characteristic length of the volume (m)

In the case of multiple ignition, two factors with opposite effects on the speed of the flame appear. The velocity field corresponding to the flows induced by the flames produce a more intense turbulence (relative to the single ignition case), which causes an enhanced acceleration of the flames. On the other hand, the fronts of the flames divide the compartment, leading to a possible significant reduction of the length of propagation of the flames. These dependences are confirmed by the experimental results presented in Chap. 4.4.3.

5.2.3 Burning Rate

The burning rate represents the rate of variation in time of the number of moles of fuel. It is first calculated for the case of single ignition such that the burning would end after a time, t_{hu}, equal to the ratio between the characteristic length and the flame velocity in the subcell.

Based on the composition of the atmosphere at ignition and on the anticipated input flow sources integrated over t_{hu}, the number of moles of H_2 and CO available to be burnt are calculated.Similarly, the number of moles of O_2 available for burning ($N_{O2\,disp.}$) is determined. The number of moles of O2 required ($N_{O2\,nec.}$) for burning the H_2 and CO (as calculated in the previous step) to the final concentration given by the combustion completeness (x_{Hf}, x_{COf}) , is then calculated. Comparing the necessary numbers of moles of O_2 ($N_{O2\,nec.}$) and the available number of moles of O_2 ($N_{O2\,disp.}$), the following situations appear:

- If $N_{O2\,nec.} < N_{O2\,disp.}$, sufficient oxygen exists and the hydrogen and the carbon monoxide are burnt to x_{Hf} and to x_{COf} respectively.

- If $N_{O2\ nec.} > N_{O2\ disp.}$, the burning occurs in deficit of oxygen. It is assumed that the available oxygen is distributed for burning H_2 and CO in a ratio proportional to their initial mole concentrations. Further, comparing the number of moles of H_2 and CO with the number of moles of O_2 assigned for burning, other situations are considered:

  a. H_2 burns to $K_H * x_{Hf}$, $K_H > 1$
     CO burns to x_{COf}
  b. H_2 burns to x_{Hf}
     CO burns to $K_{CO} * x_{COf}$, $K_{CO} > 1$
  c. H_2 burns to $K_H * x_{Hf}$, $K_H > 1$
     CO burns to $K_{CO} * x_{Hf}$, $K_{CO} > 1$

In all the calculations, it is required that the final molar fraction of O_2 should not be below $x_{O2f} = 0.05$, /20/.

For each case, the burning rate is calculated separately for hydrogen and for carbon monoxide. The burning rate expresses the rate of variation in time of the number of moles of fuel. Since the burning rate is considered constant during combustion, for burning of hydrogen, we have:

$$\dot{N}_{H2}=[n_{H2}(t_{ign})+\int_{tign}^{tign+thu} Q_{H2}dt-n_{H2}(t_{ign}+t_{hu})]/t_{hu} \qquad (53)$$

where

$n_{H2}(t)$ = number of moles of hydrogen at the time t in subcell
t_{ign} = moment of ignition
t_{hu} = L_c/V_f
L_C = characteristic length of the subcell
V_f = flame velocity in the subcell
Q_{H2} = input source flow of hydrogen
$\dot{N}_{H2}$ = burning rate of hydrogen with single ignition

and a similar expression for burning of carbon monoxide.

Since at a particular moment several flames can be simultaneously present, the effective burning rates ($\dot{N}_{H2\,eff}$ and $\dot{N}_{CO\,eff}$ respectively) are calculated by multiplying the burning rates as determined above, with the number of flames existing in the subcell.

Thus the variation during the time step of the number of modes of the various components of the atmosphere, due to combustion of H_2 and CO, can be determined for every subcell, with:

$$\Delta N_c = (S_{C,H}*\dot{N}_{H2eff} + S_{C,CO}*\dot{N}_{COeff}) \cdot \Delta t_c \qquad (54)$$

where

$S_{C,H}$, $S_{C,CO}$ = stoichiometric coefficients for the component C in the chemical reactions for burning of H_2 and CO respectively,
  < 0 for reactants
  > 0 for products
Δt_c = cell time step
ΔN_c = variation of number of moles of component c due to combustion, during Δt_c.

These values are used for recalculating the composition of the atmosphere in subcells at the beginning of the next cell time step.

The energy released in a burn is calculated at the cell level, for every time step:

$$q_{burn} = [2.86*10^{8}*\sum_{j}(\dot{N}_{H2,eff})_j + 2.83*10^{8} * \sum_{j}(\dot{N}_{CO,eff})_j]*\Delta t_c \quad (55)$$

j = subcell index

and this value is further transferred to the other models of CONTAIN.

5.2.4 Shock Waves and Detonations

The energy released in the reaction zone produces a local increase of temperature and pressure and the hot burnt gas expands. The flame acts as a piston on the unburnt gas generating a pressure/shock wave which precedes the flame and propagates in the unburnt gas with supersonic speed. Since it originates in the flame the strength of the shock increases with increasing the velocity of the flame. At fast flames a strong coupling appears such that the shock will change the state of the gas behind it, influencing the propagation of the flame itself.

Based on the equation for the unconfined planar wave approximation (Chap. 2.3)[1], a model for calculating the flow structure at burning has been implemented. It is executed optionally, only once for every subcell, at the moment of ignition. The initial state of the gas is given by p_{in}, ρ_{in}, and γ (pressure, density, and ratio of the specific heats, respectively), calculated in other sections of CONTAIN. They have the same value for all the subcells in the cell.

The ratio of the specific heats for the combustion products, γ_2, is calculated for every suocell, before the execution of this module, for the expected composition of the atmosphere after the end of combustion. It is assumed that γ_2 is independent of temperature (the molecular dissociations are neglected).

With these assumptions, the calculation of the shock speed and of the flow structure during combustion is made with an iterative scheme with the following steps:

a. Assign a guess value for the velocity of the shock, V_s^*. Since $c_0 < V_s < c_0 + V_f$, the first and the subsequent guesses for V_s^*,are obtained by consecutive partitioning of the interval $(c_0 , c_0 + V_f)$.
b. For the guess value of V_s^*, calculate the pressure, density, and velocity of the shocked gas, p_1^*, ρ_1^*, and u_1^* with the relations Rankine - Hugoniot, (18), (19), and (21).
c. Test the convergence for the flame velocity, calculated with (23).

If the convergence is not satisfied, a new guess value for the shock speed, V_s^*, is made (step a).

At convergence, the flow structure for the burnt gas (p_2, ρ_2, u_2) is recalculated with the relations (25), (26), and (14).

The output values retained as significant are those describing the shock wave and the flow field generated by burning, the shock velocity, and the relative pressure of the unburnt gas compressed by the shock, p_1/p_{in}.

---

1. Note: The notations used in this section are the same as the notations in Chap. 2.3.

This calculation model has been verified against reference data, /34/ for 4% methane-air mixtures and a good agreement has been obtained.

The calculations for detonations are made with the assumption that the detonations occur in the point Chapman-Jouguet, with a solution which corresponds to the experimental observations for self-sustained detonations, /34/. In this case, the flame front coalesces with the shock, such that

$$V_f = V_s \tag{56}$$

and a detonation wave is created.

For mixtures containing hydrogen, the velocity of the detonation wave is high such that we can consider that

$$\eta = \frac{1}{M^2_{CJDet}} \ll 1$$

with

$$M_{CJDet} = \frac{V_s - u_\infty}{C_\infty} \; (= \frac{V_f - u_\infty}{C_\infty})$$

With this assumption the equation (28) results in

$$V_s = [2Q(\gamma_2^2 - 1)]^{\frac{1}{2}} \tag{57}$$

a relation which is also recommended by various authors, /34/, /40/.

With V_s known, the pressure, the density, and the velocity of the gas in the detonation front (point a', Fig. 6) are then determined from the Rankine-Hugoniot relations.

5.2.5 Calculations and Comments

The test calculations have been performed for the constant volume combustion experiments with simultaneous multipoint ignition carried out in the Containment Test Facility at Whiteshell Laboratory, /32/.

For simulating the experiments in CTF-Pipe the measured values for the flame velocity have been used as input data. In the other cases (experiments in CTF-Sphere) the input values for the flame speed have been obtained by dividing the propagation length (sphere radius) to the time to maximum pressure at single point central ignition for the various mixtures; these values too have been used for calculating the tests with multipoint ignition.

In Fig. 37 the curves for the evolution of the pressure in CTF-Pipe for a 12% hydrogen-air mixture ignited with the ignitors I2 and I3 are presented. As a first observation one can note the significant difference of the time to maximum pressure (which is a measure of the flame speed and thus of the burning rate) for the two experiments E12 and T4. The supplementary instrumentation for measuring the arrival time (thermocouples and the associated supports, wires, etc.) during E12, acted as obstacles; in this case, the enhanced turbulence and the increased area of the reaction zone contributed to the acceleration of the flame and thus, to a higher average velocity, /32/. Also, the average velocities of the two flames developed to the right and to the left of the ignitor I2 (or I3), Fig. 13, are not equal, being influenced by the available length of propagation and, in this case,

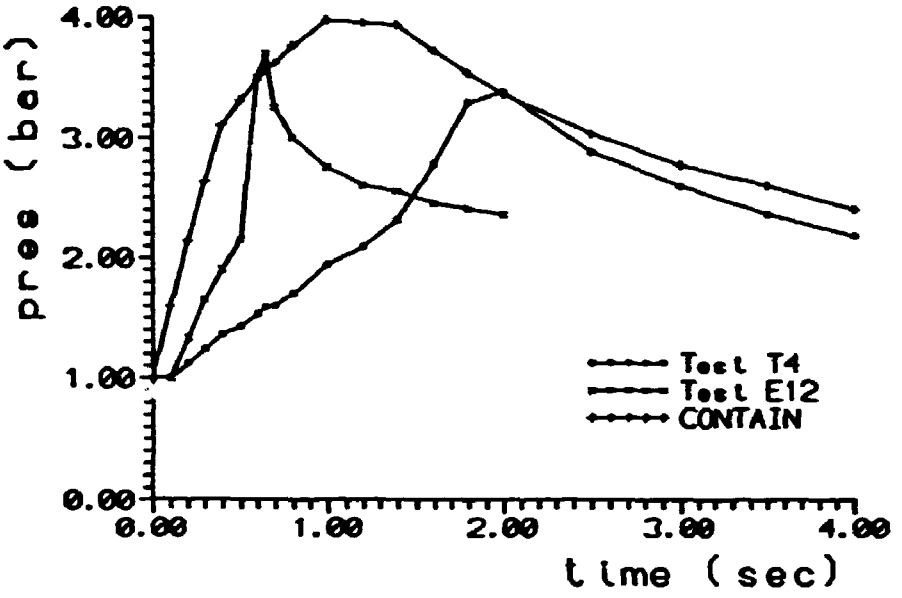

Figure 37. Pressure histories for a 12% H_2-air mixture in CFT-Pipe. Ignitors I2 and I3.

by supplementary turbulence generated due to the simultaneous presence of several flames in the vessel. We have used in this case, the velocity of the flame originating in I2 directed toward I3, which is obviously lower than the velocity of the other flame originating in I2 and directed toward the left end of the vessel (or than the velocity of the flame from I3 directed to the right end of the vessel), Fig. 13.

Regarding simulations for the reactor containments, where large empty volumes coexist with spaces filled with various equipment, the difficulties of implementing "correct" input data are obvious. It is therefore the moment to stress again the importance of the analyst achieving a best possible level of understanding of both the real (accident) situation and of the available options and assumptions for simulation available, especially when empirical correlations are used.

The values for the calculated versus measured peak pressures during combustion for various experiments in CTF-Sphere and in CTF-Pipe are given in Fig. 38 and in Fig. 39 respectively. As it can be seen, CONTAIN conservatively generates greater values for the maximum pressure than the ones observed in experiments. In general, the difference is less than 25% from the measured values, though in some cases (end ignition in CTF-Pipe for 10% and for 12% H_2-air mixtures), the overestimation is higher.

Explanations for these results can be found by a closer evaluation of the modelling characteristics of CONTAIN, such as the combustion model and the models for calculating the energy dissipation mechanisms (particularly the heat and mass transfer from the atmosphere).

Thus, since CONTAIN is a lumped parameter program, the combustion energy is uniformly distributed in the whole volume of the cell such that there are not delimited separate volumes of hot burnt gas and fresh unburnt mixture. Therefore, during the transient the heat transfer from a hot gas is replaced by one originating in an atmosphere at a lower average temperature, leading to an underestimation of the heat losses and to a corresponding overestimation of the pressure. An opposite

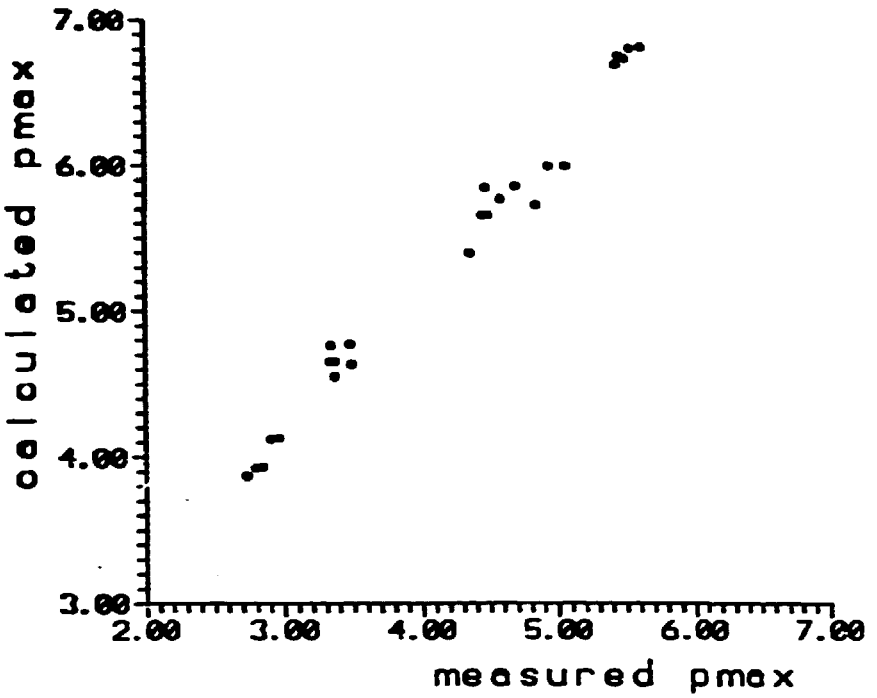

Figure 38. Calculated versus measured values for the peak pressure in CTF-Sphere.

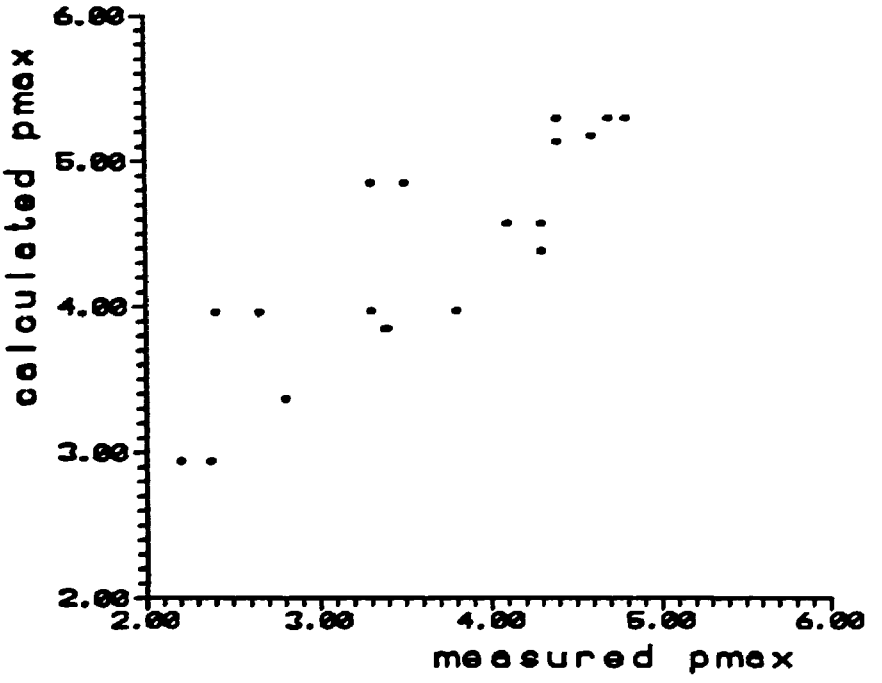

Figure 39. Calculated versus measured values for the peak pressure in CTF-Pipe.

effect is that the heat transfer surface area is always equal to the sum of the areas of all the structures in compartment, while during burning, the heat is mainly transferred only to those structure surfaces in direct contact with the hot combustion products.

On the other hand, the heat transferred is first deposited in a thin layer at the surface of the structure material (and then further dissipated by conduction) /20/, /80/, leading to the overestimation of the wall surface temperature. This contributes, not only to the reduction of the heat flux transferred by convection and radiation, but also to the underestimation of the condensation rate. Thus, the quantity of vapour extracted from the atmosphere and deposited as liquid is lower, and also the latent heat which should be transferred to the walls. The overall effect is again in the direction of overestimating the calculated pressure.

Other reasons for higher calculated pressures seem to lie in the constancy of the speed of the flame during combustion, which is a basic assumption in CONTAIN. In reality, however, the flame starts with a low value (equal to the burning velocity) and then accelerates due to various mechanisms. Therefore, the use of an average constant value for the flame speed, leads in the first part of burning to an overestimation of the burning rate and of the rate of the deposition of the combustion energy in the atmosphere of the cells. Combined with a lower dissipation rate via the heat transfer to the structures, as mentioned above, it results in a steeper rate of increase of the pressure (see also Fig. 37), which seems to have a decisive influence on the value for the maximum combustion pressure.

As one can see, the balance of these uncertainties due to modelling assumptions is shifted toward conservative results. Though acceptable from the point of view of safety evaluations, further developments would be beneficial, as for example in the direction of refining the models for high temperature heat transfer phenomena.

6 Conclusions

The presence of hydrogen in containment at reactor accidents constitute a supplementary source of risk due to the pressure and temperature effects during burning. Currently this issue is under attention due to the trend of enlarging the area of interest for reactor safety such that more and more often the severe accidents are into focus.

The study of the various aspects related to the combustion of hydrogen and their treatment in a unitary manner have constituted the introductory part of the work for this project and also, are the object of the first part of this report.

The experimental research has had as scope the study of the simultaneous multipoint ignition in dry H_2-air mixtures, for constant volume and for vented combustion under various geometrical conditions. The experimental data have shown the influence of the number and location of the ignition points, sensitivity of the mixture and the effects induced by the geometry of the vessels, on the development of the combustion pressure and on the speed of the flames. Important phenomena, as the apparition of enhanced pressure oscillations for particular geometrical conditions, and the balance between the influence of the length of propagation of the flame and the enhanced turbulence at simultaneous multipoint ignition, have been identified. Based on the experimental data, a correlation for the vent effectiveness for the simultaneous multipoint ignition at vented combustion, correlating data for mixture properties and geometry of the vent has also been developed.

The theoretical part of the activity has consisted in the development work with the computer programs licensed for the analysis of hydrogen combustion in reactor containment VENT and CONTAIN. The simulation capability and the limits of the simplifying assumption have been analyzed and the calculation results have been compared with the experimental data. The calculations have shown the trend of these two codes to produce conservative results, in the direction of overestimating the combustion pressure.

The adaptation work with the program VENT has lead to the development and implementation of a new correlation for the laminar burning velocity and of a model for allowing the simulation of the simultaneous multipoint ignition at constant volume combustion. Also, a model for calculating the energy lost during combustion which allows for more realistic results for the maximum combustion pressure, has been implemented. Since the basic input data for the combustion model is the laminar burning velocity, a model which makes possible the calculation of the influence of the flame induced turbulence on the burning velocity, based on empirical correlations has also been introduced.

The existing combustion model in CONTAIN 1.12 has been refined and completed to account for specific situations which occur during reactor accidents. Thus, a model for simulating the simultaneous or nonsimultaneous multipoint ignition in an inhomogeneous atmosphere has been developed and implemented in the code. It allows the simulation of the combustion effects due to long term stratification and formation of gas pockets with different compositions inside one compartment, the simultaneous presence of several flames and the possibility of modelling of localized continuous flames. The number of options available for calculating the flame velocities and the combustion completeness has been extended by implementing new correlations which consider the dependence upon the characteristic dimension of the compartment and upon the operation of other systems in containment (fans, sprays) during combustion. A model for optional

calculation of the combustion pressure waves and of the parameters for a Chapman-Jouguet detonation, based on the unconfined planar wave approximation, has also been introduced.

7 Acknowledgement

Funding for this project was provided by the Danish Research Academy and by Risø National Laboratory. The work has been carried out at Risø National Laboratory, Nuclear Safety Research Department, Reactor Physics Group. In the period of the project I was matriculated as a Ph.D. student at the Technical University of Denmark. In this respect, the positive attitude of these organisations is highly appreciated.

I am indebted to my advisers, Prof. P.L. Ølgaard and Dr. P.B. Fynbo for their continuous professional guidance, interest, and will to share from their expertise and experience.

The research activity has included an eleven months attachment with the Atomic Energy of Canada Limited, Whiteshell Laboratory, Containment Analysis Branch. In this respect, I want to thank all responsible factors at AECL, in particular Dr. K. Tennankore, at present Director at AECL-Research, for allowing me to work with their highly qualified and experienced staff in the frame of their commercial research activities. It is the right moment to express my gratitude and indebtedness to Dr. Grant Koroll, head of the Hydrogen Combustion Group for his open-minded professionalism, guidance and steady support, during and after the termination of the attachment, as well. I am fully thankful to Dr. K.K. Kumar and to Dr. C.K. Chan for the valuable technical discussions as well as to the technicians W. Dewit, E. Bowles, and B. Thomas for assistance in the experimental setup.

I want also to thank Dr. T.F. Kanzleiter and Dr. K. Fischer for hospitality during the visit made in the first part of the project at the Containment Facility at Battelle Institut, Frankfurt.

Last but not least, I want to thank Mrs. Inge Blyitgen for careful typing of the Risø reports related to this project.

References

1. Rasmussen, N.G., Kouts, H.J.C., Dabora, E.K., Faeth, G.M., Oppenheim, A.K., Seery, D.J., Zalosh, R.G. (1987). Technical Aspects of Hydrogen Control and Combustion in Severe Light-Water Reactor Accidents. National Academy Press, Washington D.C.
2. Jankowski, M., Tolley B., Parsons, P.D., Blahnik, C., Jahn, H., Tolstykh, V. (1991). Hydrogen in Water Cooled Nuclear Power Reactors. *IAEA* and *CEC*, Vienna, Austria.
3. Tennankore, K.N., Koroll, G.W., Kumar, R.K., Lam, A.H.T., Chan, C.K., Wren, D.J. (1987). Hydrogen Combustion Issues and Containment Integrity. AECL-9094.
4. Camp, A.L., Cummings, J.C., Sherman, M.P., Kupiec, C.F., Healy, R.J., Caplan, J.S., Sandhop, J.R., Saunders, J.H. (1983). Light-Water Reactor Hydrogen Manual. SAND 82-1137, NUREG/CR-2726.
5. Berman, M., Cummings, J.C. (1984). Hydrogen Behaviour in Light Water Reactors. *Nuclear Safety*, **25(3)**, pp 53-74
6. Bujor, A. (1991). Review on Hydrogen Generation, Transport, Combustion, and Mitigation Techniques in the Reactor Containment. Risø-I-532.
7. Lillington, J. (1991). Hydrogen Production under PWR Degraded Core Conditions. Seminar/Workshop on Hydrogen Behaviour and Mitigation in Water Cooled Nuclear Power Reactors, Bruxelles, 4-8 March 1991.
8. Christensen, H., Söderman, E. (1984). Radiolytic Gas Generation after Loss of Coolant Accident in a Boiling Water Reactor. *Nuclear Safety*, **25(3)**, pp 329-340.
9. Sugimoto, J., Hidaka, A., Soda, K. (1991). Hydrogen Generation during Reflooding of Degraded Core as an Accident Management Measure. Seminar/Workshop on Hydrogen Behaviour and Mitigation in Water Cooled Nuclear Power Reactors, Bruxelles, 4-8 March 1991.
10. Manno, V.P., Golay, M.W. (1984). Hydrogen Transport in Containments: A Survey of Analytical Tools and Benchmark Experiments. *Nuclear Safety*, **25(6)**, pp 797-814
11. Karwat, H. (1993). International Standard Problem 29: Distribution of Hydrogen within the HDR Containment under Severe Accident Conditions. Final Comparison Report. NEA/CSNI/R(93)4.
12. Maas, U., Warnatz, J. (1988). Ignition Processes in Hydrogen-Oxygen Mixtures. *Combustion and Flame*, **74**, 53-69.
13. Glassman, I. (1977). Combustion. *Academy Press.*
14. Kumar, R.K., Koroll, G.W., Dewit, W.A., Hallin, E.L., Skopik. D.M., Caplan, H.S. (1992). Ignition of Hydrogen-Oxygen-Diluent Mixtures in an Ionizing Radiation Field. *Combustion Science and Technology*, **38** pp. 145-159.
15. Kumar, R.K. (1990). Hot Surface Ignition of Hydrogen/Oxygen/Diluent Mixtures in the Presence of Radiation Fields. ASME-HTD142, Heat Transfer in Combustion Systems. Editors: Farouk, B., Grosshandler, W.L., Lilley, D.G., Presser, C. Book no. H00595.
16. Kumar, R.K. (1989). Ignition of Hydrogen/Oxygen/Diluent Mixtures Adjacent to a Hot, Nonreactive Surface. *Combustion and Flame*, **75**, 197-215.
17. Koroll, G.W., Kumar, R.K. (1991). Isotope Effects on the Combustion Properties of Deuterium and Hydrogen. *Combustion and Flame*, **84**, 154-159.
18. Plys, M.G. (1993). Hydrogen Production and Combustion in Severe Reactor Accidents: an Integral Assessment Perspective. *Nuclear Technology*, **101**, 400-410.

19. Murata, K.K., Caroll, D.E., Washington, K.E., Gelbard, F., Valdez, G.D., Williams, D.C., Bergeron, K.D. (1989). User's Manual for CONTAIN 1.1: A Computer Code for Severe Nuclear Reactor Accident Containment Analysis. SAND87-2309, NUREG/CR-5026.
20. Washington, K.E., Murata, K.K., Gido, R.G. Gelbard, F., Russel, N.A., Billups, S.C., Caroll, D.E., Griffith, R.O., Louie, D.L.Y (1991). Reference Manual for the CONTAIN 1.1 Code for Containment Severe Accident Analysis. SAND91-0835, NUREG/CR-5715.
21. Liu, D.D.S. MacFarlane, R. (1983). Laminar Burning Velocities of Hydrogen-Air and Hydrogen-Air-Steam Flames. *Combustion and Flame*, **49**, 59-71.
22. Mulpuru, S.R., Wilkin, G.B. (1982). A Model for Vented Deflagrations for Hydrogen in a Volume. AECL-6826.
23. Kumar, R.K., Koroll, G.W. (1992). Combustion Mitigation in Hydrogen-Air Mixtures by Dilution and Depletion. P.D. Vol. 41. Emerging Energy Technology. ASME, 1992, Ed.: S.R. Gollahalli.
24. Andrews, G.E., Bradley, D. (1973). Determination of Burning Velocity by Double Ignition in a Closed Vessel. *Combustion and Flame*, **20**, 77-89.
25. Berman, M. (1984). Light Water Reactor Safety Research Program, Semi-Annual Report, 1983 April-1983 September. SAND 84-0689.
26. Bujor, A. (1992). Adaptations in the Computer Program VENT for Predicting the Hydrogen Burning Effects. AECL, Propriety report, AECL/10704, RC-1041.
27. Andrews, G.E., Bradley, D., Lwakabamba, S.B. (1975). Turbulence and Turbulent Flame Propagation. *Combustion and Flame*, **24**, 285-304.
28. Abdel-Gayed. R.G., Bradley, D. (1976). Dependence of Turbulent Burning Velocity on Turbulent Reynolds Number and Ratio of Laminar Burning Velocity to RMS Turbulent Velocity. 16th Symposium (International) of Combustion, pp 1725-1735.
29. Wohl. K., Shore, L., von Rosenberg, H. (1953). The Burning Velocity of Turbulent Flames. 4th Symposium (International) of Combustion, pp. 620-635.
30. Dingman, S.E., Camp, A.L., Wong, C.C., King, D.B., Gasser, R.D. (1986). HECTR Version 1.5 User's Manual, SAND86-0101, NUREG/CR-4507.
31. Wong, C.C. (1988). Analyses of the Nevada Test Site (NTS) Premixed Combustion Experiments. SAND 87-0956, NUREG/CR-4916.
32. Bujor, A., Koroll, G.W., Dewit, W., Bowles, E. (1992). Constant Volume Combustion Experiments of Hydrogen-Air Mixtures with Simultaneous Multi-point Ignition. COG-92-233.
33. Landau, L.D., Lifshitz, E.M. (1959). Fluid Mechanics. *Pergamon Press.*
34. Lee, J.H.S., Guirao, C. (1981). Gasdynamic Effects of Fast Exothermic Reactions. Fast Reactions in Energetic Systems, pp 245-313. Ed. C. Capello, R.F. Walker, D. Reidel Publishing Comp.
35. Pai, I.S. (1959). Introduction in the Theory of Compressible Flow. D. van Nostrand Comp. Inc., N.Y.
36. Strehlow, R.A. (1968). Fundamentals of Combustion. Int. Textbook Company. Scranton, Pa.
37. Stamps, D.W. (1990). Detonation Cell Width in H_2-Air-Diluent Mixtures. Western States Section/The Combustion Institute. San Diego, California, Oct. 14-16 1990.
38. Chan, C.K. (1990). Private communication.
39. Searby, G., Quinard, J. (1990). Direct and Indirect Measurements of Markstein Number in Premixed Flames. *Combustion and Flame*, **82**, 298-311.

40. Chan, C.K., Tennankore, K.N. (1991). A state of the Art Report on Flame Acceleration and Transition to Detonation in Hydrogen/Air/Diluent Mixtures. OECD/NEA.
41. Chan, C.K., Lau, D., Radford, D. (1990). Transition to Detonation Resulting from Burning in a Confined Vortex. 23rd Symposium (International) of Combustion. The Combustion Institute.
42. *** (1993). Hydrogen Management Techniques in Containment. NEA/C-SNI/R(93)2.
43. Kumar, R.C., Koroll, G.W. (1992). Hydrogen Combustion Mitigation Concepts for Nuclear Reactor Containment Buildings. *Nuclear Safety*, 33(3), pp 398-414.
44. Haugh, J.J., Hosler, J.F., Sliter, G.E., Torok, R.C., Wall, I.B. (1991). EPRI Research on Hydrogen Combustion and Control - Hydrogen behaviour and mitigation in water cooled nuclear power reactors. Proceedings. Brussels, 4-8 March.
45. Baronov, G.S., Davidov, Y.G., Ershov, D.E., Furkasov, D.E., Kalinnicov, A.A., Keller, V.D. (1991). Hydrogen Mitigation Technical Means of Nuclear Power Plants - Hydrogen behaviour and mitigation in water cooled nuclear power reactors. Proceedings. Brussels, 4-8 March.
46. Behrens, U., Seidler, M., Wolff, U. (1991). Hydrogen Mitigation Using Catalyst Modules - Hydrogen behaviour and mitigation in water cooled nuclear power reactors. Proceedings. Brussels, 4-8 March.
47. Chakraborty, A.K. (1991). Removal of Hydrogen with Catalytic Recombiners During Severe Accident Situations - Hydrogen behaviour and mitigation in water cooled nuclear power reactors. Proceedings. Brussels, 4-8 March.
48. Koroll, G.W., Lau, D., Graham, W.R.C. (1991). Catalytic Removal of Hydrogen in Humid Hydrogen-Air Gas Streams - Hydrogen behaviour and mitigation in water cooled nuclear power reactors. Proceedings. Brussels, 4-8 March.
49. Gregoriev, S., Davidov, Y., Stolyarova, G., Khodulev, L. (1991). Some Aspects of Hydrogen Catalytic Recombiner Operation under Severe Accident Conditions - Hydrogen behaviour and mitigation in water cooled nuclear power reactors. Proceedings. Brussels, 4-8 March.
50. Techy, Z., Lajtha, G. (1991). Hydrogen Behaviour in VVER-440 Nuclear Power Plants in Case of Severe Accidents - Hydrogen behaviour and mitigation in water cooled nuclear power reactors. Proceedings. Brussels, 4-8 March.
51. Fineschi, F. (1991). A Strategy for Dealing with Risk Due to Hydrogen Explosions in the Containments of Pressurized Water Reactors of Russian Design (WWERs). *Nuclear Safety*, 32(3) pp 380-387.
52. Rohde, J., Chakraborty, A.K., Hüttermann, B. (1991). Mitigation of Hydrogen Threats to Large Dry Containments (German approach) - Hydrogen behaviour and mitigation in water cooled nuclear power reactors. Proceedings. Brussels, 4-8 March.
53. Karwat, H. (1991). Critical Review on Hydrogen Mitigation by Ignitors for Large Dry PWR Containments - Hydrogen behaviour and mitigation in water cooled nuclear power reactors. Proceedings. Brussels, 4-8 March.
54. Heck, R., Hill, A. (1992). A Two-pronged Approach to Hydrogen Reduction. Nuclear Engineering International. July, pp 21-28.
55. Boyack, K.W., Tieszen, S.R., Stamps, D.W. (1992). Loads from the Detonation of Hydrogen-Air-Steam Mixtures. SAND 92-0541.

56. Breitung, W. (1991). Conservative Estimates for Dynamic Containment Loads from Hydrogen Combustion. Pre-Conference Seminar on Containment of Nuclear Reactors. Shanghai. Aug. 14-16. SMIRT-11, Tokyo, Aug. 18-23.
57. Krieg, R. (1993). Can the Acceptance of Nuclear Reactors be Raised by a Simpler, more Transparent Safety Concept Employing Improved Containments? *Nuclear Engineering and Design*, 140 pp. 39-48.
58. Koroll, G.W. (1992). Private communication.
59. Kumar, R.K. (1989). Hydrogen Mitigation in Nuclear Containments by Combustion in Cooling Ducts, *Nuclear Engineering and Design* 113, 149-154.
60. Okai, S., Akagi, M. (1979). Multi-point Ignition Characteristics in a Fixed Volume Combustion Container. Combustion Symposium. Maezuru City, 17th. Combustion Symposium. 1-3. Japan.
61. Bujor, A., Koroll, G.W., Bowles, E. (1992). Vented Combustion of Dry Hydrogen-Air Mixtures with Simultaneous Multipoint Ignition. COG-92-235.
62. Bujor, A., Koroll, G.W. (1992). Intermediate-Scale Hydrogen Combustion Experiments with Simultaneous Multipoint Ignition. ANS/ENS International Conference on Fifty Years of Controlled Nuclear Chain Reaction: Past, Present, Future. Chicago. Nov. 15-20.
63. Kordilewski, W., Wach, J. (1988). Influence of Ducting on Explosion Pressure; Small Scale Experiments. *Combustion and Flame*, 71: 51-61.
64. Zalosh, R.G. (1980). Gas Explosion Tests in Room Size Vented Combustion. Loss Prevention, A.I. Ch. E., N.Y.
65. Markstein, G. (1982). Instability Phenomena in Combustion Waves. 19th Symposium (International) on Combustion, Pittsburgh.
66. Chu, B.T. (1952). On the Generation of Pressure Waves at a Plane Flame Front. 4th Symposium (International) on Combustion. M.I.T., Cambridge, Ms., Sept. 1-5.
67. Kumar, R.K., Dewit, W.A., Grieg, D.R. (1989). Vented Explosions of Hydrogen-Air Mixtures in a Large Volume. *Combustion Science and Technology* 66, 251-266.
68. Bradley, D., Mitcheson, A. (1978). The Venting of Gaseous Explosions in Spherical Vessels. I-Theory. *Combustion and Flame*. 32(3), 221-236.
69. Bradley, D., Mitcheson, A. (1978). The Venting of Gaseous Explosions in Spherical Vessels. II-Theory and Experiments. *Combustion and Flame*. 32(3), 237-256.
70. Cooper, M.G., Fairwater, M., Tite, J.P. (1986). On the Mechanism of Pressure Generation in Vented Explosions. *Combustion and Flame*. 65, 1-14.
71. Kinsler, L.E., Frey, A.R. (1967). Fundamentals of Acoustics. John Willey and Sons.
72. Bujor, A. (1993). A Model for Multipoint Ignition of H_2 in Containment. Risø-I-707.
73. Klazek, P. (1989). The Prediction of Gas Explosion Transients by VENT Code Calculations. 906-NK38-3461OP.
74. Babiy, V.I. (1974). Solid/Gas Phase Heat Exchange in Combustion of Powdered Fuel. Heat Transfer in Flames, Eitors N.H. Afgan and J.M. Beer; John Wiley and Sons.
75. Lignola, D.G., Raverchon, E., Bolzano, M. (1983). Heat Transfer in Mechanically Mixed CSTR for Gas Phase Reactions. *Combustion and Flame*, 51, 63-77.
76. Hadvig, S. (1970). Heat Transmission by Gas Flow Including Both Radiation and Convection. *Journal of the Institute of Fuel*, 35(129), pp. 202-211.

77. Steward, F.R., Guruz H.K. (1974). Mathematical Simulation of an Industrial Boiler by the Zone Method of Analysis. Heat Transfer in Flames. Editors N.H. Afgan and J.M. Beer; John Wiley and Sons, pp. 131-140.
78. Yaws, C.L., Miller, J.W., Shah, P.N. (1976). Correlation Constants for Chemical Compounds. Chemical Engineering, Nov. 22, pp 153-162.
79. Kumar, R.K., Bowles, E.M. (1991). Flame Acceleration in Hydrogen/Air/-Steam Mixtures in the Presence of Repeated Obstacles in a Closed Volume. Hydrogen behaviour and mitigation in water cooled nuclear power reactors. Proceedings. Brussels, 4-8 March.
80. Williams, D.C., Bergeron, K.D., Rexroth, P.E., Tills, J.L. (1987). Integrated Phenomenological Analysis of Containment Response to Severe Core Damage Accidents. *Progress in Nuclear Energy*, 19(1), 69-131.
81. Koroll, G.W., Bowles, E.M., Bujor, A. (1993). Hydrogen Combustion with Simultaneous Multiple Ignition. IPSN-COG Hydrogen Working Group Meeting, Sept. 20-22, Fontenay aux Roses.
82. Koroll, G.W., Bowles, E.M., Bujor, A. (1993). Hydrogen Combustion with Simultaneous Multiple Ignition. 2nd German-Canadian Workshop on Hydrogen, Oct. 20-22, Pinawa, Canada.

Appendix

Chemical Reactions of the H_2-O_2 System, /21/

Expressing the reaction rate k with the Arrhenius Law,

$$k = A \cdot T^{\beta} \exp\,(E_A/RT)$$

the values of the coefficients A (expressed in cm · mole · sec) and β and of the activation energy E_A (expressed in kJ/mole) for reactions between the radicals of the hydrogen-oxygen system are given in Tab. A1, /21/.

Table A1. Mechanisms of the hydrogen-oxygen reaction

		A	β	E_a
1.	$O_2 + H \rightarrow OH + O$	2.00×10^{14}	0.00	70.30
2.	$OH + O \rightarrow O_2 + H$	1.46×10^{13}	0.00	2.08
3.	$H_2 + O \rightarrow OH + H$	5.06×10^{4}	2.67	26.30
4.	$OH + H \rightarrow H_2 + O$	2.24×10^{4}	2.67	18.40
5.	$H_2 + OH \rightarrow H_2O + H$	1.00×10^{8}	1.60	13.80
6.	$H_2O + H \rightarrow H_2 + OH$	4.45×10^{8}	1.60	77.13
7.	$OH + OH \rightarrow H_2O + O$	1.50×10^{9}	1.14	0.42
8.	$H_2O + O \rightarrow OH + OH$	1.51×10^{10}	1.14	71.64
9.	$H + H + M \rightarrow H_2 + M$	1.80×10^{18}	-1.00	0.00
10.	$H_2 + M \rightarrow H + H + M$	6.99×10^{18}	-1.00	436.08
11.	$H + OH + M \rightarrow H_2O + M$	2.20×10^{22}	-2.00	0.00
12.	$H_2O + M \rightarrow H + OH + M$	3.80×10^{23}	-2.00	499.41
13.	$O + O + M \rightarrow O_2 + M$	2.90×10^{17}	-1.00	0.00
14.	$O_2 + M \rightarrow O + O + M$	6.81×10^{18}	-1.00	496.41
15.	$H + O_2 + M \rightarrow HO_2 + M$	2.30×10^{18}	-0.80	0.00
16.	$HO_2 + M \rightarrow H + M + O_2$	3.26×10^{18}	-0.80	195.88
17.	$HO_2 + H \rightarrow OH + OH$	1.50×10^{14}	0.00	4.20
18.	$OH + OH \rightarrow HO_2 + H$	1.33×10^{13}	0.00	168.30
19.	$HO_2 + H \rightarrow H_2 + O_2$	2.50×10^{13}	0.00	2.90
20.	$H_2 + O_2 \rightarrow HO_2 + H$	6.84×10^{13}	0.00	243.10
21.	$HO_2 + H \rightarrow H_2O + O$	3.00×10^{13}	0.00	7.20
22.	$H_2O + O \rightarrow HO_2 + H$	2.67×10^{13}	0.00	242.52
23.	$HO_2 + O \rightarrow OH + O_2$	1.80×10^{13}	0.00	-1.70
24.	$OH + O_2 \rightarrow HO_2 + O$	2.18×10^{13}	0.00	230.61
25.	$HO_2 + OH \rightarrow H_2O + O_2$	6.00×10^{13}	0.00	0.00
26.	$H_2O + O_2 \rightarrow HO_2 + OH$	7.31×10^{14}	0.00	303.53
27.	$HO_2 + HO_2 \rightarrow H_2O_2 + O_2$	2.50×10^{11}	0.00	-5.20
28.	$OH + OH + M \rightarrow H_2O_2 + M$	3.25×10^{22}	-2.00	0.00
29.	$H_2O_2 + M \rightarrow OH + OH + M$	2.10×10^{24}	-2.00	206.80
30.	$H_2O_2 + H \rightarrow H_2 + HO_2$	1.70×10^{12}	0.00	15.70
31.	$H_2 + HO_2 \rightarrow H_2O_2 + H$	1.15×10^{12}	0.00	80.88
32.	$H_2O_2 + H \rightarrow H_2O + OH$	1.00×10^{13}	0.00	15.00
33.	$H_2O + OH \rightarrow H_2O_2 + H$	2.67×10^{12}	0.00	307.51
34.	$H_2O_2 + O \rightarrow OH + HO_2$	2.80×10^{13}	0.00	26.80
35.	$OH + HO_2 \rightarrow H_2O_2 + O$	8.40×10^{12}	0.00	84.09
36.	$H_2O_2 + OH \rightarrow H_2O + HO_2$	5.40×10^{12}	0.00	4.20
37.	$H_2O + HO_2 \rightarrow H_2O_2 + OH$	1.63×10^{13}	0.00	132.71

Bibliographic Data Sheet **Risø-R-706(EN)**

Title and author(s)

Hydrogen Problems Related to Reactor Accidents

A. Bujor

ISBN	ISSN
87-550-1925-0	0106-2840

Dept. or group	Date
Nuclear Safety Research Department	September 1993

Groups own reg. number(s)	Project/contract no.(s)

Pages	Tables	Illustrations	References
79	11	39	82

Abstract (Max. 2000 characters)

At reactor accidents, the combustion of hydrogen causes pressure and temperature transients which pose supplementary loads in containment. In certain conditions, they could be at hazardous levels and impair the integrity of the containment and the operability of the safety systems.

The mechanisms of the chemical reactions specific for the hydrogen-oxygen system are presented in Chap. 2. The conditions in which a burning can occur and the various combustion modes, including the transition to detonation are also described.

In Chap. 3 the related safety aspects and mitigation methods are discussed. Examples for particular applications and safety approaches for various types of reactors, included those promoted for the advanced reactors are also given.

Chap. 4 is dedicated to the presentation of the experimental research completed at AECL-Research, Whiteshell Laboratory, where the multi-point ignition effects for constant volume and for vented combustion of dry hydrogen-air mixtures in various geometries have been investigated.

Various aspects of modelling and simulation for the hydrogen burning are discussed in Chap. 5. The adaptations and the new models implemented in the codes VENT and CONTAIN, aimed to broaden the simulation capabilities of their hydrogen combustion models are described. The capabilities and the limits of the modelling assumptions of these two codes are also evaluated.

Descriptors *INIS/EDB*

Available on request from Risø Library, Risø National Laboratory
(Risø Bibliotek, Forskningscenter Risø), P.O. Box 49,
DK-4000 Roskilde, Denmark
Telephone (+45) 46 77 46 77, ext. 4004
Telex 43 116 · Telefax (+45) 46 75 56 27

RISØ

OBJECTIVE

The objective of Risø National Laboratory is to further technological development in three main areas: energy, environment and materials.

USERS

Risø's scientific results are widely applied in industry, agriculture and public services. Risø contributes its share of new knowledge to the global research community.

RESEARCH PROFILE

Risø emphasises long-term and strategic research providing a solid scientific foundation for the technological development of society.

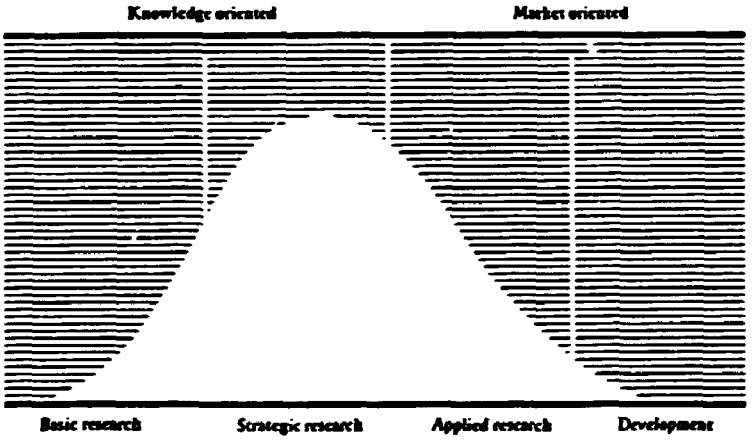

PRIORITY AREAS

- **Combustion and gasification**
- **Wind energy**
- **Energy materials**
- **Energy and environmental planning**
- **Assessment of environmental loads**
- **Reduction of environmental loads**
- **Safety and reliability of technical systems**
- **Nuclear safety**
- **Atomic structure and properties of materials**
- **Advanced materials and materials technologies**
- **Optics and fluid dynamics**

Risø-R-706(EN)
ISBN 87-550-1925-0
ISSN 0106-2840

Available on request from:
Risø Library
Risø National Laboratory
P.O. Box 49, DK-4000 Roskilde, Denmark
Phone +45 46 77 46 77, ext. 4004/4005
Telex 43116, Telefax 46 75 56 27